Nanoparticles and Photosensitisers; their Interactions and Antibacterial Properties

Naima Narband

Supervised by Prof. Ivan Parkin
And Prof. Mike Wilson

University College London
2009

I Naima Narband confirm that the work presented in this thesis is my own. Where information has been derived from other sources, I confirm that this has been indicated in the thesis.

Acknowledgements

I am grateful and thankful to God who makes all things possible. All praise is due to the Almighty. May he make our lives easier and grant us contentment.

I would like to thank a number of people who have helped and encouraged me to write this thesis. I would like to acknowledge and extend my heartfelt gratitude to my supervisor Prof. Ivan Parkin who has guided, taught and encouraged me through this project. I would also like to thank my second supervisor Prof. Mike Wilson, along with Dr. Sean Nair at the Eastman Dental Institute. Without their understanding and input this thesis would not have been possible. Many thanks go to Cale Street and Ondine Biopharma who provided the financial support for this project.

I would like to express my thanks to Dr Andrew Beeby from Durham University and Dr Mark Green from Kings College London for their enthusiastic, expert advice and input into the project. I will always be grateful to Linda Dekker and Sarah Tubby who have worked with me on the microbiology experiments. I have learnt a great deal from those who have worked with me over the years and gratefully acknowledge my debt to them, especially Dr Steve Firth, Dr Jesus Gil Tomas, Dr Andrea Sella, Dr Ian Watts and Dr Chris Balckman. I would also like to thank my first chemistry teacher Mr Gratrix who contributed in a fundamental way to my understanding of chemistry.

I am grateful to Dr Russell Binions, Dr Clara Piccirrillo and Dr Charlie Dunnill for conversations that clarified my thinking. Their friendship and professional collaboration meant a great deal to me. I will always be grateful to Dr Geoff Hyett who taught me something new almost every day with immense patience and understanding.

To all of the below individuals, and to several colleagues who have assisted me one way or another, especially in challenging me with alternative views, I feel very much indebted to you; Dr Rob Palgrave, Dr Niccochoco, Dr Uzma Quershi, Dr Jalpa Patel and Dr Christina Bashkaran. To my friends I have moaned to on bad days and celebrated with on good, I could not have accomplished this project without you; Kris Page, Stephen Potts, Paolo Melgari and Luanne Thomas. Caroline Knapp, Dr Siama

Basharat/Hussein and Asif Bhaiji have never been more than a phone call away and nothing I write here would do justice for the help and support you guys have given me. I would like to express my deep-felt thanks and gratitude to my family; Mum, Dad, Anisa Wadi, Rabiah Tashkent, Sajeda Narband, Fahmeeda Narband, Hajra Narband, Fatz, Maryam Wadi, Khadijah Wadi, Ayesha Tashkent, Ayesha Suleman, Younus Masa, Rashida Masi and all other relatives in Zambia for their patience and forbearance whilst I have spent hundreds of hours working on this thesis! I can reassure the reader that as this may be my last direct work as such, at least for a while, I have put a bit of "heart and soul" into it! Therefore, I hope that you will very much enjoy this work as well as find it immensely educative!

Abstract

This work reports on the coupling of light activated antimicrobial (LAA) agents with gold nanoparticles to provide new materials that displayed enhanced antimicrobial properties. A versatile and robust approach to the synthesis of gold-thiol-photosensitiser light activated antimicrobials has been developed. In the synthetic approach the thiols attached to the gold nanoparticles were tiopronin and glutathione. The photosensitisers attached to the thiols were toluidine blue and tin chlorin e6 respectively. It was found gold-tiopronin-toluidine blue nanoparticles at 1 μM concentration were efficient as light activated antimicrobials, that had a reduction of colony forming units (cfu) of *S.* aureus by 4.5 $\log_{10}$ compared with, 0.5 $\log_{10}$ for toluidine blue at the same concentration. The attachment of photosensitisers to thiol protected gold nanoparticles enhanced the lethal photosensitisation of bacteria. The second approach was mixing of charge stabilised gold nanoparticles with various photosensitisers. When charge stabilised gold nanoparticles when mixed with toluidine blue (20 μM), showed a reduction in colony forming units (cfu) for *S. aureus* of 2.5 $\log_{10}$ compared with 1.5 $\log_{10}$ for only toluidine blue at the same concentration. This established that covalent attachment of the photosensitiser was not necessary for the enhancement in the lethal photosensitisation of bacteria. Also, it was discovered that certain dyes which have basic, cationic natures have different interactions with charge stabilised gold nanoparticles.

A separate study focusing on semi-conductor quantum dots and the photosensitiser toluidine blue was undertaken to investigate any relationship between nanoparticles and photosensitisers. It was found that semi-conductor quantum dots enhance the effect of toluidine blue in the lethal photosensitisation of bacteria. An excess of a 1.7 $\log_{10}$ enhancement in bacterial kill was observed with quantum dot concentration of 0.0075 μM and toluidine blue concentration of 20 μM. In summary, the efficacy of photosensitisers can be enhanced by the presence of nanoparticles of gold and CdSe.

List of Figures

List of Equations

List of Tables

List of Abbreviations

AMD	Age Related Macular Degeneration
AZ A	Azure A
AZ B	Azure B
AZ C	Azure C
CFU	Colony Forming Units
CTAB	Cetyl Trimethyl Ammonium Bromide
DNA	Deoxyribonucleic acid
EDC	1-[3-(dimethylamino)propyl]-3-ethylcarbodiimide hydrochloride
G+	Gold Present
G-	Gold not Present
GS	Glutathione (bound)
GSH	Glutathione
HOMO	Highest Occupied Molecular Orbital
HRTEM	High Resolution Transmission Electron Microscopy
IR	Infra-Red
L+	Light
L-	No Light
LAA	Light Activated Antimicrobial
LAAA	Light Activated Antimicrobial Agent
LUMO	Lowest unoccupied Molecular Orbital
MB	Methylene Blue
MBC	Minimum Bacterial Concentration
MRSA	Methicillin-Resistant *Staphylococcus aureus*
MWCO	Molecular Weight Cut Off
P.	*Psuedomonas*
PBS	Phosphate Buffer Solution
PCS	Photon Correlation Spectroscopy
PDT	Photodynamic Therapy
QD	Quantum Dots
RB	Rose Bengal
Rho B	Rhodamine B

S+	Sensitiser
S-	No Sensitiser
SnCe6	Tin Chlorin e6
S. / Staph.	*Staphylococcus*
Strep.	*Streptococcus*
Sulfo-NHS	*N*-hydroxysulfosuccinimide sodium salt
TBO	Toluidine Blue
TNBPPT	5,10,15,20-tetra(*N*-benzyl-4-pyridyl)porphyrin tetrachloride
TOAB	Tetraoctylammonium Bromide
TGA	Thermal Gravimetric Analysis
Th	Thionin
UV-vis	UV-visible absorption
XRD	X-ray Diffraction

Contents Page

Chapter 1 Introduction

This thesis presents the results of an investigation into the interactions between Light Activated Antimicrobial Agents (LAAA) and nanoparticles. Light Activated Antimicrobial Agents utilise incident radiation to produce reactive oxygen species which are toxic to bacteria. Charge stabilised gold nanoparticles mixed with LAAAs' were investigated, along with monolayer protected gold nanoparticles with LAAAs' covalently attached. The nature of the protecting monolayer and LAAAs' were modified and their effect on the lethal photosensitisation of bacteria assessed. Additionally the size of the gold core was modified in an attempt to find an optimum size at which lethal photosensitisation of bacteria would be at its most efficient. Finally, in order to uncover details of the mechanism by which this enhanced kill operates, the composition of the core was changed from gold to a cadmium selenide. These semiconductor quantum dots were used in conjunction with LAAAs' in singlet oxygen detection experiments to quantify the production of toxic oxygen species.

1.1 Overview

Lethal photosensitisation of bacteria is an emerging and promising treatment, which utilises light in combating microbial infections. Its main advantage is the reduced possibility of resistance. This thesis focuses on established photosensitisers such as methylene blue, toluidine blue and tin chlorine e6, all of which have been widely recognised as effective light activated antimicrobials.

Two different types of ligand stabilised nanoparticles have been synthesised: tiopronin and glutathione, each attached to a different photosensitiser (toluidine blue and tin chlorine e6). Additionally, charge stabilised gold nanoparticles have been investigated with a wide variety of photosensitisers. Lastly, to understand the mechanisms observed for the enhanced microbial kill, the core metal was changed to CdSe semi-conductor quantum dots and singlet oxygen detection experiments were performed.

This introduction focuses on the properties and synthesis of gold nanoparticles. A brief overview on the historical aspects of colloidal gold is presented, followed by a detailed description of surface plasmon resonance (SPR). Various syntheses of gold nanoparticles are discussed along with nucleation and growth mechanisms. Finally, the lethal photosensitisation of bacteria is reviewed.

1.2 Gold

Gold has been the subject of investigation since ancient times. Its recent renaissance has lead to an exponentially increasing number of publications, especially in the field of nanoscience and nanotechnology.[1,2] The extraction of gold started in the 5th millennium B.C. near Bulgaria and reached 10 tons per year in Egypt (around 1200 - 1300 B.C).[3] Known and highly valued since ancient times, gold is found in nature as the free metal and in tellurides. It occurs naturally in veins and alluvial deposits, and is often separated from rocks and other minerals by sluicing and panning operations. The metal is recovered from its ores by cyaniding, amalgamating and smelting processes, while refining is carried out by electrolysis.[4]

Gold in its pure state is considered to be beautiful and rare, hence a valuable metal. It has a yellow colour when in bulk, though when finely divided it may be black, red, blue or purple. In the bulk form gold is a soft yellow metal, which has a face centred cubic crystal structure, and a melting point of 1064 °C. Gold is soft, ductile and malleable and is usually alloyed to improve strength and durability. Gold's reflectivity at ultraviolet and visible light wavelengths is low; however it has high reflectivity at red and infrared wavelengths.

Gold is a good conductor of heat and electricity, and is mostly unaffected by air, nitric, hydrochloric, or sulphuric acid. However, a solution of aqua regia (3:1 of hydrochloric acid:nitric acid) dissolves gold. Common gold compounds are auric chloride ($AuCl_3$) and chloroauric acid ($HAuCl_4$).

1.3 Colloidal Gold

A colloidal dispersion is a system of particles which are dispersed in a continuous phase of a different composition or state.[5] Suspensions in liquids form the basis of a wide variety of systems of scientific and technological importance, including paints, ceramics, cosmetics, agricultural sprays, detergents, soils, biological cells, and in many food preparations.[5] A colloidal system is composed of two separate phases: a dispersed phase (or internal phase) and a continuous phase (or dispersion medium). The dispersions can have the appearance of a solution when dispersion is homogeneous.

Colloidal gold was used to colour glass and ceramics. A famous example of this is the Lycurgus Cup (Figure 1-1) which is currently on display at the British Museum. This is an extraordinary item, assumed to be made in Rome around the 4th century AD,[6] and is an example of dichroic glass. Dichroic glass changes colour when held up to light. The Lycurgus cup appears green in daylight or reflected light, changing to red when illuminated from the inside or in transmitted light. These unusual optical properties are attributed to the presence of tiny amounts of colloidal gold – silver alloy present in the glass. Although this colouring of glass was described in Roman times, the production of gold – ruby glass was not rediscovered in Europe until the 17th century, when sizeable red glass vessels were manufactured by adding ‘Purple of Cassius’. Purple of Cassius is a colloid resulting from the heterocoagulation of gold particles and tin dioxide and was named after Andreas Cassius who described it in his treatise De auro in 1685.[3]

In the manufacture of Purple of Cassius, a solution of auric chloride ($AuCl_3$) was treated with tin chloride ($SnCl_2$). $AuCl_3$ is reduced to colloidal gold and $SnCl_2$ is oxidised to $SnCl_4$. The $SnCl_4$ formed undergoes hydrolysis to form $SnO_2.2H_2O$. The overall reaction can be thought of as:

$$2\,AuCl_3 + 3\,SnCl_2 + 6\,H_2O \longrightarrow 2\,Au + 3\,SnO_2 + 12\,HCl \qquad \textbf{1-1}$$

Purple of Cassius is colloidal SnO_2 with absorbed colloidal Au.

Figure 1-1 ***The Lycurgus cup, appears red in transmitted light (right) and green in reflected light (left) due to the presence of gold/silver colloids.***

An early book on finely divided gold which has been preserved, was published in 1618 by Francisco Antonii.[7] This book contained considerable information on the formation of colloidal gold, the medical uses of colloidal gold sols and successful cases where these gold sols had been used for treatment. The synthesis involved the use of plant extracts which, unbeknown to the alchemists stabilised the sols. The sols were supposedly infused with medicinal virtues, which could cure disease and improve strength. Johann Kunckels, a German chemist published a book in 1676 describing “drinkable gold that contains metallic gold in a neutral, slightly pink solution that exert curative properties for several diseases”. These diseases included heart and venereal problems, dysentery, epilepsy, and tumours. Colloidal gold was used for the diagnosis of syphilis. By the mid eighteenth century it became apparent to alchemists that ‘aurum potable’- drinkable gold was just finely divided gold in a liquid, and was devoid of any magical, medicinal or at that point therapeutic qualities.[7]

1.4 Clusters vs. Nanoparticles vs. Bulk

The properties of materials change as their size approaches the nanoscale, and as the percentage of atoms at the surface of a material becomes more significant. Bulk materials possess relatively constant physical properties regardless of their size, but at the nanoscale this is often not the case. As the material becomes smaller the percentage of atoms at the surface increases relative to the total number of atoms of the material bulk (Figure 1-2). This can lead to unexpected properties of nanoparticles which are partly due to the surface of the material dominating over the bulk properties. Size-dependent properties are observed such as quantum confinement in semi-conductor particles,[8] surface plasmon resonance in noble metal particles[2] and superparamagnetism in magnetic materials.[9]

In 1981 Schmid *et al.*[10] reported the synthesis of the cluster [$Au_{55}(PPh_3)_{12}Cl_6$], which was unique with its low size distribution (4.0 ± 0.4 nm). The synthesis of this cluster is difficult, and it was not until 1993 that the stabilisation of nanoparticles with alkanethiols was first reported by Mulvaney and Giersig.[11] The particles synthesised by Schmid *et al.*[10] displayed quantum confinement properties, where the band gap is sufficiently increased and there is quantisation of discrete electronic energy levels. These well defined phosphine stabilised particles were less than 10^{-9} m in diameter. Particles this small are better thought of as clusters of metal atoms.[12] Schmid's group reported that the [$Au_{55}(PPh_3)_{12}Cl_6$] cluster had discrete energy level spacings of 170 meV which was attributed to the Au_{55} gold core.[13]

If the diameter of a gold clusters is above 3×10^{-9} m the electronic structure of the particles shifts towards the band structure of bulk gold. The number of atoms in each particle increases and so they are not easily countable. The crystal structure becomes cubic closed packed as in bulk gold and each particle can be made up from more than one crystallite.[3] Gold particles between the size interval of 3×10^{-9} m and 5×10^{-7} m have interesting optical properties, the most dominant being surface plasmon resonance.[14] The surface plasmon resonance is a strong absorbance at a specific frequency, which induces the collective oscillation of electrons at the surface of the gold particle that gives gold colloids their characteristic colour. Particles above 5×10^{-7} m no longer display the surface plasmon resonance in the visible part of the electromagnetic spectrum and gradually move towards the properties of bulk gold.[6]

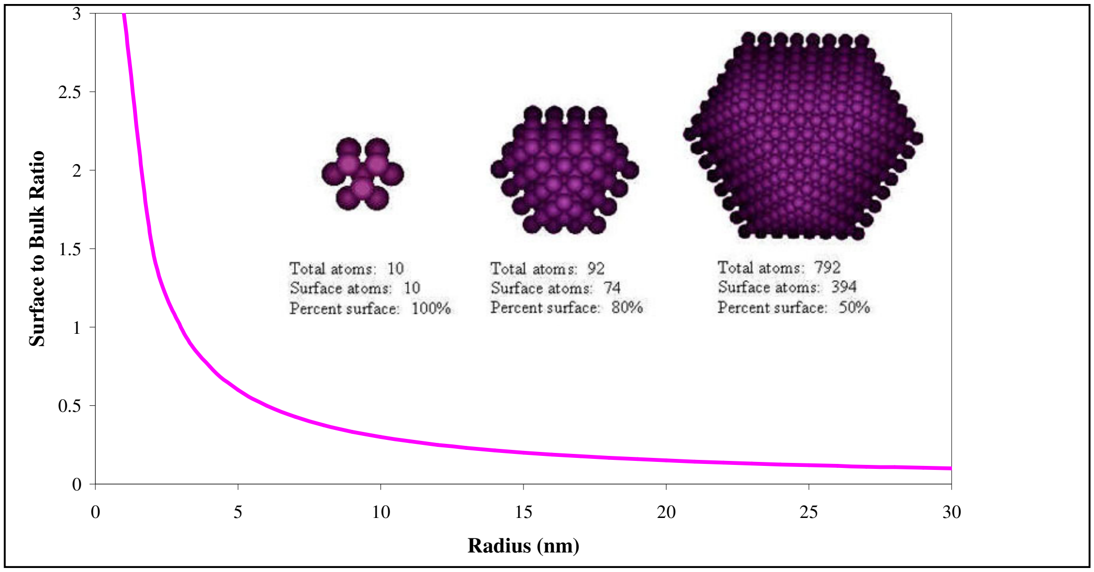

Figure 1-2 ***Graph illustrating the relationship between the radius of the particle and the surface to bulk ratio. As the particle becomes smaller the surface to bulk ratio increases. Inset is a representation of face centred cubic structure of most metals as small particles. A cuboctahedral cluster of 792 atoms has 50% contributing to the surface, and a cluster of 10 atoms has 100% of the atoms contributing to the surface.***[15]

Gold particles between the size interval of 3 × 10^{-9} m and 5 × 10^{-7} m have a large surface to volume ratio. A significant proportion of atoms in this structure are surface atoms (Figure 1-2). Therefore any reactions that occur at the surface are amplified due to the large expanse of exposed surface. A detailed review of small gold nanoparticles and their reactions has been presented by Daniel and Astruc.[3]

Nanoparticles are often described as structures with a diameter in the range of 10 – 100 nm.[6] This description is often arbitrary as some nanoparticles with larger diameters display behaviour exclusively associated with nanoparticles. Gold particles about 100 nm in diameter still display the surface plasmon, albeit with the Tyndall effect.[16] The Tyndall effect results from the scattering of light waves from the surface of a particle. When the wavelength of incident light is the same size or smaller than the particle a haze is observed from the suspensions of these particles in air or liquids.[17,18] Shorter wavelengths of light (blue) are reflected or scattered whereas longer wavelengths (red) pass straight through. In the work reported in this thesis, the gold nanoparticles synthesised typically have a diameter less than 30 nm. These particles are not large enough to display the Tyndall effect, but did have a surface plasmon resonance in the visible part of the spectrum.

1.5 Surface Plasmon Resonance

At the nanometer scale, particles display properties that are not inherent in individual atoms or to those in the bulk macroscopic material. The optical properties of gold nanoparticles are decidedly dependant on[19]:-

- Particle size
- Interparticle distance
- Type of surfactant
- Shape of the nanoparticle
- Dielectric constant of the dispersion medium

In a nanoparticle many of the atoms are located on the surface, hence unusual properties are observed which are not present in the bulk or in individual atoms. One of these optical phenomena is surface plasmon resonance. The deep coloured nature from orange through to deep purple, of colloidal gold is a result of the surface plasmon.[2] At this nanometer scale the 'quantum size effect' becomes significant as the de Broglie wavelength of the valence electrons is in the same size range as the particle itself. The particles are then considered to be zero-dimensional quantum dots or quantum boxes, and are subject to quantum mechanical rules. Freely mobile electrons are trapped effectively in quantum boxes and hence exhibit a collective oscillation frequency associated with the plasmon resonance in the presence of light. In gold nanoparticles there is a gap between the valence and the conduction bands. Hence there is a size induced metal-insulator transition where size dependent quantisation effects occur. This leads to standing electron waves with discrete energy levels.[3]

Surface plasmon resonance manifests itself when the electric field of the incoming radiation induces a dipole on the nanoparticle. There is a restoring force that tries to compensate for this dipole, so that a unique resonance frequency is formed which matches the electron oscillation frequencies within the particle (Figure 1-3). This frequency of oscillation is equal to the frequency of resonant light, and as the particle is much smaller than the wavelength of incoming light it is homogeneously polarised. The plasmon resonance band is observed at approximately 530 nm for gold nanoparticles of diameter 5-20 nm.[6]

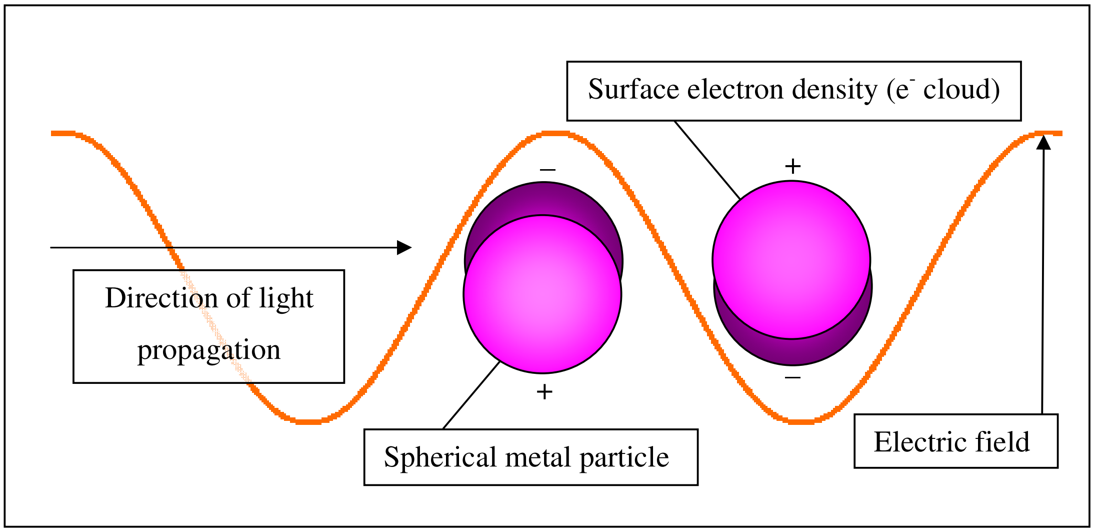

Figure 1-3 ***Illustration of the excitation of a dipolar surface electron oscillation, surface plasmon resonance by the electric field of incoming light on gold nanoparticles*.**

As mentioned above, a result of the surface plasmon effects is that the sols appear coloured. When particles are small (~10 nm) they appear ruby red due to the absorption of green light at around 520 nm. If these particles are allowed to coalesce in a controlled fashion by the addition of electrolytes, a colour change is observed. The red goes through pink and violet to blue as the nanoparticles grow. This is due to a change in the absorption spectrum upon aggregation, causing the increased absorption of red light.[1]

1.6 Theoretical Approaches to the Surface Plasmon Resonance

Existing theories that describe the interaction of light and matter have been applied to spherical and non-spherical gold particles. Mie described the surface plasmon resonance quantitatively by solving Maxwell's equations.[20] Mie theory relates the surface plasmon resonance to the complex dielectric constant of the metal. The total extinction cross section (σ_{ext}) composed of absorption and scattering is given as a summation over all electric and magnetic multiple oscillations. Mie theory is conceptually simple and has been applied in explaining experimental results.[21]

In particles where the wavelength of incident radiation is much smaller than the particle itself, the polarisation of the particle is such that only dipolar surface plasmons are excited. In these cases the wavelength (λ) of incident light is ($\lambda >> 2R$) where R is the radius. In the case of gold where $2R < 25$ nm only the dipole absorption of the Mie equation contributes to the extinction cross section of the nanoparticles (σ_{ext}). Mie theory is then reduced to a dipole or quasi–static approximation where the surface plasmon resonance frequency is largely size independent:

$$\sigma_{etx} = \frac{9V\varepsilon_m^{3/2}}{c} \times \frac{\omega\varepsilon_m(\omega)}{[\varepsilon_1(\omega)+2\varepsilon_m]^2+\varepsilon_2(\omega)^2}$$

1-2

where V is the volume of a spherical particle, c is the speed of light, ω the angular frequency of the exciting frequency, and ε_m is the dielectric constant of the surrounding medium (assumed to be frequency independent). $\varepsilon_1(\omega)$ and $\varepsilon_2(\omega)$ are the real and imaginary parts respectively of the frequency dependant dielectric function of gold.[14] The imaginary part of the dielectric function of the surrounding medium is assumed to be zero. This is a reasonable approximation for most non metals at visible frequencies. From equation (1-2) it is deduced that resonance occurs when $\varepsilon_1(\omega) \approx -2\,\varepsilon_m$ if ε_2 is small. With this dipole quasi–static approximation, the size of the particle is not explicitly included in the equation, but inferred through the volume (V) which is solely dependant on the radius (R).[14] Nonetheless, experimentally it has been found that there is a strong size dependence of the surface plasmon band width and position. The position of the absorption maximum is affected through a blue shift as the particles get smaller and a red shift as the particle grows.[20] Modifications of Mie theory can be made, to take into account the size dependence using the Drude model.[6] The dielectric function of the gold nanoparticle is assumed to become size dependant [$\varepsilon = \varepsilon\,(\omega, R)$]. This results in a size absorption cross section even within the dipole approximation.[6]

Equation (1-2) can be used to describe the lifetime of the surface plasmon resonance. The decay of surface plasmon oscillations mostly occurs through non–radiative pathways, such as scattering from the metal surface, electron–phonon and electron–electron scattering or transfer of energy from the collective electron oscillations to individual electron excited states. Additionally, radiative decay through electron–photon decay also occurs.[22]

1.7 Synthesis of Colloidal Gold Nanoparticles

Gold nanoparticles were largely overlooked by research chemists before the 1850's; however they were used to decorate ceramics and glass. In 1857, Michael Faraday performed the first reliable systematic investigation of gold colloids.[23] The methods of producing colloidal gold solutions involved using single phase and two phase systems with different solvents and reducing agents, some of which were extremely hazardous. Faraday synthesised gold nanoparticles by the reduction of $AuCl_3$ by phosphorous. The paper was innovative because it contained the first mention of the sensitivity of gold nanoparticles to electrolytes. Another important feature in this paper was the account of using macromolecules as 'protective agents' or surfactants to stabilise these nanoparticles against aggregation. As a testimony to the accuracy of his paper, several of Faraday's original nanoparticle solutions still exist today, and are kept at the Royal Institution where he worked. Subsequently, the solution phase synthesis of gold nanoparticles has been almost exclusively achieved by the reduction of hydrogen tetrachloroaurate.

$$[HAuCl_4] + 3e^- \longrightarrow Au^0 + H^+ + 4Cl^- \tag{1-3}$$

Hydrogen tetrachloroaurate is a fairly strong oxidising agent ($E^\circ = +1.002$ V),[24] therefore mild reducing agents can be used to reduce the gold to Au(0). When synthesising gold nanoparticles, the main emphasis has been placed on keeping the reaction simple to produce uniform particles that are of controllable diameter. A variety of methodologies have been reported using different reducing agents, stabilising agents and solvating media.[3] All methods vary considerably but have in common the use of hydrogen tetrachloroaurate ($HAuCl_4$). Hydrogen tetrachloroaurate can be prepared by dissolving gold in aqua regia and evaporating the acid by heating. A few cycles of HCl addition followed by evaporation are required. Afterwards, some cycles of water addition followed by evaporation are needed to remove the excess acid. The final product is a hygroscopic yellow/orange solid which has a pH of *ca*. 1 when dissolved in water.[25] A solution of hydrogen tetrachloroaurate in methanol or water is usually used to synthesise gold nanoparticles. Typical reducing agents used to form gold nanoparticles include citrate, tannic acid, amino acids and sodium borohydride.

Improvements in analytical techniques throughout the 19th and 20th century have stimulated interest in nanoparticular science. In the late nineteenth century breakthroughs in the synthesis of colloidal gold were made by Zigsmondy, as colloidal gold was the main experimental subject used when developing the ultramicroscope.[7] He described methods for the synthesis of colloidal gold with different particle sizes, using hydrogen peroxide, phosphorus and amines as reducing agents. In 1925 Zigsmondy was awarded the Nobel Prize in Chemistry 'for his demonstration of the heterogeneous nature of colloid solutions and for the methods he used, which have since become fundamental in modern colloid chemistry'.[7] In 1924 Ostwald[26] synthesised gold nanoparticles using an electrical arc. Around this time the composition of colloidal gold was determined to be an elemental gold core with an anionic protective double layer of charges (Figure 1-4).[27]

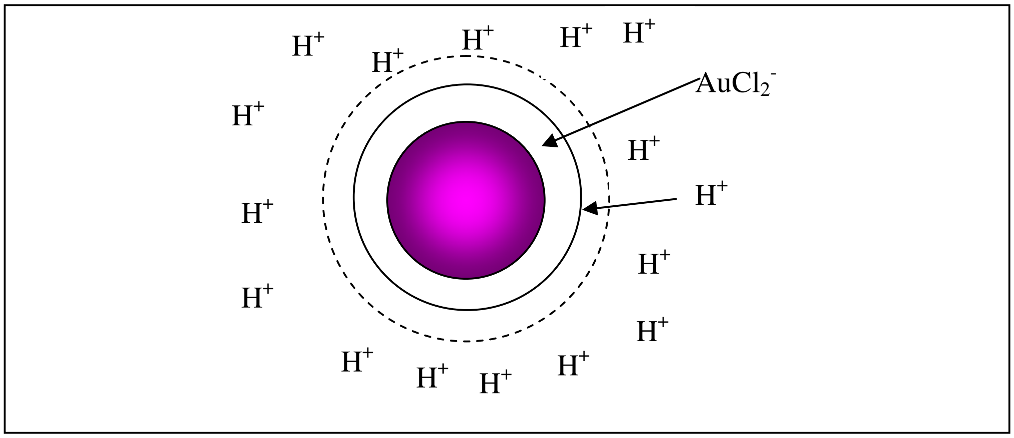

Figure 1-4 ***Crystalline core of elemental Au with adsorbed $AuCl_2^-$ ions which make up the inner layer of the ionic double layer on a gold nanoparticle, synthesised by a citrate reduction.***

A straight forward synthesis of gold nanoparticles was reported by Turkevich *et al.* in 1951.[28] Their study focused on the process of nucleation and growth in the synthesis of nanoparticles. The synthesis required the use of inexpensive sodium citrate as the reducing agent, in a solution of chloroauric acid. This method produced gold nanoparticles of about 20 nm with 12.5% standard deviation in particle size. The synthesis involved dissolving gold chloride in water and boiling the solution. Another solution of trisodium citrate in water was prepared and added to the boiling water and dissolved gold chloride. The gold ions were reduced by the citrate and gold particles are stabilised against aggregation by the citrate:

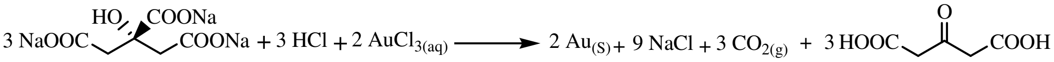

1-4

Turkevich's paper would have gone largely unnoticed without Fren's landmark paper in 1973.[18] Fren found that by controlling the amount of citrate added to the chloroauric acid solution, the size of nanoparticles obtained could be varied. Although monodispersity over 30 nm was poor, this was the first reliable attempt to regulate the size of gold nanoparticles. Fren's paper has been cited 2273 times (as of 19th November 2008), and is among the most cited paper in colloidal science; noted for is simplicity in synthesis of colloidal gold and its potential applications, from other areas of particle science to cell biology.

Slot and Gueze[29] used tannic acid in conjunction with sodium citrate in a modified Turkevich synthesis of gold nanoparticles. The concentration of tannic acid was found to be responsible for the final diameter of the nanoparticles, which can be as small as 3 nm. If the concentration in the final volume of tannic acid was very high, K_2CO_3 was used to neutralise the solution. Tannic acid is a rapid reductant and sodium citrate is a slower reductant. Therefore by modifying the ratio of these two components the desired diameter was obtained.[29] In 1981 they used ascorbic acid as a reducing agent.[30] Whilst using ascorbic acid as a reducing agent, K_2CO_3 was again used to neutralise the solution. This method yielded nanoparticles with a diameter of approximately 12 nm.

Mulvaney and Giersig[11] further developed the Turkevich synthesis by stabilising the gold nanoparticles against aggregation with alkanethiols. They found that the gold sols crystallise in a hexagonal close packed lattice and that the mean particle spacing depends on the thickness of the stabilising layer – the chain length of the stabilising alkanethiol.

The syntheses described so far have all been in aqueous media. The popularity of Turkevich's and related syntheses has been due to their simplicity. The gold ions and stabilising citrate are both soluble in water; therefore reduction can be done in one simple step, usually without the need for additional reagents. Bio-conjugation of gold nanoparticles and DNA or enzymes can be achieved through aurophilic sulphur containing biological compounds such as cystine.

There are some disadvantages to the syntheses of gold nanoparticles carried out in aqueous media. Control over particle size and monodispersity is more difficult in water. The ionic interactions of the particles in water limit the concentration of gold nanoparticles in solution to very dilute levels. Consequently, the nanoparticles can not be removed from aqueous media to form a re-dispersable powder.

Synthesis of gold nanoparticles in organic media has overcome some of the disadvantages presented by aqueous methods. Highly monodisperse gold nanoparticles have been synthesised, with control over particle size. Higher concentrations of gold nanoparticles can be prepared and they can be removed from the solvent and stored in air without aggregation. This was achieved by Brust in 1994.[31]

The Brust-Schiffrin method[31] for gold nanoparticle synthesis takes inspiration from Faraday's original paper.[23] The two phase system they developed uses thiol ligands that strongly bind to gold due to their mutual soft character (Figure 1-5). In Pearson's terms, a gold ion is a soft acid. In general, soft acids have low positive charge and have unshared pairs of electrons in their valence shells. They have high polarisability and low electronegativity (low LUMO). Accordingly thiols (RSH) are soft bases; they have low electronegativity (high HOMO), hence hold their valence electrons loosely and are easy to polarise. Soft acid (low LUMO) and soft base (high HOMO) interactions results in the orbitals being closer in energy which in turn gives a covalent bond.[32]

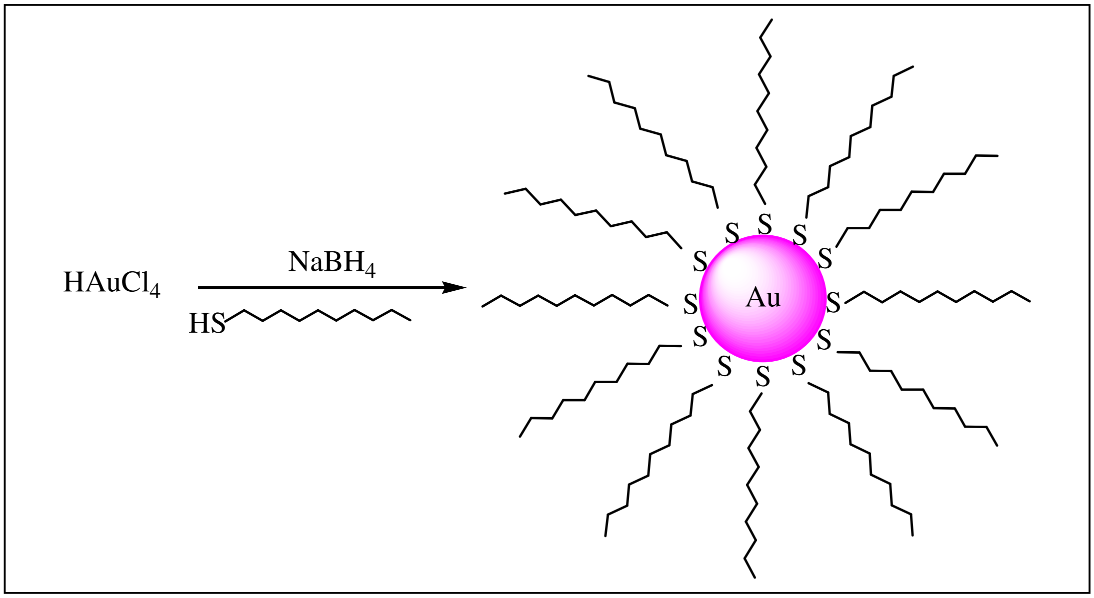

Figure 1-5 ***Schematic representation of the Brust-Schiffrin method of synthesis of thiol capped gold nanoparticles using sodium borohydride as the reducing agent.***

In the Brust-Schiffrin method for the synthesis of thiol capped gold nanoparticles, $AuCl_4^-$ ions were dissolved in an aqueous phase. These were transferred to the organic phase with the aid of a phase transfer reagent, tetraoctylammonium bromide (TOAB). The gold ions were then reduced by sodium borohydride in the presence of dodecanethiol, which capped the nanoparticle. The gold nanoparticles remained in the organic phase, which was indicated by the colour change of the organic phase from colourless through orange to deep brown.

The Brust-Schiffrin synthesis allowed the facile synthesis of thermally stable and air stable gold nanoparticles which had a narrow size distribution. These nanoparticles could be repeatedly isolated and re-dispersed in common organic solvents without irreversible aggregation and decomposition, a highly desirable property which could allow further manipulation.

Brust *et al.*[33] in 1995 used sodium borohydride to reduce a solution of $HAuCl_4$ in a single phase reaction. This reaction was carried out in methanol and the capping thiol was *p*-mercaptophenol. Acetic acid was added to prevent the de-protonation of *p*-mercaptophenol. Sodium borohydride is a very potent reducing agent, hence the reaction was extremely rapid and the particles obtained had a diameter of *ca.* 2 nm.

The nanoparticles synthesised by the Brust method could be handled and modified just as stable organic and molecular compounds. This instigated the investigation into various surfactants and incorporated the use of more bulky ligands.[3] The development of thiol stabilised gold nanoparticles allowed the fuctionalisation of the organic chains of the surfactants. Murray *et al.*[34] described 'place exchange' reactions, where a controlled proportion of thiol molecules around the gold core were exchanged with functionalised thiols, and the subsequent reaction of the functionalised gold nanoparticles.

In addition to the two main synthetic approaches of Turkevich and Brust, many other methods have developed to produce gold nanoparticles. These methods include seeded growth of gold nanoparticles and the use of microemulsions.

Seed mediated synthesis approaches were introduced by Nikoobakht and El-Sayed[35] to grow gold nanorods. Spherical gold nanoparticles have also been grown using this method. Studies have shown that successful control of size can be achieved by modifying the ratio of seed to metal salt.[36] A step–by–step particle enlargement is more successful than a one step seeding method as this avoids secondary nucleation. Brown *et al.*[36] described a synthesis where gold seeds were prepared by borohydride reduction. They improved on this synthetic protocol, by developing a room temperature seeding method of using NH_2OH / Au^{3+} to grow nanoparticles up to 100 nm.[37] This iterative seeding method is consistent and reproducible and can be used to rapidly produce large colloidal gold nanoparticle solutions that exhibit excellent monodispersity. Spherical nanoparticles of 50 nm can be synthesised from 12 nm seeds.[36]

A non-iterative seeding method of producing gold nanoparticles was reported by Sau *et al.*[38] They used photochemically prepared seeds to grow monodisperse highly spherical gold nanoparticles. Seeds were synthesised from chloroauric acid in water by irradiation by UV light from a germicidal lamp in air. Reduction of gold ions was carried out in the presence of a poly(oxyethylene)iso-octylphenyl ether (Triton X-100) which acted as a capping agent and reductant. These seeds could be prepared with average diameters ranging between 5 to 20 nm. The seeds were then grown to diameters of 25-110 nm by varying the ratio of seed to Au^{3+} in the solution and using ascorbic acid as the reductant.

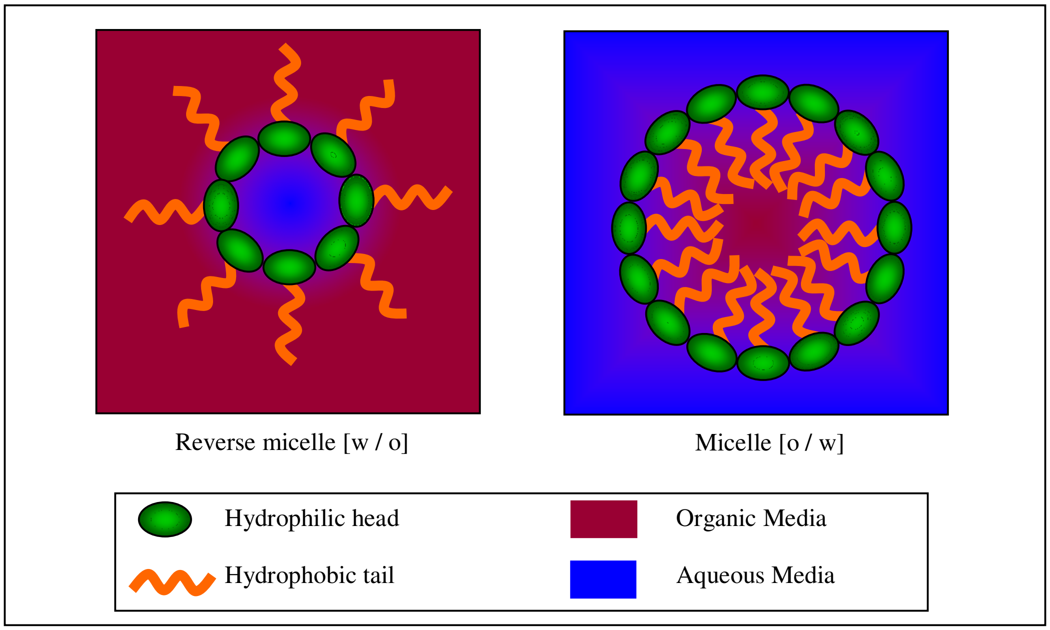

Figure 1-6 ***Representation of reverse micelle, water – in – oil [w/o](left) and normal micelle, oil – in – water [o/w](right) phases. The reverse micelle, water – in – oil [w/o](left), can be used in the synthesis of gold nanoparticles.***

The use of microemulsions, co-polymer micelles and reversed micelles has also been used in the synthesis of gold nanoparticles. Microemulsions are transparent, isotropic, thermodynamically stable dispersions of two immiscible liquids. These liquids are commonly an oil and water, which are stabilised by surfactants. These systems can form normal micellar oil – in – water [o/w] or reverse micellar water – in – oil [w/o] phases (Figure 1-6). An important feature of water – in – oil microemulsions is their ability to solubilise guest molecules such as inorganic precursor salts. In one synthesis of gold nanoparticles, $HAuCl_4$ is dissolved in the aqueous droplets stabilised by cetyl trimethyl ammonium bromide (CTAB), reduced with sodium borohydride, and then removed from the solvent. The water droplets act as microreactors for the nucleation and growth of the particles. The size of the aqueous core of the micelle controls the size of the resulting nanoparticles.[39]

As described above many methods of gold nanoparticle synthesis have been developed using different reducing agents, stabilising agents and solvents. The reducing agent reduces Au(III) to Au(0), and since $HAuCl_4$ is a strong oxidising agent many reducing agents can, and have been used.

One of the main reasons why so many synthetic approaches to the synthesis of gold nanoparticles have been developed is to achieve particles of specific sizes with narrow particle size distributions, and low standard deviations. Narrow size distributions are highly desirable because, the application of mathematical models on physical and optical properties of gold on nanoparticles assumes monodispersity. These models are more accurate if the sizes of the nanoparticles in the sample are identical.

Monodispersity, where all particles are identical in shape and size, is extremely advantageous but rarely achieved. Therefore, monodisperse is a term applied to samples where particles have size distributions with standard deviations less than 15%,[40] and samples with standard deviations less than this are termed highly monodisperse. Particle size distributions are commonly measured using high resolution Transmission Electron Microscopy (TEM) or Scanning Electron Microscopy (SEM) images. More recently, dynamic light scattering equipment has been used to measure particle size distributions in solutions. A major advantage of this technique is the speed at which results and particle size distributions are obtained. However, the results need to be interpreted with caution as the size obtained is often a hydrodynamic radius and not the nanoparticle core size. Therefore, if large organic groups with many charges on the outside are used to coat the gold particles, or due to the nature of the coating many particles are attracted to each other in solution, the total hydrodynamic radius is observed and not the core size.

In order to achieve monodisperse particles the nucleation and growth mechanisms need to be understood and controlled. It is commonly believed that in order to achieve monodisperse particles in the liquid phase, homogeneous precipitation and the separation of nucleation and growth phases is required. In homogeneous precipitation a single burst of nucleation occurs when the concentration of the constituent species reaches a critical supersaturation. The nuclei obtained are allowed to grow by the diffusion of solutes from the solution to the surface until a stable final size is achieved. This is heterogeneous growth of surface reactions which leads to the addition of atoms to the nucleated particle, increasing its size. When this heterogeneous step is slower and uniform the resultant particles are monodisperse. This model was first proposed by LaMer *et al.*[41] deduced from their work on particles of sulphur. Their conclusions have since been applied to the nucleation and growth of any solid particles from the liquid phase.

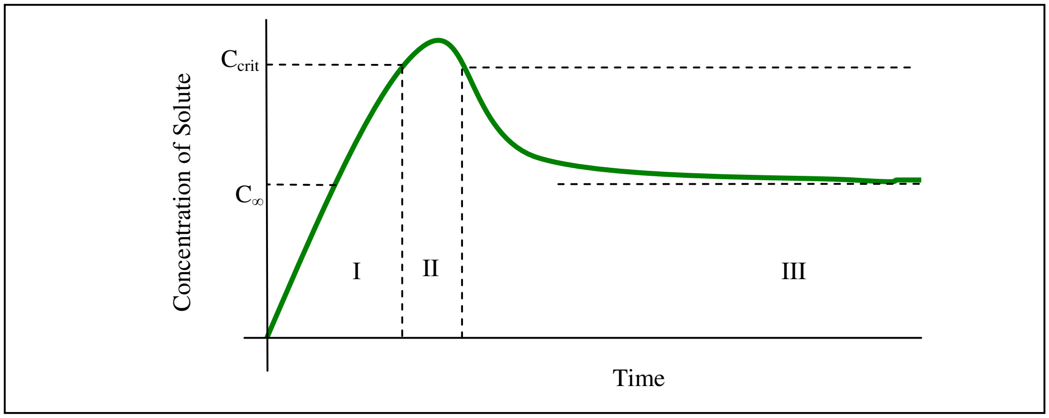

Figure 1-7 ***LaMer diagram as a schematic explanation for the formation process of monodisperse particles, where C_∞ and C_{crit} are the equilibrium concentration of solute with the bulk solid and the critical concentration as the minimum concentration for nucleation, respectively. The regions I, II, and III represent the prenucleation, nucleation, and growth stages, respectively***

LaMer's model is shown in Figure 1-7, where the concentration of the precursor solute, C, increases to the critical level for nucleation (I), C_{crit}. At this concentration there is a balance between the supply rate of the precursor solute, and the consumption rate for the nucleation and the growth of the generated nuclei (II). There is an increase in the consumption of the solute needed for the growth of the generated nuclei the nucleation ends (II) as solute concentration reaches C_{crit} again. The concentration of the solute continues to decrease resulting from the growth of the generated stable nuclei, under the supersaturation level, which is below the critical level for nucleation with out renucleation (III). The final number of the monodisperse particles are determined by the nucleation stage and kept constant through the growth stage.

A problem with LaMer's model when applied to the formation of gold sols using Turkevitch's method is that the particles growing homogeneously and spontaneously from solution need to achieve a critical size before growth is energetically favourable. Below this size the particles spontaneously dissolve. Different materials at various reaction conditions predictably have different critical sizes and for gold it is thought to be a cluster of 20 atoms.[28] LaMer explained the spontaneous formation of particles greater than its critical size by statistical fluctuations.[41] However, Turkevitch believed the formation of colloidal gold was through a mechanism of chelation of multidente agents that produced clusters of un-reacted gold.[28] These loosely bound clusters of polymeric gold / reducing agent grows to a critical size which results in the rapid reduction to form an Au(0) nucleus.

Monodisperse uniform particles have also been obtained from multiple nucleation events. The uniformity of the final particles can be explained by self-sharpening or Ostwald ripening (Figure 1-8). Ostwald ripening involves atoms from one particle dissolving and transferring to another. This is a dynamic process where both particles exchange atoms, but the rate of loss from smaller particles is higher. This is because atoms in smaller particles have lower average coordination numbers at the surface which facilitates ease of removal. The process is driven by a reduction in surface energy. This results in the larger particles growing at the expense of the smaller particles, which shrink and eventually disappear.[42]

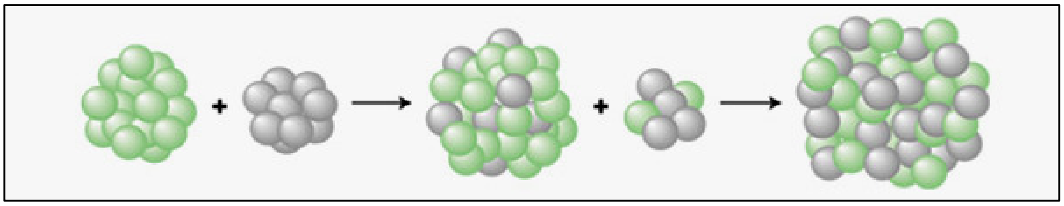

Figure 1-8 ***Schematic representation of Ostwald ripening of nanoparticles. This is a dynamic process which occurs by evaporation, recombination of atoms from one cluster to another.***

Nucleation and growth of Turkevitch's particles may be the result of a multifaceted mechanism where more than one process is involved. It was found by Chow and Zukoski that the number of nuclei continues to increase even at the very final stages of the precipitation reaction.[43] They postulated two mechanisms for the increasing concentration of nuclei over the course of the reaction.

1. Nuclei continuously form and grow over the course of the reaction
2. Particles nucleate in small bursts and agglomerate weakly. They continue to grow within agglomerates, and as the reaction proceeds the agglomerates fall apart, giving rise to the continual increase in the number density of nuclei.

Their investigation concluded that the synthesis of gold nanoparticles in Turkevitch inspired reactions proceed through a mechanism which involves the formation of large particles that shrink with time over the course of the reaction. This conclusion was arrived at by monitoring the shift in wavelength of the maximum absorption λ_{max} which is associated with the surface plasmon. The λ_{max} initially lies near 590 nm giving a purple appearance to the solution. Over the course of the reaction, λ_{max} shifts towards 525 nm where it remains constant and corresponds to a red colour. They correlated this to the loss of Au(III) in solution, indicating that the large particles must contain Au(0), in the reaction medium.[43]

In essence, modification of LaMer's model is needed, which allows the inclusion of nuclei particles being able to reversibly aggregate. These larger particles then fall apart as the reaction proceeds resulting in uniform sols. Aggregation of particles is an energetically favourable process, as the surface of a material is a region of high energy. Since nanoparticles have a high surface–to–bulk ratio, aggregation of these particles becomes highly energetically favourable. Aggregation can continue after the exhaustion of the solution phase constituents of the particles, by the particles themselves coalescing. When the particles collide they can merge and form a larger particle, increasing stability. Smaller particles are more likely to be consumed by larger particles because of their extremely high surface to bulk ratio. This process can lead to the loss of all of the small particles, resulting in the loss of properties associated with the nanoscale, with a fine metallic powder being deposited. Therefore a key aspect of the synthesis is the role of stabilising agents to prevent agglomeration.

For gold nanoparticles there are two main types of stabilising agents, ionic and non-ionic. Ionic stabilising agents include the citrate anion, which stabilise Turkevitch's sols. Citrate anions are attracted electrostatically to the gold particle surface.[44] Here the reducing agent is also the stabilising agent. These particles are said to be charge stabilised. Non-ionic stabilising agents include amines[45] and thiols.[31] These can form chemical bonds to the surface of the gold particles. This is certainly the case for thiols, sulphur is extremely aurophilic in nature due to their soft character. Additionally, gold and sulphur have electronegativity values (χ) of 2.54 and 2.58 Pauling units respectively,[46] which confirm their mutually strong covalent character. These particles are said to be ligand stabilised. Both charge stabilised and ligand stabilised particles prevent agglomeration by providing a physical barrier between particles.

Ligand stabilised nanoparticles can undergo further surface modification.[47] This can aid solubility in whichever polar or non-polar solvent is desired. Surfactants having hydrophilic and lipophilic natures are chosen for this purpose. For example, long chain thiols have been chosen so the particles could be dispersed in organic solvents[33] where as shorter thiols containing polar groups have been chosen for re-dispersion in aqueous media.[48] Dispersion in aqueous media is necessary for the use of gold nanoparticles in biological systems.

1.8 Biocompatible Nanoparticles

Biocompatibility of gold nanoparticles has become highly desirable for application of nanoparticles in biology.[7] The term biocompatibility refers to the materials ability to perform its function, usually medical, without exertion of undesired local or systemic effects. Nanoparticles are now extensively studied because of their size dependant chemical and physical properties; these properties have been commercially explored. Gold nanoparticles have found applications in a number of biological fields including;

- Fluorescent biological labels[49]

- Drug and Gene delivery[50,51]
- Bio-detection [52,53]
- Detections of Proteins[48,54]
- Probing DNA structures[55]
- Tissue engineering[56]
- Tumour destruction by heating (photothermal therapy, hyperthermia)[57,58]
- Separation and purification of biological molecules and cells[59,60]
- MRI contrast agents[61,62]

Nanoparticles exist in the same size domain as proteins which make them perfect for tagging and labelling. Individual DNA strains are 2.5 nm wide and proteins are 1-20 nm in diameter.[63] However, the size is just one of the many characteristics that nanoparticles need to possess in order for them to be successful biological moieties. In order for gold nanoparticles to effectively interact with a biological target, a biological molecular coating or a layer which can act as a bio-inorganic interface needs to be attached. This bio-inorganic interface could be composed of antibodies,[64] biopolymers (collagen[56]), or a monolayer of small peptide based molecules to make the nanoparticle biocompatible (thiols,[31] amines[45]). There are two strategic approaches to making gold nanoparticles biocompatible; functionalisation of the ligand before assembly onto the nanoparticle, and functionalisation of assembled nanoparticles.

1.9 Ligand Protected and Functionalised Gold Nanoparticles

Faraday reported the first comprehensive study on gold nanoparticles.[23] The gold nanoparticles synthesised by him were all synthesised in aqueous media. The synthesis of gold nanoparticles in non-polar organic media is relatively recent, which was sparked by Brust *et al*.[31] with a synthesis previously described in this chapter. The synthesis involved the transfer of chloroaurate ions in to the organic phase using a phase transfer reagent such as tetraoctylammonium bromide (TOAB). The gold ions are then reduced using sodium borohydride to yield monodisperse thiol capped gold nanoparticles. Usually this renders the gold nanoparticles hydrophobic, and only soluble in organic media. These surfactant stabilised gold nanoparticles behave like new compounds which can be easily separated out of solution in the form of a microfine powder and re-dissolved in a different organic media without significant variation in particle size distribution.[31]

The Brust method has since inspired a plethora of gold nanoparticle syntheses using alkane thiols,[65] dialkylsulphides,[66,67] alkylamines[45] and thiolated cyclodextrins[68] as stabilising ligands. Adding functionality to the protecting ligand, for example a carboxylic acid group to the terminal end of a thiol, results in the modification of the chemical and physical properties of the gold nanoparticles. This dramatically increases the potential applications of these nanoparticles especially in the biological field. Another method of adding functionality to gold nanoparticles is by using a simple place exchange strategy (Figure 1-9) described by Murray *et al.*[34] Alkanethiolate protected gold nanoparticles could be functionalised with another thiolate according to equation 1-5, where x and m are the numbers of new and original ligands, respectively.

$$x(\mathrm{R'SH}) + (\mathrm{RS})_m\mathrm{Au} \longrightarrow x(\mathrm{RSH}) + (\mathrm{R'S})_x(\mathrm{RS})_{m-x}\mathrm{Au} \qquad \textbf{1-5}$$

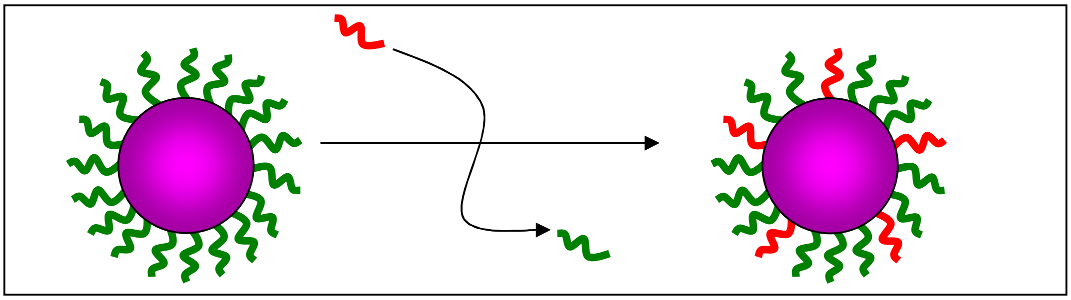

Figure 1-9 ***Schematic illustration of place exchange reactions where one thiol is replaced by another on a gold nanoparticle surface.***

There are a number of interactions that are involved in place exchange reactions, which include gold-thiol interactions; incoming thiol bound thiolate interactions, and incoming thiol-surface monolayer interactions. A complete understanding of place exchange reactions is still to be achieved, although it is generally thought to follow an associative mechanism, where the incoming thiol attaches to the surface and the bound thiol leaves the gold in a simultaneous process. A gold nanoparticle is rarely a perfect sphere and is usually in-homogeneous. Place exchange reactions are thought to initiate on the surface where the monolayer packing is less dense, such as edges and vertices of gold nanoparticles and diffuse into the rest of the particle until an equilibrium is reached.[69]

Hong *et al.*[70] demonstrated that a primary thiol is more active than its corresponding secondary and tertiary thiols for place exchange reactions. This implies that steric hindrance near the thiol group significantly reduced its reactivity in place exchange reactions. Conversely, it was found that bulky groups exhibited higher activity to place exchange than linear thiols of the same molecular weight. This enhanced reactivity was rationalised by considering that place exchange reactions are thought to start predominantly at the vertices of the nanoparticle, where the monolayer is least dense. These sites can therefore open–up enough to accommodate branched bulky ligands. Once these bulkier ligands are attached they may pack better, and therefore aid the exchange. The branched thiol occupies additional space on the particle surface and therefore destabilises the surrounding thiols more efficiently.[70]

Place exchange reactions can be used to introduce polar terminal functional groups such as carboxylic acid, ammonium ions, sulphonic acid *etc*. to the unbound end of a ligand on the nanoparticle surface. One way to exploit this added functionality to the unbound end of a ligand is to perform further chemistry and attach a light activated antimicrobial agent (LAAA), for use in antibacterial photodynamic therapy.

1.10 Photodynamic Therapy

This thesis reports on the coupling light activated antimicrobial (LAA) agents with gold nanoparticles to provide new materials that display enhanced antimicrobial properties. Light activated antimicrobial (LAA) agents can be used in photodynamic therapy. Photodynamic therapy (PDT) combines light and light sensitive agents (such as porphyrins) in an oxygen-rich environment. These absorb photons of energy from light and transfer this energy to surrounding oxygen molecules. Toxic oxygen species, such as singlet oxygen and free radicals are formed. These species are very reactive and can damage bacteria proteins, lipids, nucleic acids and other cellular components.[71]

The history of PDT goes back to the attempts of ancient Egyptians to treat skin diseases with light-absorbing compounds.[72] Ancient Egyptians applied vegetable substances to produce photoreactions in tissues for the treatment of de-pigmented skin lesions (vitiligo). These lesions used to be regarded as manifestations of leprosy. Egyptians utilised natural photosensitisers such as psoralens, which were in many plants such as parsnip, parsley, and Saint-John's-wort. Egyptians made a powder of these plants and applied it to de-pigmented skin lesions and then exposed the skin to bright sunlight. The sun activated the applied photosensitisers, resulting in the lesions becoming less pigmented.[73] The Hindus of India in *ca.* 1400 BC also treated the skin psoriasis using dyes in combination with sunlight.[72]

PDT has been applied to skin cancer patients and the results obtained have opened up new prospects for PDT.[71] In Europe the potential of photosensitisers was first realised by Raab in 1898.[73] He was studying the effects of light and dyes such as acrydine on paramecia, unicellular ciliate protozoa. He noted that an acrydine solution killed paramecia when irradiated with light, and no such effect was observed in the absence of light. Raab and Tappeiner hypothesised that fluorescing dyes convert the energy of light into an active chemical energy which kill paramecia.[72]

At around the same time as Raab’s observations the French neurologist Prime, was treating epileptic patients with the dye eosin.[73] He reported on photosensitive reactions occurring in sun-exposed areas in a patient who had been administered eosin for epilepsy. On the basis of this new knowledge about photodynamic effects, H. Tappeiner and H. Jesionek, performed the first PDT session on a patient with skin carcinoma, where a topical application of eosin was used as a photosensitiser and white light to treat the tumour. This was the first application of PDT to treat cancer. In 1904 Tappeiner and Jodlbauer demonstrated that oxygen was integral to photosensitisation reactions.[72-74] From these origins photodynamic therapy has been increasingly adopted through-out the clinical world.

Currently photodynamic therapy has successfully been used to treat cancer of the bladder using the photosensitiser Photofrin®.[75] Other cancers approved to be treated by PDT include bronchial,[76] and skin cancers.[77] Clinical trials are currently being conducted on the treatment of prostate cancer.[78] PDT in the past decade has been used for the treatment of age-related macular degeneration (AMD). This is the leading cause of blindness in the elderly in the Western world. Treatment involves the intravenous injection of the photosensitiser Visudyne® and has been used in over two million cases to date.[79]

Work on the lethal photosensitisation of bacteria began in the early 1960's. Macmillan *et al.*[80] used toluidine blue as a photosensitiser to kill bacteria, algae and yeast. They found 99% kills were obtained for most of the bacteria tested, after 30 min of exposure to a gas laser (21-30 mW). A few years later Bellin *et al.*[81] suggested that the photosensitiser, toluidine blue acts on the cell membrane. Additionally, they studied the effects of other thiazine dyes such a methylene blue. A range of dyes were investigated, including rose bengal, erythrosine B, eosine Y, neutral red, acridine orange, crystal violet, pyrorine Y, and rhodamine 6G. They concluded that cationic dyes act as photosensitisers at an alkaline pH, and anionic dyes act as photosensitisers at a pH slightly lower than their pK_a. Furthermore, they demonstrated the presence of oxygen was required for the successful kill of bacteria.

Antimicrobial PDT produces bactericidal and bacteriostatic effects on bacteria due to the generation of singlet oxygen and peroxide radicals. These substances are generated by extracellular and intracellular photosensitisers. Their action brings about a chain of phototoxic reactions. Schneider *et al.*[82] investigated antimicrobial PDT with methylene-blue dye. Irradiation was performed using a wideband white light source, which produced radiation at wavelengths of 400 to 700 nm. It was found that such antimicrobial PDT inactivated bacteria RNA in *vitro*. The RNA was cross-linked to plasmatic proteins. In some cases, oxidant stress inhibited the growth of bacterial cultures in *vitro*.

Antimicrobial PDT usually requires the involvement of an external photosensitiser. After absorbing light of certain energy, the photosensitiser may undergo electronic transition from its ground state to an excited singlet state (electron spins paired). Depending on the molecular structure of the photosensitiser and its environment the molecule may lose energy by being quenched by other surrounding molecules, thus returning to the ground state (Type I). The other pathway available is to undergo intersystem crossing, to a triplet excited state, where the electron spins are unpaired (Type II). At this point the photosensitiser can lose its energy: by quenching from surrounding molecules and electronic decay back to the ground state, from undergoing redox reactions with the surrounding environment, or the excitational energy maybe transferred to molecular oxygen where singlet oxygen is generated (Figure 1-10).[83]

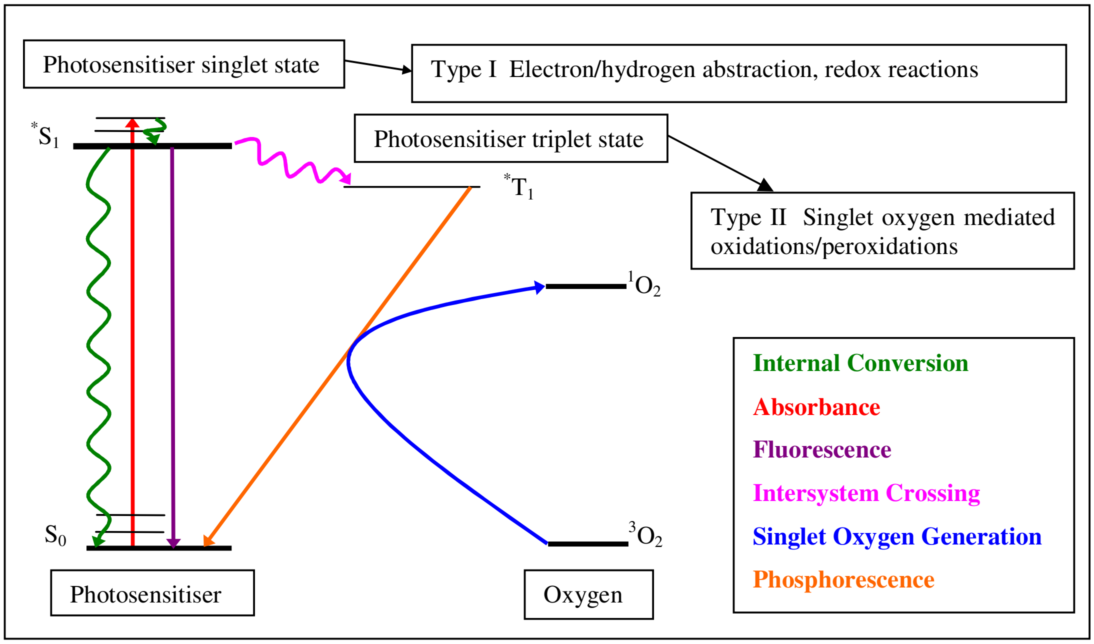

Figure 1-10 ***Simplified energy level diagram of a photosensitiser, displaying key energy transitions in the formation of singlet oxygen and consequent Type I and Type II processes.***

Type I reactions can cause photo-damage by hydrogen or electron abstraction by the photosensitiser. Subsequent redox reactions and oxygenation products depend on the proximity of the photosensitiser and the bacteria. In aqueous media type I reactions can produce hydroxyl radicals which can also react with biomolecules on the surface of the bacteria, or combine together to give hydrogen peroxide that subsequently has cytotoxic effects. On the bacterial cytoplasmic membrane, abstraction of allylic hydrogens from unsaturated molecules such as phospholipids also occurs.[84] The radical species which is produced reacts with oxygen to yield lipid hydroperoxide, which is detrimental to membrane integrity. This leads to the loss of fluidity and increased ion permeability. Other targets of type I reactions include aminolipids and peptides, hence inactivation of membrane enzymes and receptors is also possible.[85]

Type II reactions involve the formation of singlet oxygen. The short half-life of singlet oxygen ensures that there is a localised response. This singlet oxygen formed reacts rapidly with the environment; cell wall, nucleic acids, peptides *etc*. General belief is that the singlet oxygen produced in a Type II process is the major pathway which is responsible for the photo-oxidative microbial cell damage.[86] Analogous to type I reactions singlet oxygen also reacts with the cell wall and the cell wall components.[84] In particular, type II reaction pathways are thought to interfere with the amino acids histidine, tryptophan, and methionine, and to DNA bases (largely guanine). It has been difficult to obtain direct spectroscopic evidence for the involvement of singlet oxygen in photodynamic therapy.[83] Experiments have shown the emission of singlet oxygen from porphyrins adsorbed onto cell surfaces,[87] but these experiments have proved difficult to reproduce, because of the rapid reaction of singlet oxygen. Additionally some protection from photodynamic therapy has been displayed in the presence of singlet oxygen scavengers.[86,88,89]

Photosensitisers are usually aromatic molecules which are efficient in the formation of long lived triplet excited states. Long lived triplet states increase the probability of efficient singlet–oxygen production. Photosensitisers with an affinity for microbial cells and a broad spectrum of action, as well as being able to damage to the host tissue and prevent re-growth of the pathogens after the treatment, are also required. Membrane photosensitisation can lead to a decrease in plasma membrane potential, inhibition of molecular transport across the membrane and the inhibition and activation of membrane associated enzymes. Cellular response to membrane photosensitisation includes apoptosis.[74]

The sites of photosensitiser action and the effects of lethal photosensitisation are dependant on the photosensitiser used and the target bacteria. For example, toluidine blue when used against *Escherichia coli* (gram negative bacteria) is known to be membrane active and increase permeability.[84] Methylene blue, which belongs to the same family of thiazine dyes, affects the same organism's nucleic acid and causes strand breaks.[84] However, methylene blue affects *Proteus mirabilis* in a different way and causes photodamage to the cell envelope and enhanced cell lysis, as well as DNA photo-damage.[84]

The field of antimicrobial photodynamic therapy is rapidly expanding and benefiting from new technology and research. More effective photosensitisers are being developed, and unusual materials such as fullerenes are now being considered.[90] Research is being conducted on the targeting of photosensitisers which exhibit higher selectivity of microbial cells, reducing the collateral damage.[91]

Current applications of antimicrobial photodynamic therapy include the treatment of periodontal diseases.[92] Periodontal diseases are characterised by the severe inflammation of the gums and are a result of chronic infections caused by a mixture of Gram-positive and Gram-negative biofilm infections. These infections can eventually lead to tooth loss. Current treatment involves the removal of the biofilm mechanically, often in laborious and unpleasant procedures. Wilson *et al.*[93] have made pioneering advances in the treatment of periodontal disease using PDT. In *vitro* studies have shown that several pathogens were successfully eradicated by photodynamic therapy, both in aqueous suspensions and in biofilms. In *vivo* studies have displayed toluidine blue photosensitiser mediated photodynamic therapy, selective killing of *P. gingivalis* in the oral cavity with significant decrease in the level of bone loss in rats affected by periodontitis.[92] Early commercial application of their work is currently being tested out in Canada. Treatment method entails the deposition of photosensitiser in the appropriate place and irradiation by laser delivered by a fibre optic dentist tool. The treatment is over in a few minutes and has considerable advantages over treatment with antibiotics and antiseptics, which have problems associated with selectivity and resistance.

Antibacterial photodynamic therapy has been used in the treatment of Acne Vulgaris. The condition is caused by the proliferation of bacteria such as *P. acnes* and *P. granulosum.* These bacteria are known to produce large amounts of porphyrins, and can be inactivated when irradiated with high intensity light. It has been shown that efficient inactivation can be achieved with blue light irradiation, and that blue light therapy results in a significant decrease in the progression of acne lesions.[94]

Wounds can often be infected by bacteria, and such contamination normally leads to extended healing times and prolonged hospitalisation. Usually the bacterial infection in wounds is treated with antibiotics, and would therefore be subject to resistance and selectivity. In such cases photodynamic therapy would be an ideal treatment with its broad spectrum of action against bacterial infection by the appropriate choice of photosensitiser. Hamblin *et al.* have performed clinical experiment and have shown eradication of *S. aureus* in burn wound infections.[95]

Oral Candidiasis (oral thrush) is caused by a fungal infection, which is also susceptible to photodynamic inactivation. Topical application of methylene blue on the tongues of rats has shown the complete eradication of these microbes when irradiated by red light. Applying photosensitiser directly on infected areas minimises collateral damage.[96] This is particularly beneficial for patients with deficient immune responses such as HIV sufferers as less burden is placed on the immune system.

The expansion of applications of antimicrobial photodynamic therapy is a relatively recent development considering photodynamic therapy has been used to treat cancer since 1900. There are two main factors which have contributed to this. The first of these factors are that some prolific pathogens, especially specific kinds of gram negative bacteria and protozoa are poorly responsive to traditional photosensitisers such as acridine which have been used to treat carcinomas.[74] However, new research has developed photosensitisers which are specific in the killing of such microbes.[91,97] The second factor has been the development of antibiotics. The discovery of effective antibiotics gave the impression that microbe infection would be gradually reduced to a level which would not harm human health. The widespread use and the rapid emergence of microbes resistant to antibiotics have raised the interest in light activated antimicrobial therapy. Antibiotic abuse, with excessive prescription, inclusion in feed for live stock, frequent transmission of microbes by global travelling, poverty leading to depressed immune systems and microbes having their own internal mechanisms for development have all contributed to bacterial antibiotic resistance. Photodynamic therapy is becoming an increasingly important tool to help combat these problems and provide an alternative treatment method.[74]

There are many advantages that light activated antimicrobial therapy can provide. One photosensitiser can have a broad spectrum of action and can act on multiple bacteria strains.[84] The efficacy of the photosensitiser is independent of antibiotic resistance developed by any particular microbial strain and the probability of the onset of mutagenicity, and resistance is low.[98] Photosensitisers can be topically applied which can lead to extensive reduction in pathogen population with limited damage to the host tissue, and this has been improved upon by targeting with biological recognition peptides which increases specificity.[8,83,88]

1.11 Thesis Structure

This thesis reports on coupling LAA agents with gold nanoparticles to provide new nano bio-materials that displayed enhanced antimicrobial properties. The gold nanoparticle forms the central core of the nano-biomaterial. Organic molecules can be adsorbed onto the surface or they can be chemically attached. In this thesis both approaches have been investigated. Charge stabilised gold nanoparticles have been investigated with a wide variety of photosensitisers. The charge stabilised nanoparticles were synthesised by a modified Turkevich synthesis and it was found that association of some photosensitisers to gold nanoparticles enhanced the lethal photosensitisation of bacteria. Additionally alkane thiol protected nanoparticles have been synthesised, where light activated antimicrobial agents have been chemically attached to the monolayer (Figure 1-11).

The monolayer protected nanoparticles that were synthesised in this project had some strict regulations which needed to be adhered to. The central material needed to be gold based on some evidence which suggested that gold enhanced the antibacterial effect of photodynamic therapy agents.[99] The monolayer performed two functions; providing stability against aggregation in solvents and air and allowing solubility in aqueous media by having polar groups in the alkane chain. All microbiology experiments were carried out in aqueous media as potential final applications in biological systems would also require aqueous solubility.

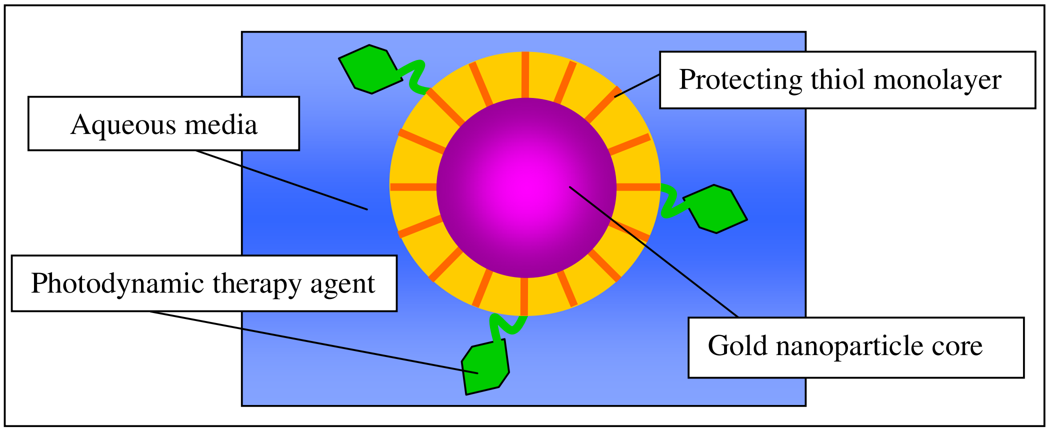

Figure 1-11 ***Schematic representation of ligand stabilised gold nanoparticles synthesised, with attached photodynamic therapy agent***

The next two chapters describe the synthesis and antibacterial properties of two novel light activated antimicrobials with motifs gold-thiol-photosensitiser. The first of these are gold nanoparticles with a tiopronin monolayer that has the photosensitiser toluidine blue attached (gold-tiopronin-toluidine blue), and the second are gold nanoparticles with a gluthathione monolayer that has the photosensitiser tin chlorin e6 attached (gold-glutathione-tin chlorin e6).

Chapter 2 Toluidine blue–Tiopronin–Gold Nanoparticles

This chapter describes the functionalisation of tiopronin monolayer coated nanoparticles in aqueous media with toluidine blue.[100] *The tiopronin coated nanoparticles were prepared in organic media, isolated and purified. The terminal carboxylic acid group on the tiopronin was utilised as a handle to tether a toluidine blue molecule via a condensation reaction forming an amide bond in aqueous media. This is the first application of a covalently linked photodynamic therapy agent to a gold nanoparticle, to function as a light activated antimicrobial (LAAA).*[84,93,101,102] *Unexpectedly, the gold–tiopronin–toluidine blue conjugate displayed, significantly enhanced antimicrobial activity, the minimum bacterial concentration (MBC) being at least 4 fold lower than that of free TBO.*

2.1 Introduction

Gold nanoparticles have well characterised physical properties, which have subsequently been exploited, such as coatings on glass to produce a desired hue.[103] An unusual property of gold nanoparticles is that they can act as an anchor for light activated antimicrobial agents (LAAA), which consequently increases its potency. This increase in potency is a result of the close proximity between the gold nanoparticle and LAAA molecule.

Organothiolate monolayer protected nanoparticles have attracted a lot of interest recently because there is greater synthetic control over particle size, dispersity, and surface functionality. Concequently, size dependant optical, catalytic and capacitance properties are easily tuned. Additionally, the stability of the thioalkane protected nanoparticles to air, allows long term storage and their solubility in solvents with temperature and concentration extremes increases.

A typical thiol, $HS(CH_2)_nX$, where n denotes chain length and X denotes a functional group allows the versatility needed for bio-application of organothiolate protected gold nanoparticles. Chain length and chemical identity of the terminal functional group can be modified by changing n and X respectively. This can be achieved by appropriate choice of thiol, ligand exchange and chemical modification by reaction with an appropriate terminal group on the thiol.

There are many attributes of organothiolate protected nanoparticles. They are relatively simple to prepare, handle and functionalise, just like stable organic and molecular species.[31] Additionally, depending on and the nature of $HS(CH_2)_nX$, the capped nanoparticles can be isolated and re-suspended in a variety of polar and non polar solvents. These properties of organothiolate protected gold nanoparticles make them attractive moieties in biological chemistry. Applications include; biosensors for binding reactions with cluster functionalised receptors,[104] and biolistics[105] where DNA is attached to the organothiolate protected gold nanoparticles and accelerated through plant cells leaving the DNA behind in the cell.

Nanoparticles for use in biological systems need to adhere to some requirements which result from the physiological environment they would be used in. The surface layer of these nanoparticles can be modified for increased aqueous stability, biocompatibility, and biorecognition.[106]

The standard synthetic method for the production of organothiolate protected gold nanoparticles involves extraction of tetrachloroaurate (III), $[AuCl_4]^-$, from aqueous media to organic media followed by the addition of a thiol, $HS(CH_2)_nX$. This mechanism is thought to follow a saturation – nucleation – growth process.[31] The first step produces gold (I) thiolate polymer or oligomer $(-AuS(CH_2)_nX-)_m$ through sacrificial reduction of the thiol. This polymer is then reduced by the addition of aqueous $NaBH_4$, yielding gold nanoparticles coated in organothiolates.[107] Factors which affect the size of the gold nanoparticles obtained include the $HS(CH_2)_nX$: $[AuCl_4]^-$ ratio, temperature and rate of reductant addition.[108] In general smaller particles are favoured by low temperatures, increased rates of reductant addition and high thiol:gold ratios.[31] Templeton *et al.*[109] developed a single phase synthesis to produce tiopronin coated nanoparticles which were soluble in water.

Tiopronin can be used as a drug preventing kidney stone formation in patients. It is a chelating agent and removes the surplus cystine from the urine.[110] It is also used in the treatment of Wilson's disease, which is a result of an overload of copper in the body.[111] Tiopronin has also displayed therapeutic effects in the treatment of certain types of arthritis, though it is not an anti-inflammatory.[112]

For the purposes of this study, tiopronin has been used to coat gold nanoparticles. One of the main advantages of using tiopronin is that tiopronin facilitates the solubility of the nanoparticles in water. The solubility arises from the introduction of polar groups between the thiol group and the terminal carboxylic acid (Figure 2-1). Another advantage of these particles is that they can be isolated and re-suspended repeatedly.

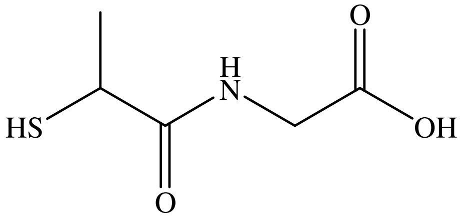

Figure 2-1 ***The structure of tiopronin***

Tiopronin (N-(2-mercaptopropionyl)glycine) (Figure 2-1) monolayer protected gold nanoparticles are air stable over many months and can be re-suspended in aqueous media. Crucially, tiopronin has a free terminal $-CO_2H$ group which provides a tether for further manipulation. One such manipulation has been attaching a chromophore to a tether.[113] The optoelectronic properties of the gold nanoparticle can be tailored by organising chromophores of specific properties and function onto the surface of the gold, and can yield photoresponsive organic–inorganic nanohybrid materials. This nanoparticle–thiol–chromophore moiety of a packed organic photoresponsive shell encapsulating a metal nanoparticle core offers exciting opportunities for the design of novel photon based devices with applications in sensing, switching and drug delivery along with photodynamic therapy.

Toluidine blue is a basic dye, which is used as an antimicrobial agent and nuclear stain.[114] It metachromatically stains certain structures such as granules in mast cells and

RNA in electrophoresis. It also antagonises the anticoagulant action of heparin.[114] Light activated antimicrobials such as toluidine blue (TBO) have the ability to kill a wide range of bacteria including methicillin-resistant *Staphylococcus aureus* (MRSA).[90] These light activated antimicrobial agents operate by producing free radicals and reactive oxygen species when irradiated by white light or a laser of the appropriate wavelength. Toluidine blue is membrane active as it increases permeability, resulting in nucleic acid photo damage.[115] Unlike antibiotics which usually have a single target to operate, LAAA are indiscriminate in their mode of action, and have many targets. This minimises the development of resistance to LAAA therapy. Additionally it has been shown that increasing the proximity of the surface of gold nanoparticles to the photodynamic therapy agent results in increased cell death.[99]

The rest of this chapter describes the synthesis of tiopronin-gold nanoparticles, and the further functionalisation of these particles to form TBO-tiopronin-gold nanoparticles. These particles were characterised and their efficacy tested as light activated antimicrobials.

2.2 Experimental

Chemicals: $HAuCl_4 \cdot 3H_2O$ (99.99%), N-(2-mercaptopropionyl)glycine (tiopronin, 99%) and sodium borohydride (99%) were purchased from Aldrich. TBO (90%) was purchased from Acros Organics. Buffers were prepared according to standard laboratory procedure. All other chemicals were reagent grade and used as received.

Synthesis of tiopronin–gold nanoparticles: Tiopronin–gold nanoparticles were prepared by modification of previously reported methodology.[109] Tetrachloroauric acid (0.62 g, 1.57 mmol) and of *N*-(2-mercaptopropionyl)glycine (tiopronin, 0.77 g, 4.72 mmol) were dissolved in of ethanol (60 mL) with acetic acid (10 mL). This resulted in a ruby red solution. $NaBH_4$ (1.21 g, 32 mmol) in distilled water (30 ml) was added dropwise with rapid stirring. The temperature of the solution immediately increased from (room temperature) to 44 °C and turned black. The solution returned to room temperature after approximately 15 min. The pH of the solution increased from 1.2 to

5.1. After cooling to room temperature the black suspension was stirred for an additional 30 minutes, and the solvent then removed under vacuum at ≤ 40 °C.

The reaction crude was completely insoluble in methanol but relatively soluble in water. It was purified by dialysis. The crude product was dissolved in 80 ml of water and the pH was adjusted to 1 by addition of concentrated HCl. This solution was loaded into a 20 cm segment of cellulose ester dialysis membrane (Spectra/Por CE, molecular weight cut-off (MWCO) = 12000), and placed in a 4 L beaker distilled water. This was stirred slowly, recharging with fresh water every 12 h over the course of 72 h. The dark tiopronin–gold nanoparticles solution was collected from the dialysis tube, and the solvent was removed by freeze-drying. Elemental analysis of the dialysed tiopronin-gold nanoparticles gave the following. Anal. found: C, 10.70; H, 1.65; N, 2.55; S, 5.73. Calcd. for $C_{425}H_{680}O_{255}N_{85}S_{85}Au_{201}$: C, 9.56; H, 1.28; N, 2.23; O, 7.65; S, 5.11; Au, 74.17%.

Preparation of TBO–tiopronin–gold nanoparticles: In a typical reaction, tiopronin–gold nanoparticles (MW = 53376.38 g mol^{-1}, 100 mg, 1.87 mmol) were dissolved in 30 mL of 50 mM 2-(*N*-morpholino)ethanesulfonic acid (MES) buffer (pH 6.5) and the solution then made up to 0.1 M in 1-[3-(dimethylamino)propyl]-3-ethylcarbodiimide hydrochloride (EDC) and 5.31 mM in *N*-hydroxysulfosuccinimide sodium salt. TBO (61 mg, 0.2 mmol) was added, and the solution was stirred for 24 h. Then, the reaction mixture was dialyzed as described above for 144 h. The dark purple TBO–tiopronin–gold nanoparticle solution was collected from the dialysis tube, and the solvent was removed by freeze-drying. Elemental Analysis found: C, 14.45; H, 1.91; Cl, 0.86; N, 3.35; S, 5.58. Calcd for $C_{656}H_{895.6}Cl_{15.4}O_{239.6}N_{131.2}S_{100.4}Au_{201}$: C, 13.63; H, 1.56; Cl, 0.94; N, 3.18; O, 6.63; S, 5.57; Au, 68.49%. The number of molecules of TBO coupled to each nanoparticle was 15.4. This value was verified by elemental analysis and TGA. The gold nanoparticles were water-soluble. This is accounted for on the basis of the high cationic character of the TBO group.

Thermogravimetric analysis (TGA): Thermogravimetric analysis (TGA) was performed on the NETZSCH STA 449C TGA, equipment. Dry, purified sample (*ca.* 7 mg) was placed in an alumina crucible under a nitrogen flow, with a flow rate of 50 ml min^{-1}. The data was recorded from 25 to 1000 °C at a heating rate of 10 °C min^{-1}. X-Ray diffraction (experiments were measured with a Bruker discover diffractometer using Cu Kα radiation), was used to analyse the residue left in the pan from the TGA experiment.

UV-visible absorption spectra: Spectra were taken between 200–1100 nm, 1 nm resolution of aqueous *ca.* 3.5 mg per 50 ml solutions in 1 cm quartz cells were recorded with a ThermoSpectronic, Heλios-λ UV-visible absorption spectrometer.

Infra-Red spectra: Data were collected for solid tiopronin and TBO–tiopronin–gold nanoparticle samples pressed into a KBr plate. These were recorded from 3800 to 500 cm^{-1} with a Shimadzu 8700 FT-IR spectrometer.

High resolution transmission electron microscopy (HRTEM): Samples were prepared by evaporating the required specimen on a carbon coated copper grid. Bright field TEM images were acquired using with an electron microscope operated at 100 kV (Joel 100CX). Typical magnification of the images was 100 000. Analysis of the images was performed using the software program Image J.[116]

Bactericidal assays: The bacterial assays were carried out at the Eastman Dental Centre by Miss Sarah Tubby. An overnight culture of *Staphylococcus aureus* NCTC 6571 (1 mL, grown aerobically at 37 °C, with shaking, in Nutrient Broth) was centrifuged and the pellet re-suspended in 1 mL phosphate buffered saline (PBS). The optical density at 600 nm was adjusted to 0.05 in PBS, in order to give an inoculum of approximately 10^7–10^8 colony-forming units (cfu) mL^{-1}. The TBO–tiopronin–gold nanoparticle conjugate was suspended in PBS at a concentration of 4.6 mg mL^{-1} (final TBO content approximately 1 mM). The conjugate solution was then diluted in PBS to give final concentrations of 2 μM, 1.0 μM, 0.5 μM and 0.25 μM respectively.

In a 96-well micro-titre plate, 50 μL aliquots of the conjugate were added to 50 μL of the bacterial suspension and a 4 mm diameter magnetic stirrer bar was added to each well. The plate was placed on a magnetic stirrer and triplicate wells were then exposed to either white light or laser light (see below) for various periods of time during which the contents of the wells were stirred to ensure irradiation of all bacteria in each well. Three control wells were not exposed to light to determine the effect on bacterial viability of the conjugate alone. Six additional wells containing the bacterial suspension plus PBS instead of conjugate solution were prepared, three of these were exposed to light to determine the effect of light alone on bacterial viability, while the remaining three were kept in the dark as an overall control and to determine the initial concentration of bacteria in the suspensions. After irradiation or incubation in the dark, samples were serially diluted 1 in 10 to a dilution factor of 10^{-4} and spread in duplicate onto 5% horse blood agar plates. The plates were then incubated aerobically at 37 °C for approximately 48 hours. After incubation, the number of bacteria surviving each treatment was determined and the concentration of survivors expressed as cfu mL^{-1}.

The white light source used in the study was a General Electric 28 W Biax 2D compact fluorescent lamp that emits light across the visible spectrum. Prominent peaks were present at 435, 495, 545, 588 and 610 nm. The light intensity at the surface of the microtitre plates was measured using a digital luxmeter (Hagner Photometric Instruments Ltd., Bosham, United Kingdom) and was found to be 3600 ± 20 lux . The exposure time was varied in different experiments. The laser used was a 35 mW helium neon (HeNe) gas laser (Model 05-LHP-928, Melles Griot, Carlsbad, CA, USA). This delivers light with a wavelength of 632.8 nm in a collimated beam with a diameter of 2.5 mm. A convex lens was used to increase the beam diameter to 6.6 mm so that it matched that of a well of the microtitre plate. A one minute exposure time delivered an energy dose of 2.1 J at an energy density of 6.14 J cm^{-2}.

Experiments were also carried out to determine the effect of a TBO-free gold–tiopronin conjugate on the viability of *S. aureus* in the presence and absence of TBO. Using a similar experimental protocol to that described above, various concentrations of the gold–tiopronin conjugate were exposed to white light (35 minutes) or 633 nm laser light (1, 2 or 5 minutes) in the absence or presence of TBO. The survivors were enumerated by viable counting as described above. All of the experiments described above were carried out on two separate occasions using different overnight cultures of *S. aureus*.

2.3 Results

The tiopronin-gold nanoparticles were synthesised by a previously reported reaction.[109,117] Hydrogen tetrachloroaurate was dissolved in acidified methanol and reduced by an aqueous solution of sodium borohydride, at room temperature (Figure 2-2).

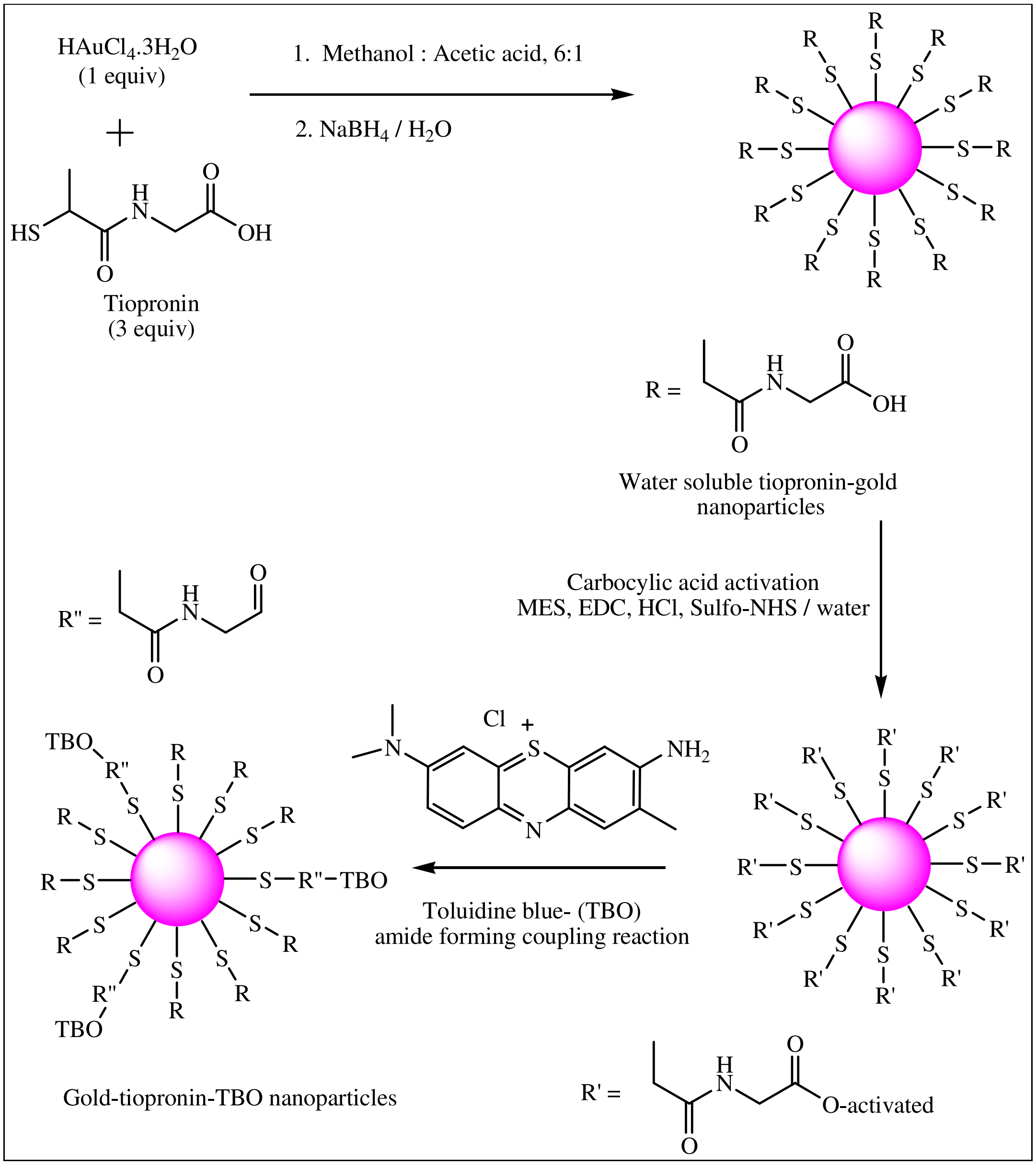

Figure 2-2 ***Synthesis of gold-tiopronin-toluidine blue nanoparticles in a two stage synthesis. The first stage is the synthesis of gold-tiopronin nanoparticles from auric acid and tiopronin in acidified methanol. The second stage is the attachment of toluidine blue to the gold-tiopronin nanoparticles.***

The tetrachloroaurate (III), $[AuCl_4]^-$ ions were soluble in acidified methanol and therefore did not require extraction from aqueous to organic media by a phase transfer agent. The acidity is essential for the reaction to yield stable monodisperse nanoparticles. This suggests that the emerging nanoparticles coated in tiopronin are unstable when the tiopronin is de-protonated in methanol. The gold–tiopronin nanoparticles formed are insoluble in methanol, but soluble in water. Once isolated and purified they have the consistency of a finely divided black powder which can be re-dissolved in water and stored indefinitely in air. The first step in the reaction also yielded undesired, water soluble by-products (NaCl, disulfide, NaOAc, HOAC), which were removed by dialysis, along with un-reacted starting reagents. Dialysis has proven to be an excellent method of removing by-products and un-reacted reagents.

The next step in the reaction involves the coupling of a toluidine blue molecule to the carboxylic acid end of the tiopronin, by forming an amide linkage *via* a condensation reaction. This process was done in the presence of the sodium salt of *N*-hydroxy sulfossuccinimide (sulfo-NHS) and 1-[3-(dimethyl amino)propyl]-3-ethyl-carbodiimide hydrochloride (EDC). Sulfo-NHS was used to convert the carboxylic acid group on the tiopronin to an amine reactive sulfo-NHS ester. This process is catalysed by EDC which behaves as a dehydrating carbodiimide. EDC is not an effective dehydrating and crosslinking molecule by itself, because failure to react quickly with the amine will result in the hydrolysis and regeneration of the carboxylic acid (Figure 2-3).

EDC reacted with the carboxylic acid group of the tiopronin, forming an amine reactive *O*-acylisourea intermediate. This intermediate may react with the amine on toluidine blue yielding a conjugate of the two molecules joined by a stable amide bond. However, this conjugate is also susceptible to hydrolysis making it unstable and short lived in aqueous solutions. The addition of sulfo-NHS stabilises the amine reactive intermediate by converting it to an amine reactive sulfo-NHS-ester. This increases the efficiency of EDC mediated coupling reactions. The amine reactive sulfo-NHS ester intermediate has sufficient stability to permit a two step crosslinking reaction.[100,118]

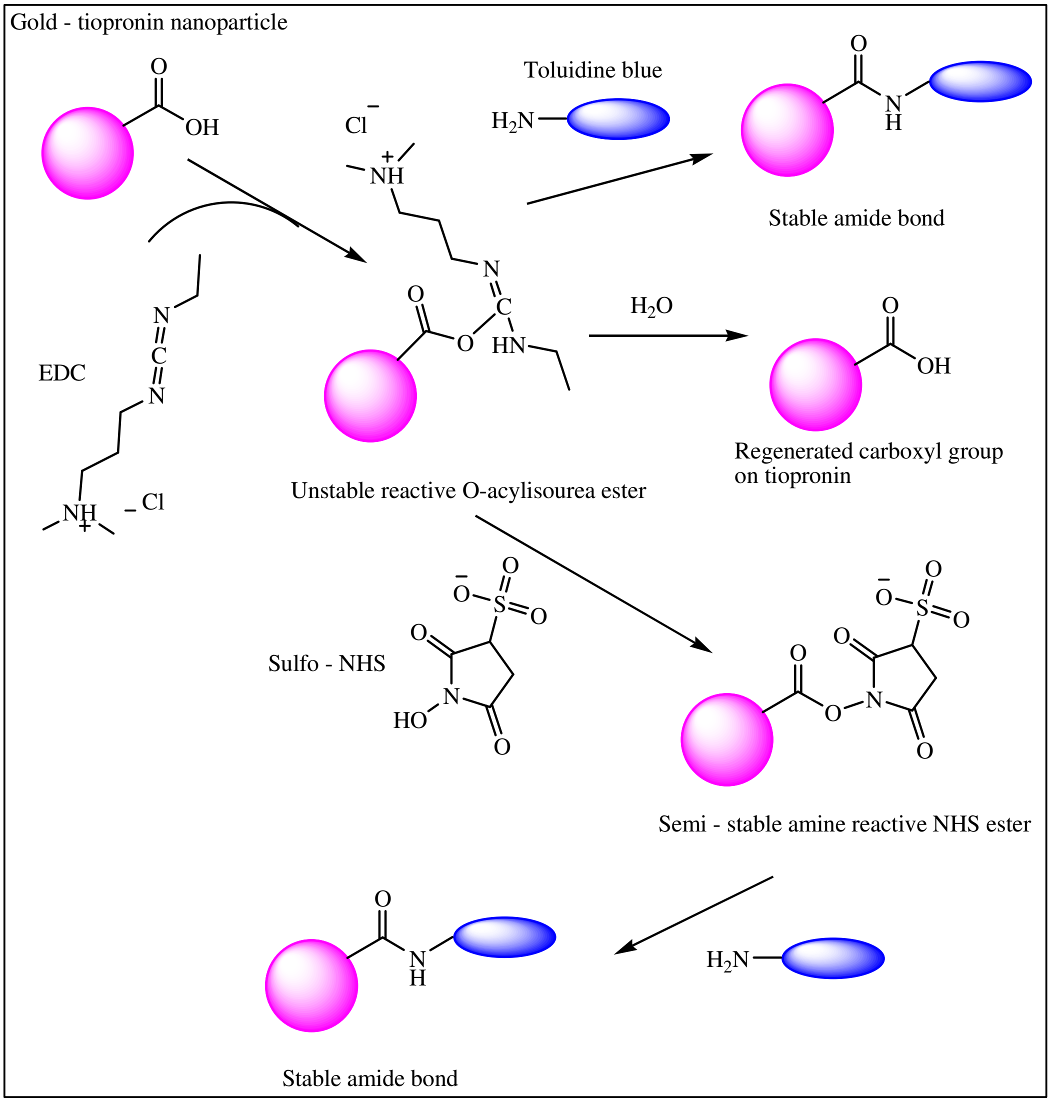

Figure 2-3 ***Routes possible when coupling TBO to tiopronin–gold nanoparticles***

The coupling reaction between tiopronin and toluidine blue required a ratio of 1.1 : 1 (mole ratio of amines on TBO to tiopronin–gold nanoparticle carboxylic acid groups) and produced clusters that contained on average 11 TBO sites per gold nanoparticle. Varying this procedure by modifying the TBO concentration so that the ratio between TBO and tiopronin gold nanoparticles was 1.5 : 1, conjugates with an average of 15.4 TBO molecules per gold nanoparticle were synthesised. TBO–tiopronin–gold nanoparticles with an average of 15.4 TBO per nanoparticle were insoluble in water, but soluble in phosphate buffer (pH = 7.01), whereas the particles with 11 TBO sites per gold nanoparticle were water-soluble. This is accounted for on the basis of the high cationic character of the TBO group.

The TBO–tiopronin–gold nanoparticle conjugate produces an intense black colour when isolated as a solid. However a blue-violet colour was observed when crushed with KBr for the IR experiments. The conjugated TBO–tiopronin–gold nanoparticles are air stable as a solid. They can be easily re-suspended and showed the same characteristics and functional properties after 9 months. In solution, the conjugated nanoparticles were stable for at least six months in water or PBS solution.

In general the UV-visible absorption spectra of gold nanoparticles are dependant on the particle size. Particles less than 2-3 nm in diameter do not exhibit surface plasmon resonance absorption. The UV-visible absorption spectrum of the tiopronin–gold nanoparticles was also dependent on the core size (Figure 2-4). The UV absorbance profile of the nanoparticles decayed almost exponentially into the visible. There was no detectable surface plasmon band in the visible region which indicates that the diameter of the gold nanoparticles was less than *ca.* 3 nm across. There were no identifiable features in the UV-visible absorbance profile of the tiopronin–gold nanoparticles.

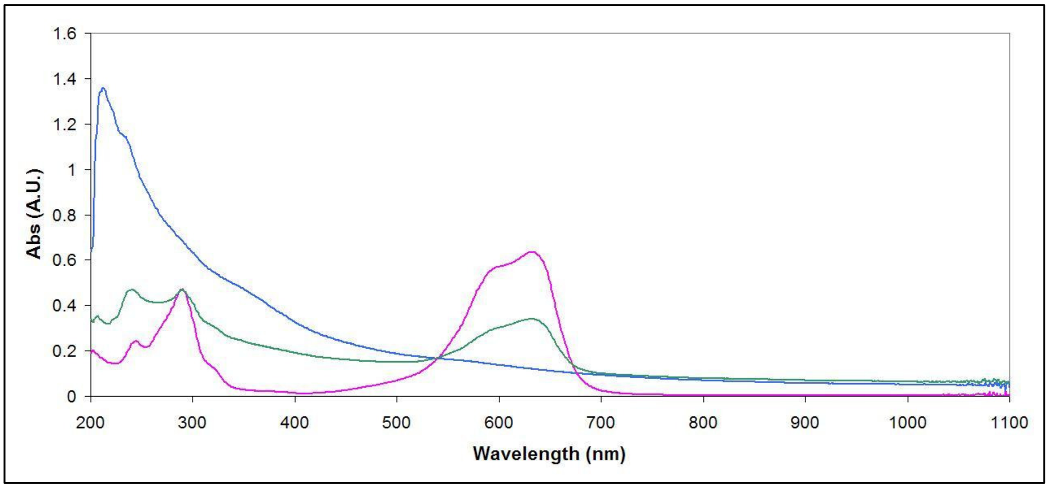

Figure 2-4 ***UV-visible spectra (in phosphate buffer, pH 7.01) of: (Blue) tiopronin–gold nanoparticles, 1.9 µM; (Green) TBO–tiopronin–gold nanoparticles, 1.2 µM; (Pink) TBO, 20 µM***

The absorbance profile of free toluidine blue and tiopronin-gold bound toluidine blue are very similar (Figure 2-4). Both exhibit a maximum absorbance at 633 nm. A band at 245 nm is significantly weaker in the bound toluidine blue spectrum. This may be due to that particular wavelength of lights absorption being reduced by being bound. Additionally the molar extinction coefficient in phosphate buffer for TBO–tiopronin–gold nanoparticles is significantly higher ($\varepsilon = 5.2\times10^{5}$ l mol^{-1} cm^{-1}; $\lambda = 633$ nm) than of the corresponding one for TBO ($\varepsilon = 2.8\times10^{4}$ l mol^{-1} cm^{-1}; $\lambda = 633$ nm).

The thermal decomposition of tiopronin–gold nanoparticles occurred in two steps; a well-defined step that began at approximately 90 °C and was completed by 450 °C, and a second step from 600 °C to 1000 °C (Figure 2-5). The percentage weight losses for the organic fragments were 23.49% for tiopronin–gold nanoparticles. These values combined with the C, H, N, S and Cl microanalytical results for the clusters give molecular formulae of $C_{425}H_{680}O_{255}N_{85}S_{85}Au_{201}$ for the tiopronin–gold nanoparticles. These formulae indicate that each gold nanoparticle has coordinated on average 85 tiopronin molecules.

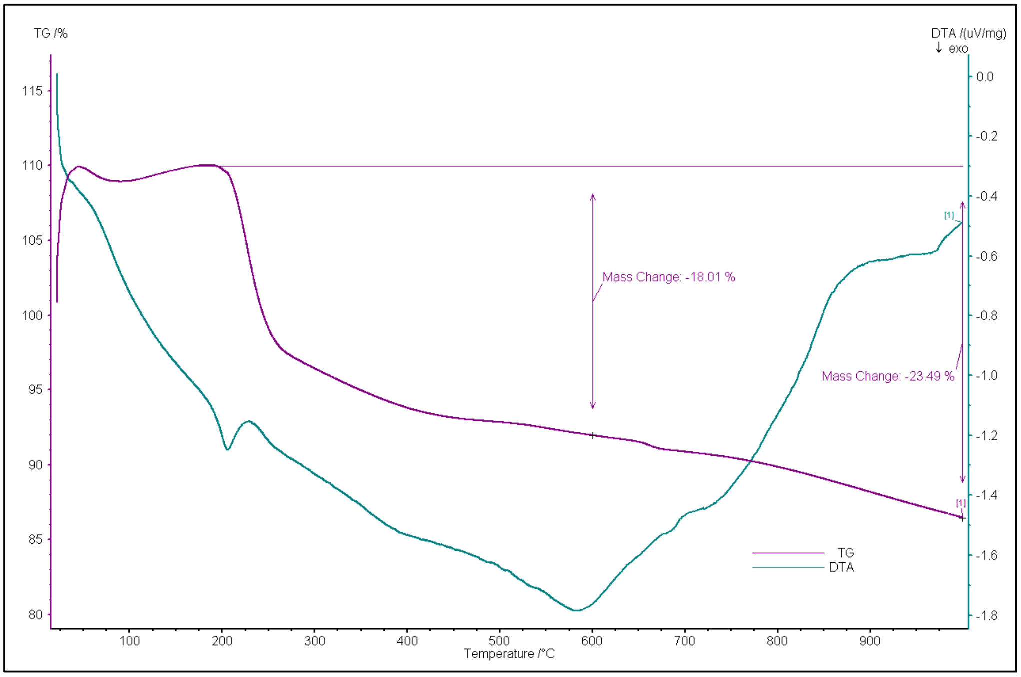

Figure 2-5 ***Thermal Gravimetric Analysis (TGA) of tiopronin–gold nanoparticles synthesised by reaction of auric acid and tiopronin in acidified methanol.***

Thermal gravimetric analysis of the TBO–tiopronin–gold nanoparticles occurred in two steps; a well-defined step that began at ~200 °C and was completed by 450 °C, and a second step from 600 °C to 1000 °C (Figure 2-6). The percentage weight losses for the organic fragments were 24.21% for the TBO–tiopronin–gold nanoparticles. These values combined with the C, H, N, S and Cl microanalytical results for the clusters give molecular formulae $C_{656}H_{895.6}Cl_{15.4}O_{239.6}N_{131.2}S_{100.4}Au_{201}$ for the TBO–tiopronin–gold nanoparticles (15.4 TBO per cluster unit). On reaction with TBO either 15.4 or 11 TBO molecules (depending on the two concentrations of the TBO used) are covalently bonded to the tiopronin and hence directly connected to the gold nanoparticle.

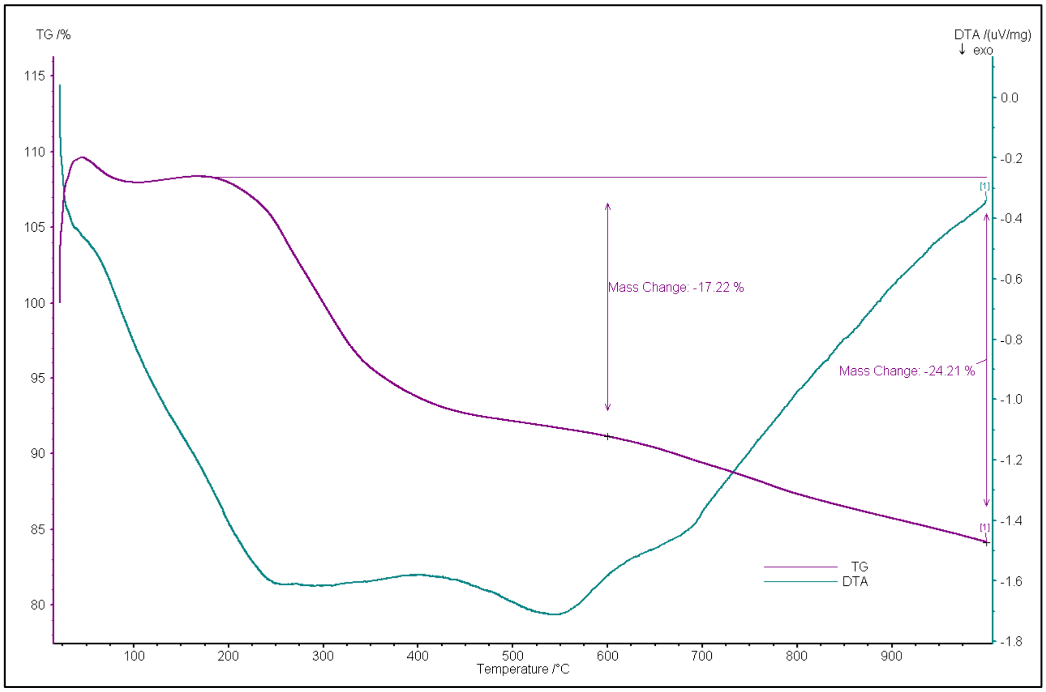

Figure 2-6 ***Thermal Gravimetric Analysis (TGA) of toluidine blue–tiopronin–gold nanoparticles, synthesised by the coupling of toluidine blue to tiopronin-gold nanoparticles.***

The residue from the TGA experiments was shown by X-ray powder diffraction to be highly crystalline gold metal (Figure 2-7). In both TBO–tiopronin–gold and tiopronin–gold nanoparticles, this residue was found to be elemental gold, which is consistent with previous TGA work on alkanethiolate–gold nanoparticles.[119]

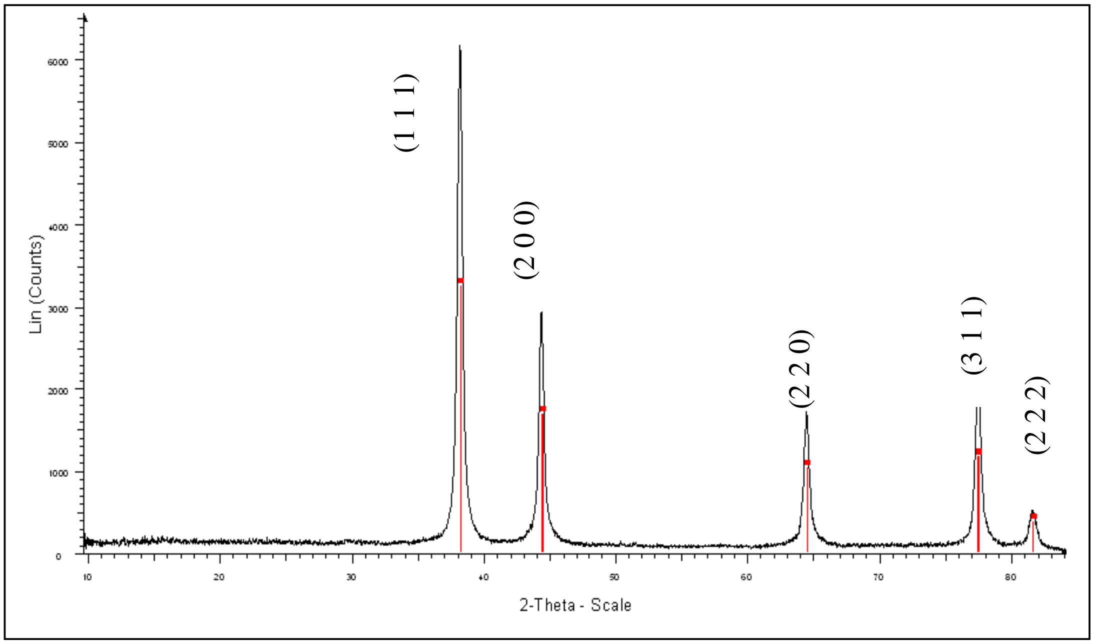

Figure 2-7 ***XRD of the residue left in the pan after TGA confirms presence of elemental gold. The pattern is indexed and shows the expected stick pattern (red) for gold metal.***

High-resolution transmission electron microscopy of the TBO–tiopronin-gold nanoparticles showed particles that are spherical in shape and of uniform size with average core dimensions of 1.8–2.0 nm (Figure 2-8).

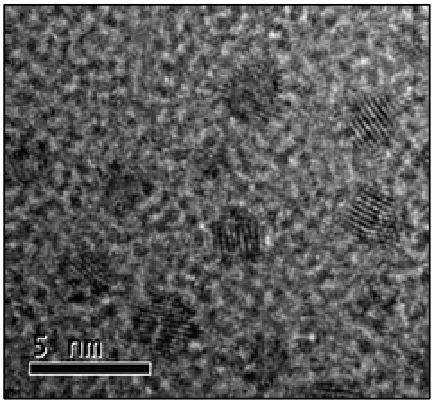

Figure 2-8 ***High Resolution Transmission Electron Microscopy (HRTEM) image of TBO–tiopronin-gold nanoparticles***

The HRTEM image illustrates the highly crystalline nature of the gold core. Additionally, the distance between the lattice fringes was measured to be 2.42 Å from the HRTEM image. The interplanar distances measured on the HRTEM images are in good agreement with that of bulk gold (111) plane, which is 2.355 Å. Furthermore, each nanoparticle has a single gold domain. The gold particles are seen to be separated on the TEM and this is further evidence of the presence of coordinating tiopronin and TBO–tiopronin groups.

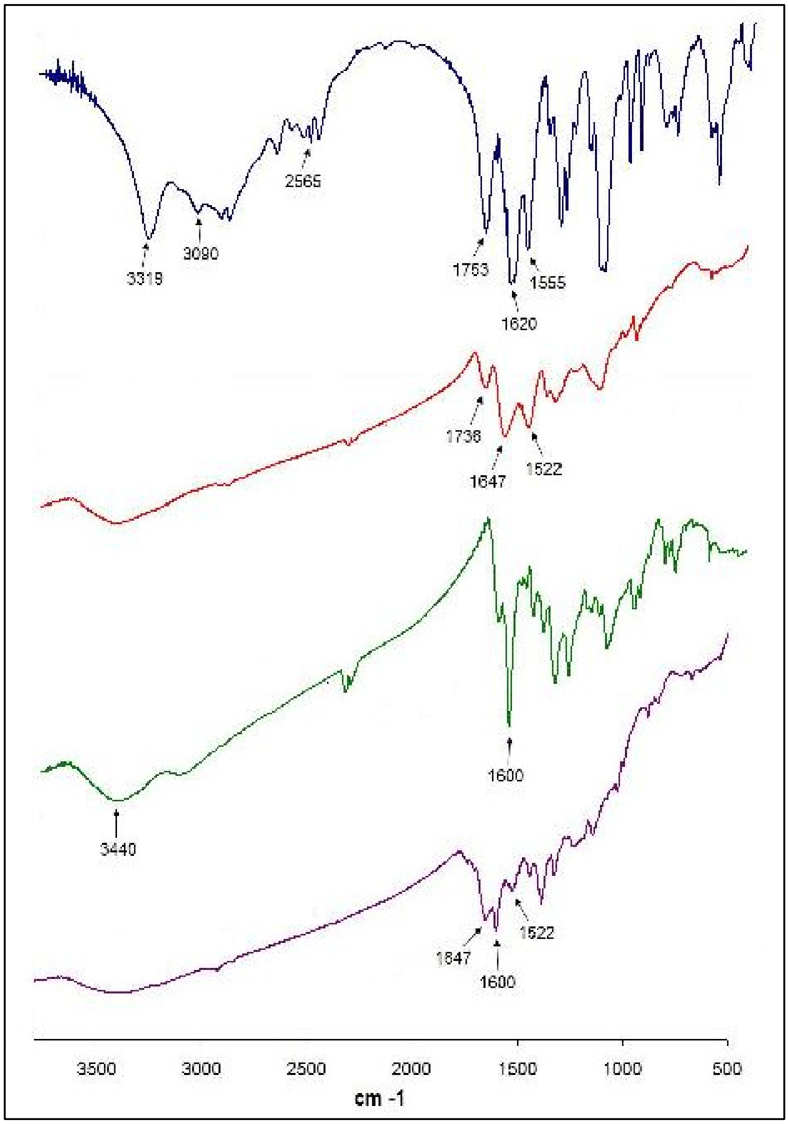

Figure 2-9 ***Transmission Infra-red spectra of: (Blue) tiopronin, (Red) tiopronin–gold nanoparticles, (Green) TBO and (Purple) TBO–tiopronin–gold nanoparticles. All spectra were acquired in the form of KBr plates, and intensities of the bands are uncorrected for sample quantity.***

Infra-red spectroscopy of the gold–tiopronin nanoparticle showed that the bands for the tiopronin group are readily seen (Figure 2-9). The S–H vibration band of free tiopronin is observed at 2565 cm^{-1}. This band is absent in the infra red spectrum of gold–tiopronin and gold–tiopronin–toluidine blue nanoparticles indicating that the sulphur has been de-protonated and coordinated to the gold nanoparticle surface. The N–H vibration has moved to a slightly lower frequency indicating a change in hydrogen bonding.

The bands due to the aromatic rings at ~1600 cm^{-1} from the TBO monomer, is present on the TBO–tiopronin–gold nanoparticles infra-red spectra. Additionally the N–H stretching band of the TBO monomer attributed to the primary amine at ~3440 cm^{-1} is absent from the TBO–tiopronin–gold nanoparticles IR spectrum. This is evidence for the conversion of the primary amine to amide. Analysis of the IR spectra provides some evidence for interparticle hydrogen bonding for both the gold–tiopronin and gold–tiopronin–TBO nanoparticles.

The characterisation data confirm the successful formation of both gold–tiopronin and covalently linked gold–tiopronin–TBO nanoparticles. Taking into account all the characterisation data, a calculated number of TBO molecules per gold nanoparticle was obtained. This has been crucial in the microbiology because a direct comparison of the antimicrobial properties of the gold–tiopronin–TBO nanoparticles with free TBO could be made.

The antimicrobial activity of the TBO–tiopronin–gold conjugate when exposed to white light or to 632.8 nm light from a HeNe laser was assessed using *S. aureus* in aqueous suspension. An extensive series of controls was used to determine the antimicrobial activity of TBO, TBO-tiopronin-gold and tiopronin-gold nanoparticles.

To ensure that the bacterial suspension of *S. aureus* NCTC 6571 did not have any endogenous photosensitisers activated by either 632.8 nm laser light or white light, 50 µl of the bacterial suspension was added to 50 µl of PBS, and irradiated with 632.8 nm laser light for one minute or with white light for 30 minutes (Figure 2-10 & Figure

2-11). In neither case was the viability of the *S. aureus* suspension affected and it was ascertained that the organism could not be killed at these light energy doses in the absence of an exogenous photosensitiser. In order to have successfully synthesised a light activated antimicrobial, controls on the tiopronin–gold and TBO–tiopronin–gold nanoparticles in the dark were also performed.

In the absence of white light, the TBO–tiopronin–gold nanoparticles exhibited no antibacterial activity at any of the concentrations tested. However, the viable count of *S. aureus* on irradiation with white light for 30 min reduced depending on the concentration. The highest kill of approximately 5.5 $\log_{10}$ was observed at a concentration of 2.0 µM. Substantial kills were also observed at concentrations as low as 0.5 µM. The TBO–tiopronin–gold nanoparticles killed more effectively at a concentration of 1.0 µM than free TBO, which only had significant kills at double the concentration of 2.0 µM (Figure 2-10).

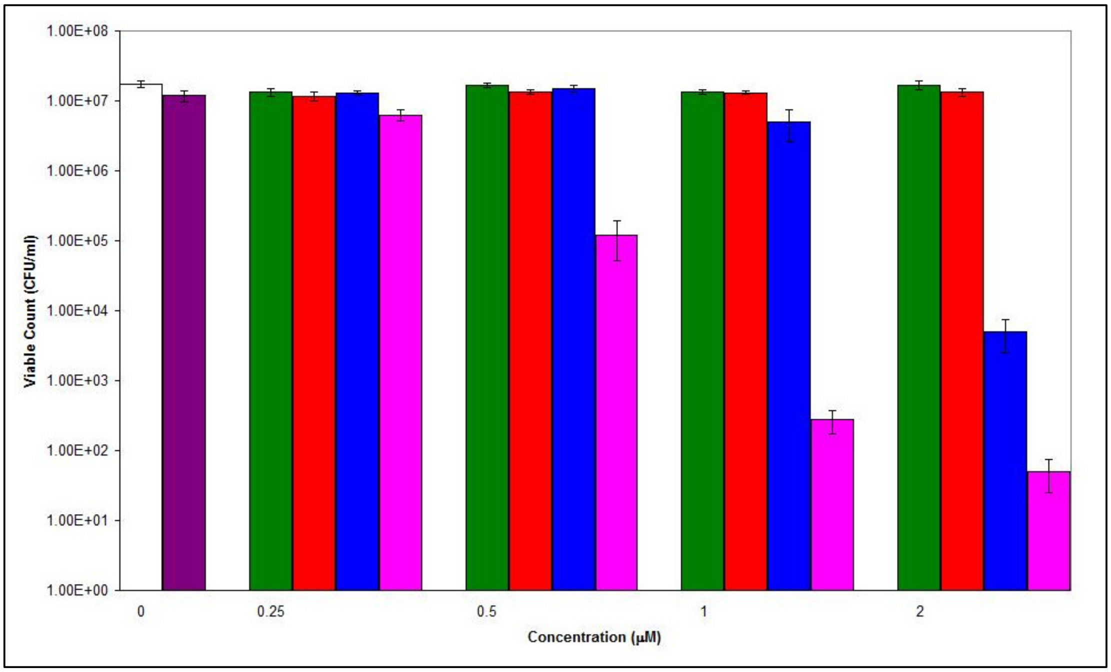

Figure 2-10 ***Effect of TBO (Blue) and the TBO–tiopronin–gold nanoparticle conjugate (Pink) on viability of S. aureus 6571 following exposure to white light for 30 minutes, or incubation in the dark with TBO (Green) or the TBO–tiopronin–gold nanoparticle conjugate (Red). The white bar denotes the viable count of the original bacterial suspension, and the purple bar represents the viable count of the bacterial suspension after exposure to white light.***

Additionally it was observed that the kills achieved by the TBO–tiopronin–gold nanoparticles were light dose dependent. As exposure time was increased from 15 to 45 minutes, lethal photosensitisation of the bacteria was more effective (Figure 2-11).

To ensure that the action of light on the toluidine blue was the mechanism of killing the bacteria, experiments were carried out using either (TBO free) tiopronin–gold nanoparticles (Figure 2-12) or a mixture of tiopronin–gold nanoparticles with un-conjugated TBO (Figure 2-13). Positively, no significant reduction of *S. aureus* at any of the concentrations tested (0.4–40.5 μM), were observed on exposure to white light for the tiopronin–gold nanoparticles. Additionally mixtures of various ratios of the tiopronin–gold nanoparticles and a sub-optimal concentration of TBO did not result in killing of the *S. aureus* on irradiation with white light.

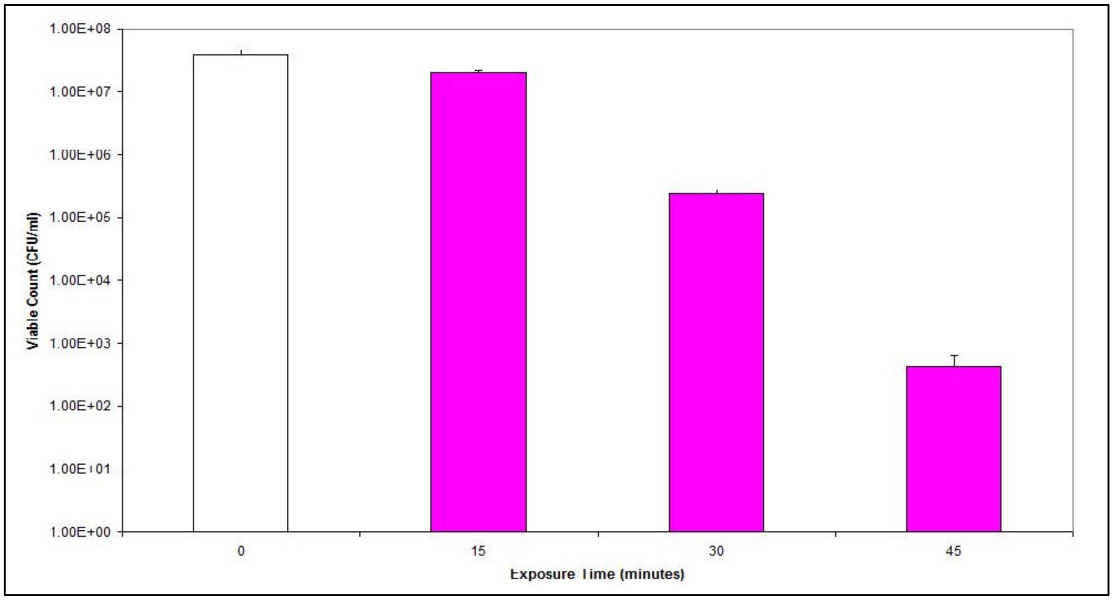

Figure 2-11 ***Effect of white light dose on the killing of S. aureus by the gold–tiopronin–TBO conjugate (concentration = 4 μM). The exposure time was varied from 15 to 45 minutes.***

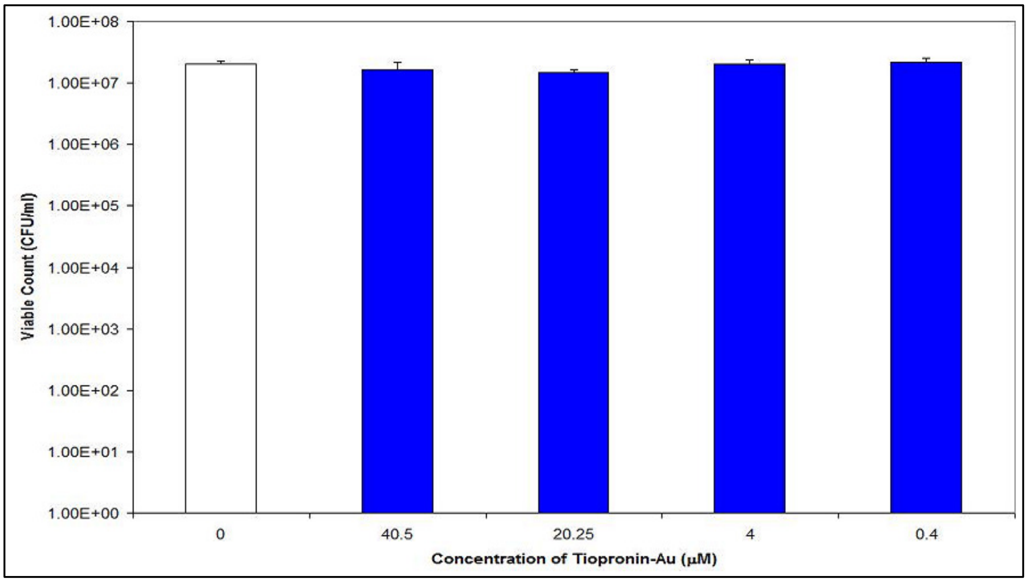

Figure 2-12 *Effect of various concentrations of the gold–tiopronin conjugate on the viability of S. aureus following exposure to white light for 35 minutes. The white bar represents the viable count of the original bacterial suspension.*

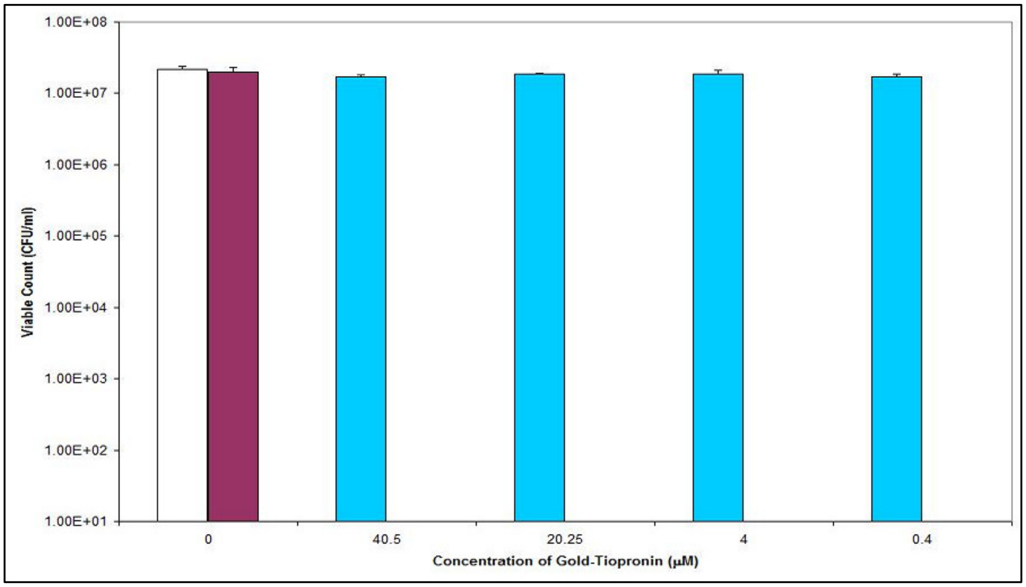

Figure 2-13 *Effect of mixtures of ratios of the gold–tiopronin conjugate and TBO (TBO concentration = 1 µM) (Blue) and TBO alone (Purple) on the viability of S. aureus following irradiation with white light for 35 minutes. The white bar represents the viable count of the original bacterial suspension*

These results provide strong evidence that TBO–tiopronin–gold nanoparticles enhance antimicrobial response using both a laser and a white light source. The most striking result in the kills was observed at 1 μM concentration whilst using white light for 30 minutes. The conjugate showed a reduction in cfu of 4.5 $\log_{10}$ that is a 99.995% kill compared with a 0.5 $\log_{10}$ or 50% kill for TBO of the same concentration. Regardless of the light source used, the kills achieved by the TBO–tiopronin–gold conjugate were two $\log_{10}$ units greater than those found using TBO when each LAAA was used at a concentration of 2.0 μM, the lowest concentration at which TBO displayed any activity.

2.4 Discussion

Gold–tiopronin nanoparticles were synthesised in methanol purified and isolated as a solid. This solid was then further utilised in the second step of the reaction. Gold–tiopronin–TBO nanoparticles were successfully achieved in aqueous solution, purified and isolated as a blue black solid, by attachment of the TBO molecules to gold–tiopronin nanoparticles. The number of TBO molecules groups attached to the gold–tiopronin nanoparticles, could be controlled by the concentration of TBO used. Some control was achieved in the number of TBO groups attached to the gold–tiopronin nanoparticles. In this study 11 and 15.4 toluidine blue molecules per gold nanoparticle were synthesised by using tiopronin-gold : TBO ratios of 1 : 1.1 and 1 : 1.5. The molecular formula of the nanoparticles was obtained from the characterisation data. The TGA and elemental analysis data were in excellent agreement with each other. However these molecular formulae should be used as a weighted average as the TEM size analysis indicated that the gold cores of the nanoparticles were not monodispersed. Although, *ca.* 90% of the gold cores had diameters in the region of 1.8–2 nm, (determined by TEM image analysis) which results in the molecular formula being fairly accurate.

The plasmon resonance band in the UV-visible spectrum, which is usually an excellent indicator for the presence of gold nanoparticles, was not observed for the gold–tiopronin nanoparticles–TBO and gold–tiopronin nanoparticles. This is because there were no gold cores larger than 4 nm, providing additional evidence that synthetic control over particle size was achieved.

Nanoparticles often agglomerate and precipitate when in solution over periods of time. This is thought to be due to the fact that Au(I) atoms with a d^{10} closed shell electronic configuration tend to form aggregates through aurophillic interactions. This relatively strong non covalent Au(I)–Au(I) interactions is attributed to hybridisation between empty 6s/6p shells and filled $5d^{10}$ shells which are stabilised and destabilised, respectively, due to the relativistic effect. Conversely the gold–tiopronin–TBO nanoparticles were stable indefinitely, when suspended in water and phosphate buffer solution, and when kept as a solid in air. The TBO–tiopronin–gold nanoparticles are unusual in having both ligand stabilisation of the gold core, *via* the tiopronin groups, together with charge stabilisation, as the TBO is a cationic dye with one chloride counter ion per molecule. Therefore the TBO–tiopronin–gold nanoparticles are both ligand stabilised and charge stabilised.

This study has shown that covalently linked TBO–tiopronin–gold nanoparticles are very effective LAAAs. They are more active than free TBO, when compared on molar basis. Furthermore, the attachment of TBO molecules to tiopronin–gold nanoparticles is essential for it to function as an antimicrobial. There was no observed enhanced killing for the tiopronin–gold nanoparticles presence of free TBO. This is the first reported instance of covalently linking a photodynamic therapy agent to a gold nanoparticle enhancing the effectiveness of the LAAA.

There is a four fold reduction in inhibitory MBC of the TBO–tiopronin–gold nanoparticles compared to free TBO. Part of the mechanism of this enhanced kill can be explained by the increased extinction coefficient of the TBO–tiopronin–gold nanoparticles (ε = 520371 l mol^{-1} cm^{-1}) compared to free TBO (ε = 28225 l mol^{-1} cm^{-1}). Enhanced extinction coefficients for dyes absorbed on nanoparticulate surfaces have been reported previously. Malicka *et al.*[120] showed that indocyanine green had a 20-fold increase in extinction coefficient when directly bound to nanoscale metallic islands of silver. This was explained in terms of the excited fluorophore interacting with the freely mobile electrons on the metal resulting in increased rates of radiative decay.

Additionally this conjugation procedure results in a directional binding of the dye to the gold nanoparticle, providing a fixed distance for energy transfer.

A comparison of the antimicrobial effectiveness of the TBO–tiopronin–gold conjugate with other photosensitisers is difficult, because of the different types of bacteria and protocols adopted. However the MBC of LAAAs is typically in the range of 1–50 µM. The most effective LAAA against *S. aureus* in terms of the MBC published was 5,10,15,20-tetra(*N*-benzyl-4-pyridyl)porphyrin tetrachloride (TNBPPT) which was effective at 0.63 µM after 1 h of irradiation with a 500 W halogen–tungsten lamp.[121] Notably, no kill was observed after 30 minutes of irradiation. This is unlike these experiments with the TBO–tiopronin–gold nanoparticles MBC was 0.5 µM using 30 minutes of irradiation with a much less powerful lamp (28 W). The energy density necessary to achieve significant kills in the above experiments (6 J cm^{-2} with the HeNe laser) was considerably lower than that required with TNBPPT (133 J cm^{-2}). Therefore the TBO–tiopronin–gold nanoparticle has the lowest MBC necessary to kill *S. aureus* of any LAAA and, taking into account light intensity, it is significantly more effective than TNBPPT.

Close vicinity of chromophores to the gold core alters the excited deactivation pathways of the surface bound molecules. For example, Dulkeith *et al.*[122] observed a distance dependant quenching of the excited states of chromophores on the metal surface. Other studies have shown significant suppression in the quenching of the singlet excited of chromophores when they are densely packed onto a gold surface.[123] There are four possible deactivation pathways of the excited chromophore bound to the gold nanoparticle:

1. Intermolecular interactions
2. Energy transfer
3. Electron transfer
4. Emission from the chromophore

It is possible, by binding a TBO molecule, in manner which results in its close proximity to the gold core surface, there in an enhanced energy transfer. This would give an increased yield in singlet oxygen when light of the appropriate wavelength is applied. The enhanced kill of bacteria which was observed could therefore be explained.

It is thought that the sulphur atom in the aromatic system of the toluidine blue molecule on the TBO–tiopronin–gold nanoparticle could chelate back, and attach itself onto the gold nanoparticle surface. Although this is possible as the sulphur atom would be expected to be exceptionally aurophilic, it was not possible to prove.

It is important that for clinical use, a light-activated, or indeed any, antimicrobial agent is effective at low concentrations. TBO is a potent photodynamic therapy agent, which is effective at killing a wide range of microbes at low light energy doses both *in vitro* and *in vivo*. The TBO–tiopronin–gold nanoparticles increase this antimicrobial efficacy by association to the gold surface. This was the first time that a moiety of gold-thiol-photosensitiser had been applied to the lethal photosensitisation of bacteria. An LAAA of such potency could be useful as a rapidly acting photosensitiser, in the photodynamic therapy of a wide range of topical infections such as wound and burn infections, caries and periodontitis.

2.5 Conclusion

A novel highly effective and potent light activated antimicrobial was synthesised. The conjugation of toluidine blue to tiopronin–gold nanoparticles moiety has proved to be exceptionally effective at killing *Staphylococcus aureus*. TBO–tiopronin–gold nanoparticles killed bacteria using both a 632.8 nm laser light and white light. It was found that these novel LAAAs killed significantly better than free TBO. For example at 1 μM concentration and using white light for 30 minutes, the conjugate showed a reduction in cfu of 4.5 $\log_{10}$ compared with 0.5 $\log_{10}$ for TBO at the same concentration. Regardless of whether white light or laser light was used, the MBC of the conjugate was 0.5 μM compared to 2 μM for TBO. The superior performance of the conjugate was attributed to the enhanced extinction coefficient of TBO–tiopronin–gold nanoparticles, a result of the association to the gold core surface, when compared to free TBO. In terms of their MBCs, the covalently linked TBO–tiopronin–gold nanoparticle conjugates are the most potent light-activated antimicrobial agents reported to date.

Chapter 3 Tin Chlorin e6-Glutathione-Gold Nanoparticles

This chapter describes the synthesis and antimicrobial activity of tin chlorin e6–glutathione-gold (Au-GS-Snce6) nanoparticles. The gold glutathione protected gold (Au-GS) nanoparticles were synthesised in a one step reaction in acidified methanol. These nanoparticles were further functionalised by the attachment of a light activated antimicrobial reagent (tin chlorin e6). These Au-GS-SnCe6 nanoparticles were tested for anti-microbial activity by lethal photosensitisation of bacteria experiments, at the Eastman Dental Institute. The introduction describes key components of this novel moiety and its overall application in combating microbial infections.

3.1 Introduction

Glutathione (GSH) is a bulky tripeptide composed of cystine, glutamic acid, and glycine (Figure 3-1). The active thiol group which binds to gold nanoparticles is located on the cystine residue. Glutathione is a ubiquitous molecule that is synthesised in all organs of the human body, particularly the liver. The intracellular concentration of glutathione can be between 1 – 10 mM.[124] Free glutathione is present mainly in its reduced form, which can be oxidised and reduced by the action of the enzyme glutathione reductase.[125] Glutathione is important in the function of the central nervous system and protects cell membranes from oxidative damage.[125] It has been shown that glutathione can serve as a trigger for drug release from gold nanoparticle carriers.[126]

Glutathione is an attractive ligand for making water soluble gold nanoparticles. It has favourable properties such as the presence of thiol, carboxylic acid, and amino groups, which provide water solubility at relevant biological pH, biological compatibility, and ease of functionalisation. In 1998 Whetten *et al.*[127,128] first synthesised glutathione protected gold clusters by a sodium borohydride reduction of a mixture of tetrachloroauric acid and glutathione in methanol–water at a ratio of 2:3. They obtained gold clusters with the dominant core size of 0.9 nm. Tsukuda *et al.*[129,130] made significant progress using similar synthetic procedures to Whetten *et al.*, by introducing extensive electrophoretic separation techniques and high resolution mass spectrometry in the purification and characterisation of glutathione protected gold clusters. The study by Tsukuda *et al.* revealed that by varying the reaction temperature, the size of the clusters could be varied. Au_{10}, Au_{15} and Au_{18} were obtained as the major product by increasing the temperature respectively. In both studies, the size of the clusters formed was between 0.8 and 1.1 nm. Although the preparation of the glutathione protected gold nanoparticles were well-established and their composition was extensively characterized, the issues of further functionalisation of the nanoparticles to suit particular applications, such as biomolecular labelling, were not addressed in these studies. These issues are very important for the utility of the nanoparticles in applications that require functionality and size control. Aziwa *et al.*[131] have shown that glutathione forms a compact monolayer on polycrystalline gold surfaces retaining its non-sulph-hydryl biological activity.

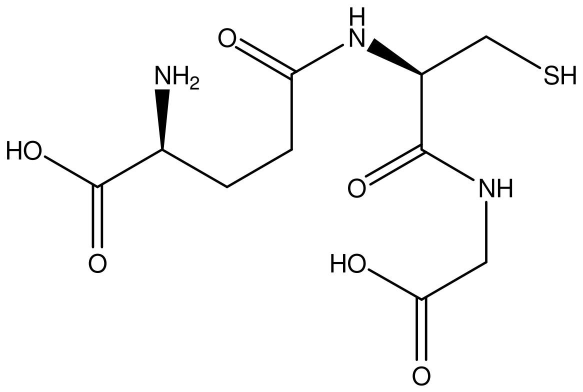

Figure 3-1 ***Structure of Glutathione***

In 1995 Brust *et al.*[33] reduced tetrachloroauric acid using sodium borohydride in the presence of organothiols in a single phase reaction to obtain thiol protected gold nanoparticles 5 nm in diameter. It is thought that the first step in the reaction, where the pale yellow colour disappears and goes clear is the result of the formation of polymeric structures with –Au–S(R)– repeating bonds units.[132,133] The thiolate polymer is formed through sacrificial reduction of the thiol. Gold(I) has a d^{10} closed shell electronic configuration which tends to form aggregates thorough aurophillic interactions. The relatively strong non covalent Au(I)–Au(I) interaction is attributed to the hybridisation between empty 6s/6p shells and filled $5d^{10}$ shells which are stabilised and destabilised respectively.[129] The second step in the reaction is where the polymer is then reduced by the addition of aqueous $NaBH_4$, yielding gold nanoparticles coated in a thiol such as glutathione. The net result is a quantitative conversion of the –Au–S(R)– polymer into intensely coloured, highly water soluble Au:S(R) cluster compounds whose stability is indicated by their resistance to excess strong reducing agents.[127] Since the preparation methods are based on nucleation of gold cores in the presence of thiols, the sizes of the resulting cores are inevitably distributed, due to the statistical fluctuations in the nucleation process.

The presence of carboxylic acid and amino groups on glutathione, when complexed with Au(I) have the potential advantage of creating pH-sensitive compounds. This compound can adopt different conformational states and sizes depending on the pH of the solution.[107] Hainfeld *et al.*[107]controlled the final diameter of the gold core by varying the size of the nanoparticle precursor [Au(I)SG] through pH manipulation. The size of the final nanoparticles was varied from 2 to 6 nm. Furthermore, the functionalisation of glutathione gold nanoparticles was demonstrated by the introduction of a nitrilotriacetic acid (NTA) moiety.

The glutathione is tethered to the surface of a gold nanoparticle through the sulphur atom. There are a number of functional groups on the rest of the glutathione molecule where further chemistry of the gold nanoparticle is possible. One possibility is the attachment of a light activated antimicrobial such as the metalloporphyrin tin chlorin e6. The structure of tin chlorine e6 is based on 16 atom rings containing four nitrogen atoms (porphyrins).

Porphyrins (Figure 3-2) are of perfect size to bind many metal ions. Metalloporphyrins are found in heme proteins which are ubiquitous in nature. They serve many roles including oxygen storage and transport. Related macrocycles include chlorophylls, which have a central magnesium ion. By varying the metal centre, the bonding and characteristics of the metalloporphyrin may be dramatically affected. This diversity is one of the reasons why metalloporphyrins have been widely used in the production of dyes, semiconductors and catalysts.[134]

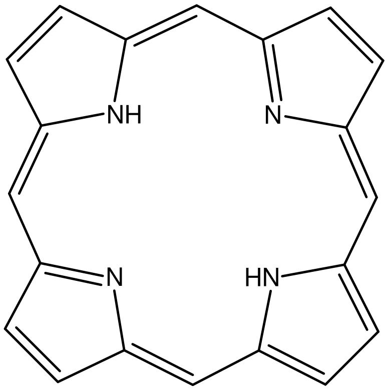

Figure 3-2 ***Porphine, the simplest porphyrin***

Tin(IV) chlorin e6 (SnCe6) is a metalloporphyrin photosensitiser, that is known to be lethal to bacteria when exposed to a HeNe laser, which emits red light at a wavelength of 632.8 nm.[91] Tin (IV) chlorin e6 (SnCe6) absorbs light at 632 nm and has an improved yield of singlet oxygen over related chlorins.[135] In addition, tin chlorin e6 possesses reactive carboxyl groups on side chains outside the polycyclic core enabling conjugation to targeting molecules,[97] and nanoparticles (Figure 3-3).

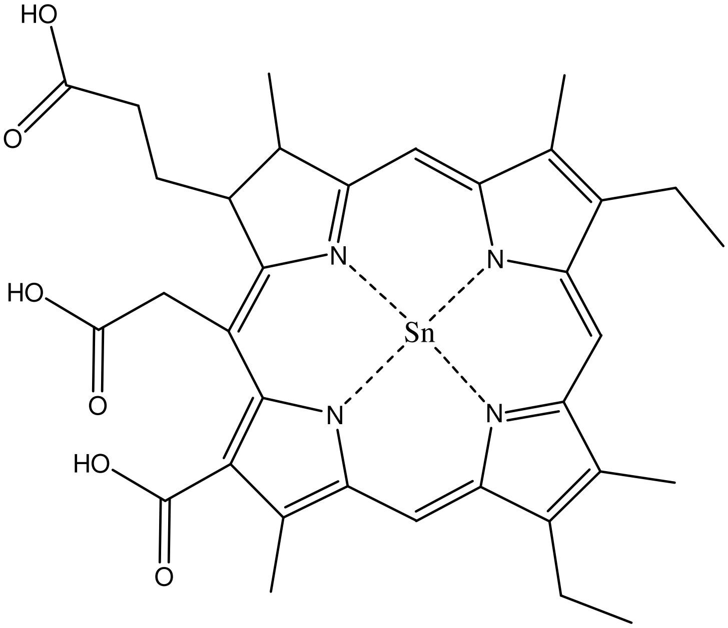

Figure 3-3 ***Structure of tin chlorin e6***

Tin chlorin e6 has been used in photodynamic therapy (PDT) as a light-activated antimicrobial agent to achieve lethal photosensitisation of infecting microbes.[91] This involves treating the microbe with a light-activated chemical, a photosensitiser such as tin chlorin e6. Generally a photosensitiser has no, or negligible, bactericidal activity alone. However, upon exposure to light of a wavelength absorbed by the photosensitiser, the photosensitiser undergoes a transition from a lower-energy 'ground state' to a higher-energy 'triplet state'. The triplet state photosensitiser can react with solvent and substrate molecules to produce free radicals and radical ions, or with molecular oxygen resulting in the generation of singlet oxygen. These toxic species in particular singlet oxygen, can damage plasma membranes leading to cell death.

There are major advantages to using photodynamic action in the treatment of microbial infections, especially methicillin resistant *Staphylococcus aureus* (MRSA) bacteria, over conventional antiseptics and antimicrobials. Neither the light nor sensitiser is inherently bactericidal, so the antibacterial effect is limited to light irradiated regions of the sensitiser treated area. This avoids the disruption of the normal microflora at sites away from those being targeted. Also, the development of resistance to photochemically induced killing would be unlikely, because the radicals formed attack bacteria by a number of pathways.

While excellent clinical results are obtained using current photosensitisers,[92,102,115] improvements could be made which enhance the efficiency of lethal photosensitisation of bacteria. These improvements include developing photosensitisers which absorb wavelengths of light in the far infrared region of the electromagnetic spectrum. These wavelengths of light are able to access infections deeper in the body as they are preferentially transmitted by human tissues.[136] Another approach is to enhance the efficiency of singlet oxygen production, reducing the concentration of photosensitiser required to treat the infection. This was achieved by Wieder *et al.*[99] who attached phthalocyanine photosensitisers to the surfaces of gold nanoparticles. They found that the surface bound photosensitiser exhibits a remarkable enhancement of the singlet oxygen quantum yield. This was attributed to the presence of the phase transfer reagent tetraoctylammonium bromide (TOAB) used in the synthesis of gold nanoparticles. It is thought that the TOAB increases the triplet energy transfer to molecular oxygen.

In this study gold nanoparticles protected by glutathione were synthesised, isolated and purified. These nanoparticles were further functionalised by conjugation of the photosensitiser tin chlorin e6 to the amino terminal of glutathione *via* a condensation reaction. The light activated antimicrobial moiety synthesised was a three component system, consisting of a gold core, protecting coating and photosensitiser. Attempts were made to modify the diameter of the gold core, by varying the gold : thiol ratio.

3.2 Experimental

Chemicals: $HAuCl_4 \cdot 3H_2O$ (99.99%), glutathione (99%) and sodium borohydride (99%) were purchased from Aldrich. Tin chlorin e6 (SnCle6) was purchased from Frontier Scientific. Buffers were prepared according to standard laboratory procedure. All other chemicals were reagent grade and used as received.

The synthesis of SnCle6-glutathione-gold nanoparticles were carried out in two steps: (1) Synthesis of glutathione-gold nanoparticles; and (2) Preparation of SnCle6-glutathione-gold nanoparticles.

Synthesis of glutathione-gold nanoparticles: Glutathione-gold nanoparticles were prepared by adaption of previously reported methodologies.[117,118,127] In a typical reaction methanol (120 mL) acetic acid (20 mL) were mixed in an Erlenmeyer flask with stirring for 2-5 min. Tetrachloroauric acid (0.788 g, 2 mmol) and glutathione (GSH, 0.307 g, 1 mmol) were added to the above mixed solvents and dissolved by stirring for 5 min, resulting in a clear yellow solution. A sodium borohydride solution was prepared by dissolving $NaBH_4$ (1.211 g, 32 mmol) in water (60 mL). The $NaBH_4$ solution was added dropwise into the tetrachloroauric acid and glutathione solution with rapid stirring. The particle solution was transferred into filter tubes (50K MW cut-off, Millipore) and purified by centrifuging at 3500 rpm and washed with water 4 times, and then freeze dried. The particles were obtained as a dark blue / black powder. The glutathione monolayer protected gold nanoparticles were soluble in water, and when diluted the solution became clear purple. The ratios and masses used were:

	Au	Glutathione
NNG.1		
Mass (g)	0.394	0.2117
Ratio	1	0.344
NNG.4		
Mass (g)	0.394	0.1829
Ratio	1	0.3
NNG.7		
Mass (g)	0.394	0.1535
Ratio	1	0.25

Table 3-1 ***Ratios and masses used in the synthesis of gold–glutathione nanoparticles.***

Preparation of SnCle6-glutathione-gold nanoparticles: SnCle6-glutathione-gold nanoparticles were prepared by modification of previously reported methodologies for making glutathione-gold nanoparticles.[100,118] In a typical reaction, tin chlorin e6 (SnCle6, 29 mg, 34.1 μmol) was dissolved in 20 mL of 50 mM 2-(*N*-morpholino)ethanesulfonic acid (MES) buffer (pH 6.5) and the solution then made up to 5.1 mM in 1-[3-(dimethylamino)-propyl]-3-ethylcarbodiimide hydrochloride (EDC) and 5.1 mM in *N*-hydroxysulfosuccinimide sodium salt. After stirring for 40 min, glutathione-gold nanoparticles (110 mg) were added, and the solution was stirred for 24 h. Then, the reaction crude was purified by dialysis, in which the pH of the crude product was adjusted to 1 by dropwise addition of concentrated HCl. This solution was loaded into a 20 cm segment of cellulose ester dialysis membrane (Spectra/Por CE, MWCO = 12000), placed in a 4 L beaker of water, and stirred slowly, recharging with fresh water ca. every 12 h over the course of 168 h. The dark SnCle6-glutathione-gold nanoparticle solution was collected from the dialysis tube, and the solvent was removed by freeze-drying. An NMR spectrum that could be resolved was not obtained.

Thermogravimetric Analysis (TGA): Thermogravimetric analysis (TGA) was performed with a NETZSCH STA 449C TGA system, on 8.84 mg of dry, purified glutathione-gold nanoparticles, under He (flow rate of 50 mL min^{-1}), recording data from 25 to 1000ºC at a heating rate of 10 ºC min^{-1}.

X-Ray diffraction: These experiments were measured with a Bruker discover diffractometer using Cu Kα radiation. These were used to analyse the residue left in the pan after the TGA experiment. In both, TBO-tiopronin- and tiopronin-gold nanoparticles, this residue resulted to be elemental gold, which is consistent with previous TGA work on alkanethiolate-gold nanoparticles.[6,7]

High resolution transmission electron microscopy (HRTEM): Samples were prepared by evaporating the required specimen on a carbon coated copper. Bright field TEM images were acquired using with an electron microscope operated at 100 kV (Joel 100CX). Typical magnification of the images was 100 000. Analysis of the images was performed using the software program Image J.[116]

Infra-Red Spectroscopy: Spectra were recorded on a Perkin Elmer Spectrum RX1 spectrometer. Samples were made in the form of dispersed pellets. Spectra were collected at a resolution of 1 cm^{-1}.

UV-visible absorption spectroscopy: Spectra were recorded using a Perkin Elmer Lambda 25 Spectrometer. Samples were dissolved in phosphate buffer solution or deionised water and placed in plastic cuvettes. Data were collected between the range of 300 and 1000 nm.

3.3 Results

The gold–glutathione (Au-GS) nanoparticles were synthesised by a previously reported reaction.[117,129] Tetrachloroauric acid was dissolved in acidified methanol, under rapid stirring. This was reduced by a freshly prepared sodium borohydride solution under rapid stirring, at room temperature. The tetrachloroaurate (III), $[AuCl_4]^-$ ions were soluble in acidified methanol and therefore did not require extraction from aqueous to organic media by a phase transfer agent, which is the conventional Brust[31] method for preparing thiol protected gold nanoparticles. The acidity is essential for the reaction to yield stable monodisperse nanoparticles. This suggests that the emerging nanoparticles coated in glutathione are unstable when the glutathione is de-protonated in methanol. The gold–glutathione nanoparticles formed are insoluble in methanol, but soluble in water (Figure 3-4). Once isolated and purified they have the consistency of a finely divided black / blue powder which can be dissolved in water and stored in air. The first step in the reaction also yielded undesired, water soluble by-products (NaCl, disulfide, NaOAc, HOAC), which were removed by dialysis, along with any un-reacted starting reagents.

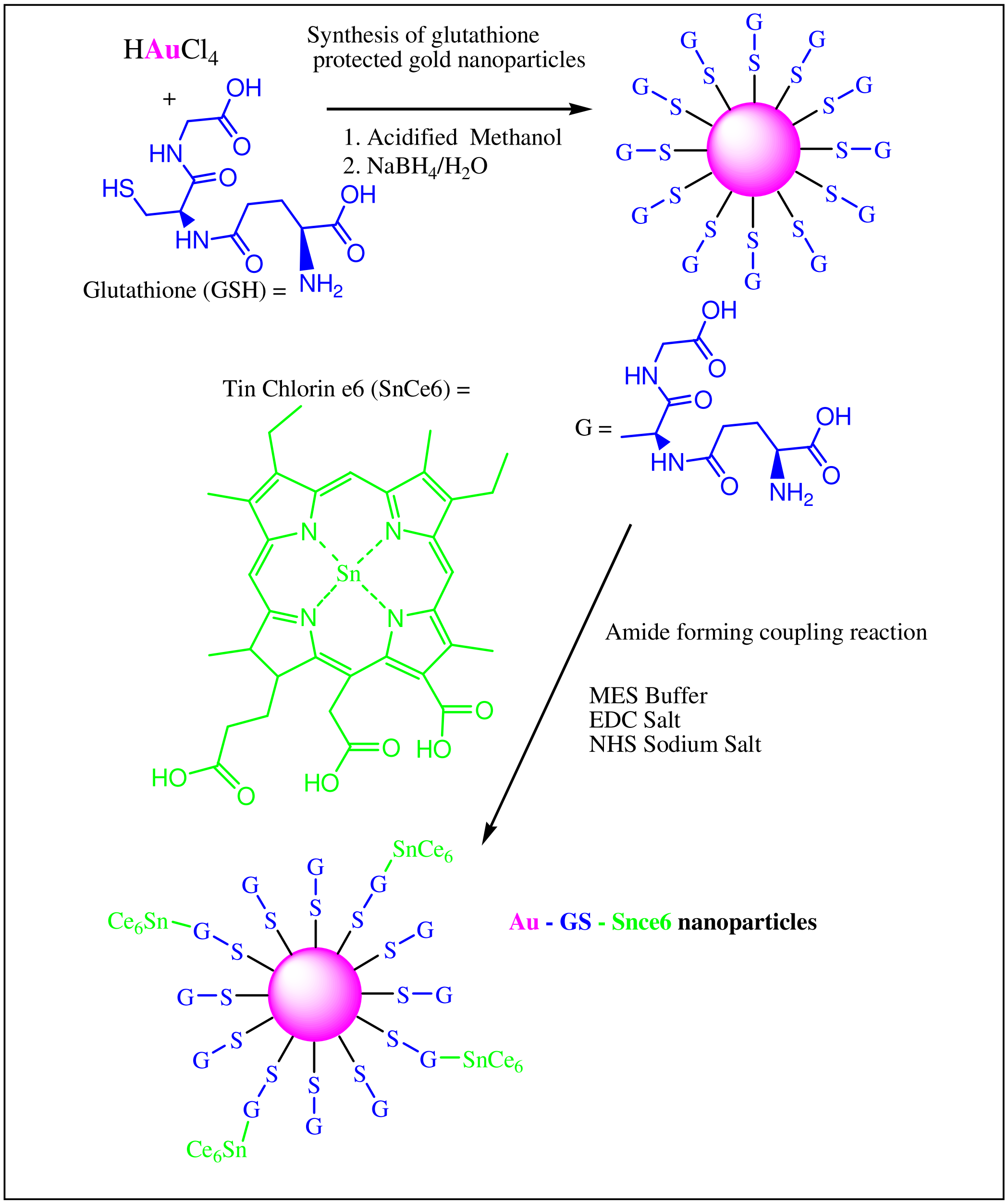

Figure 3-4 ***Detailed scheme of the synthesis of gold–glutathione (Au-GS) nanoparticles and the functionalisation of these particles to obtain gold–glutathione–tin chlorin e6 (Au-GS-Snce6).***

The next step in the reaction involved the coupling of a tin chlorin e6 molecule to the amino end of a glutathione on the surface of the gold nanoparticles (Figure 3-5). This is achieved by the formation of an amide linkage *via* a condensation reaction. This reaction takes place in the presence of the sodium salt of *N*-hydroxysulphosuccinimide (sulfo-NHS) and 1-[3-(dimethyl amino) propyl]-3-ethyl-carbodiimide hydrochloride (EDC). Sulfo-NHS is used to convert a carboxylic acid group on the tin chlorin e6 to an amine reactive sulfo-NHS ester. This process is catalysed by EDC which behaves as a dehydrating carbodiimide. EDC is not an effective dehydrating and crosslinking entity by itself, because failure to react quickly with the amine results in the hydrolysis and regeneration of the carboxylic acid (Figure 3-5).

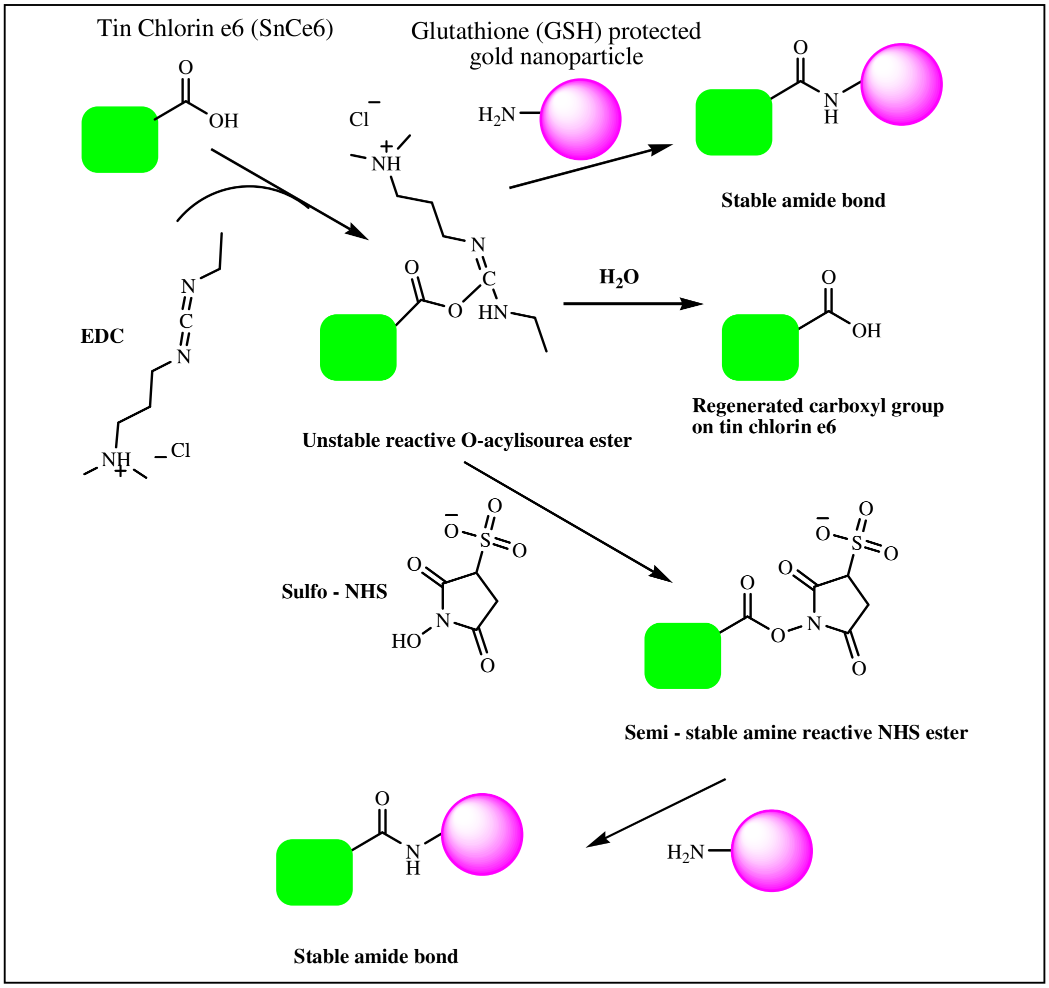

Figure 3-5 ***Routes possible when coupling tin chlorin e6 to glutathione-gold nanoparticles using 1-[3-(dimethyl amino) propyl]-3-ethyl-carbodiimide hydrochloride (EDC) and N-hydroxysulphosuccinimide (sulfo-NHS)***

EDC reacts with the carboxylic acid group of the tin chlorin e6, forming an amine reactive *O*-acylisourea intermediate. This intermediate then can be reacted with the amine on the glutathione of the Au-GS nanoparticles. This yields a conjugate of the two entities joined by a stable amide bond. However this conjugate is also susceptible to hydrolysis making it unstable and short lived in aqueous solutions. The addition of sulfo-NHS stabilizes the amine reactive intermediate by converting it to an amine reactive sulfo-NHS-ester. This increases the efficiency of EDC mediated coupling reactions. The amine reactive sulfo-NHS ester intermediate has sufficient stability to permit a two step coupling reaction.

There are three carboxylic acid groups on each tin chlorin e6 molecule. Therefore the ratio of tin chlorin e6 to EDC was kept 1:1, in order to activate only one acidic group on each molecule. The tin chlorin e6-glutathione-gold (Au-GS-SnCe6) nanoparticles produced an intense green / black colour when isolated as a solid. However, a faint green colour was observed when crushed with KBr for IR experiments. The conjugate was air stable for at least 4 months and could be dissolved in water or phosphate buffer (PBS) solution.

In order to change the core size of the nanoparticles three different Au:thiol ratios were used. Sample NNG.1 (Au-GS) had gold:thiol ratio of 1:0.344. This gave an average particle size of 2.6 ± 0.6 nm in the first step of the reaction. This sample was further functionalised with the coupling reaction and the addition of tin chlorin e6. The product of this reaction (Au-GS-SnCe6, NNG.3) had an average particle size of 2.3 ± 0.5 nm. Sample NNG.4 (Au-GS) had gold:thiol ratio of 1:0.3. This gave an average particle size of 5.2 ± 1.2 nm in the first step of the reaction. This sample was further functionalised by a coupling reaction and the addition of tin chlorin e6. The product of this reaction (Au-GS-SnCe6, NNG.5) had an average particle size of 5.4 ± 1.3 nm. Sample NNG.6 (Au-GS) had gold:thiol ratio of 1:0.25. This gave an unusual result and two particle size distributions were observed, 6.07 ± 1.4 nm and 1.97 ± 0.8. This sample was further functionalised with the coupling reaction and the addition of tin chlorin e6. The product of this reaction (Au-GS-SnCe6, NNG.7) also produced two average particle size distributions of 6.24 ± 1.2 nm and 1.73 ± 0.6. Particle size distributions were calculated from high resolution TEM images with sampling sizes of approximately 100 particles. It can clearly be seen in (Figure 3-6) that NNG.6 and NNG.7 have two distinct particle size distributions.

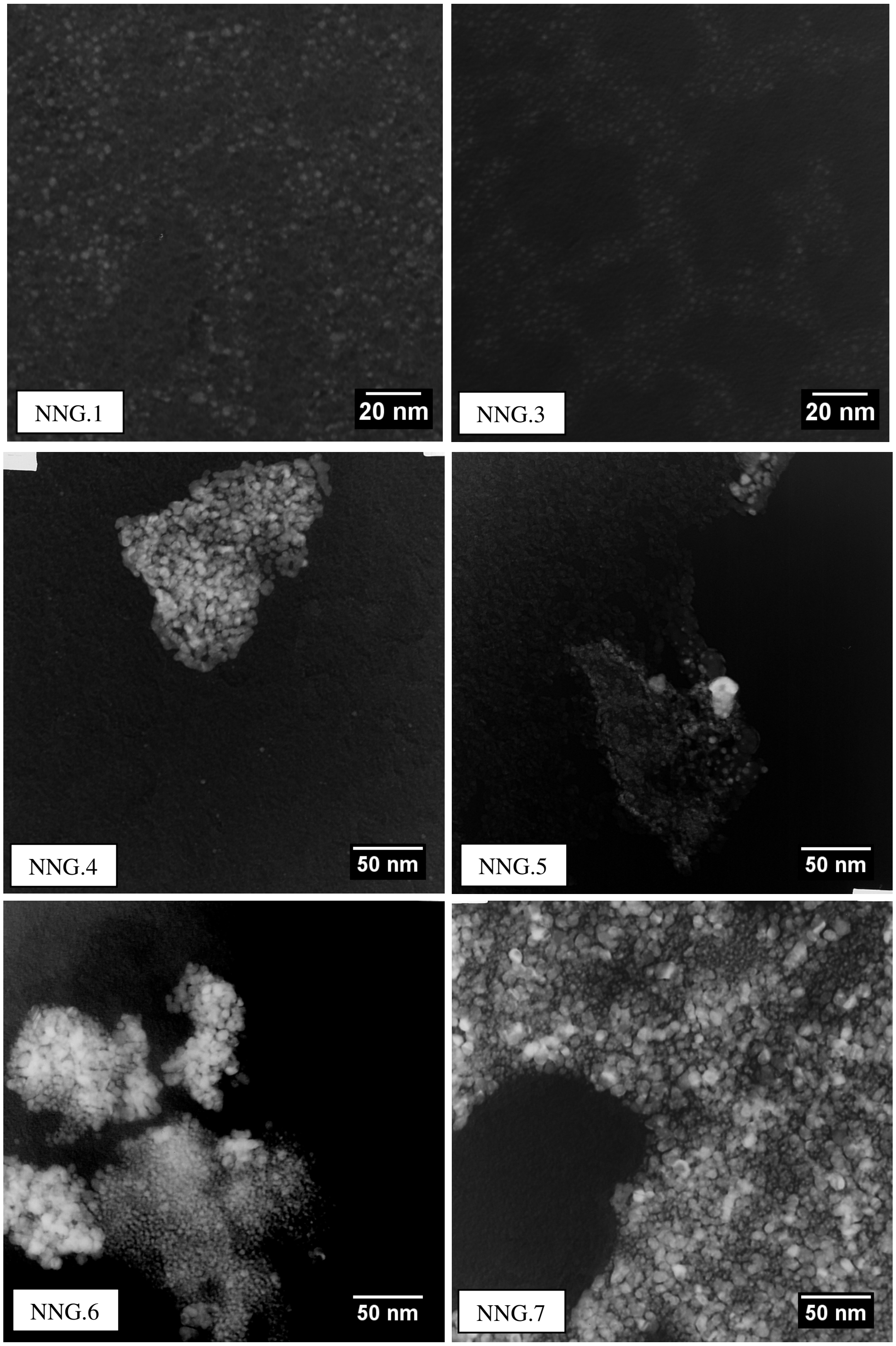

Figure 3-6 ***Transmission Electron Microscopy images of glutathione-gold (Au-GS) particles, samples NNG.1 (2.6 nm), NNG.4 (5.2 nm) and NNG.6 (6.07 and 1.97 nm), and their conjugated products (Au-GS-SnCe6), NNG.3 (2.3 nm), NNG.5 (5.4 nm) and NNG.7 (6.24 and 1.73 nm) respectively.***

Elemental analysis was performed on all samples, and using these data the mass of tin chlorin e6 per 100 mg of samples NNG.3, NNG.5, NNG.7 was calculated. The resulted are presented in (Table 3-2).

Sample	%C	%H	%N	%S	%Cl	Mass of SnCe6/100 mg
NNG.1	8.88	1.21	2.82	2.33	-	-
NNG.3	9.56	1.26	2.85	2.04	2.56	4.53
NNG.4	7.64	1.01	2.46	1.76	-	-
NNG.5	9.88	1.18	2.59	I/S	3.54	7.68
NNG.6	8.65	1.22	2.83	2.18	-	-
NNG.7	9.97	1.27	2.95	1.53	1.91	4.73

Table 3-2 ***Summary of elemental analysis and calculated mass of tin chlorin e6 (SnCe6) per 100 mg of gold-glutathione-tin chlorin e6 of nanoparticles (Au-GS-SnCe6). I/S =Insufficient Sample***

The mass of tin chlorin e6 per 100 g of sample for samples (NNG.3, NNG.5 and NNG.7) was calculated using only the elemental analysis results. The method used was as follows:

Number of carbon atoms in SnCe6 = 34
Mass of SnCe6 = 850
Number of carbon atoms in Glutathione = 10
Total mass of Carbon = MC

$$\text{Mass on SnCe6} = \underset{\substack{\downarrow \\ \text{Fraction of Carbon} \\ \text{that is in SnCe6}}}{\left(\frac{34\times x}{10+34+x}\right)}\times\left(\frac{MC}{12\times 34}\right)\times 850 \tag{3-1}$$

x = Number of SnCe6 molecules per glutathione

Number of carbon atoms in glutathione = 10
Total mass of carbon in 1 glutathione = 120
Number of nitrogen atoms in glutathione = 3

Total mass of nitrogen in glutathione = 42
Number of nitrogen atoms in SnCe6 = 4
Total mass of nitrogen in SnCe6 = 56
Therefore the carbon to nitrogen ratio is:

$$\frac{C}{N} = \frac{120 + x \times 408}{42 + x \times 56} \tag{3-2}$$

The $\frac{C}{N}$ was calculated from the elemental analysis data for samples (NNG.3, NNG.5 and NNG.7) and the equation was rearranged for x.

$$x = \left(\frac{120 - \frac{C}{N} \times 42}{\frac{C}{N} \times 56 - 408} \right) \tag{3-3}$$

The thermal decomposition of Au-GS nanoparticles (samples NNG.1, NNG.4 and NNG.6) are shown in Figure 3-7. The thermal decomposition of the smallest particles (NNG.1), with an average diameter of 2.6 nm occurred in two steps; a well-defined step that began at approximately 190 °C and was completed by 420 °C, and a second step from 420 °C to 650 °C. The percentage weight losses for the organic fragments were 31.6% for sample NNG.1. The thermal decomposition mass loss of samples NNG.4 and NNG.6 occurred in one step, which began at 190 °C and was completed by 1000 °C. The total mass loss was 20.9% and 18.2% respectively.

The thermal decomposition of gold-glutathione-tin chlorin e6 nanoparticles (samples NNG.3, NNG.5 and NNG.7) are shown in Figure 3-8. The thermal decomposition of the smallest particles (NNG.3), with an average diameter of 2.3 nm occurred in two steps; a well-defined step that began at approximately 190 °C and was completed by 500 °C, and a second step from 500 °C to 1100 °C. The percentage weight losses of the organic fragments was 23.7% for sample NNG.3 consisting of Au-GS-SnCe6 particles. The thermal decomposition mass loss of samples NNG.5 and NNG.7 occurred in one step, which began at 190 °C and was completed by 1000 °C. The total mass loss was 18.4% and 21.0% respectively.

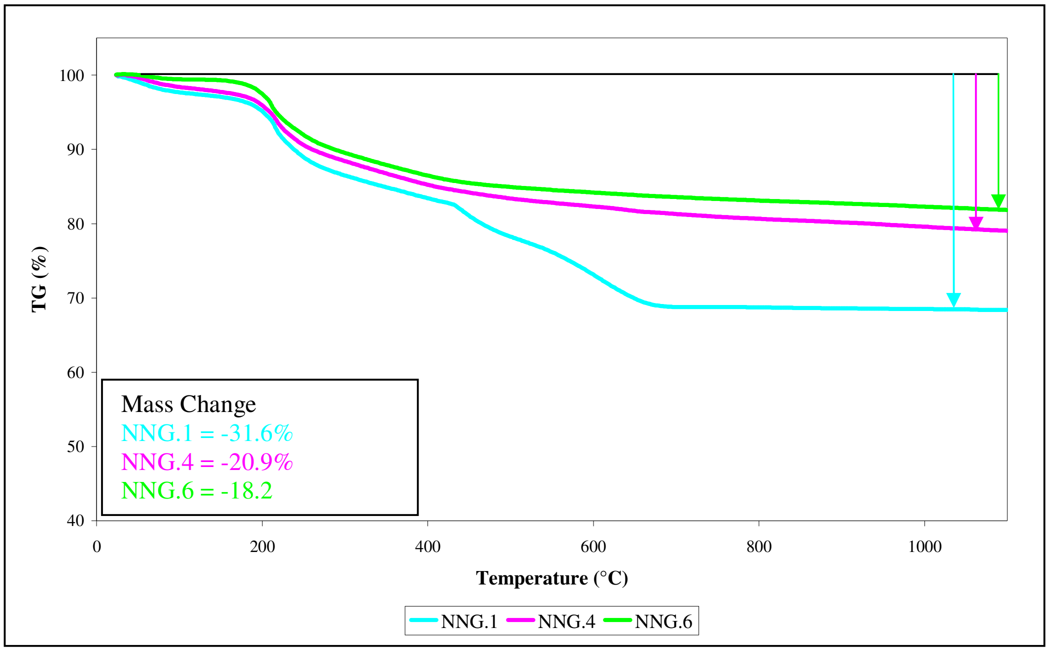

Figure 3-7 ***Thermal Gravimetric Analysis (TGA) of glutathione-gold (Au-GS) particles, samples NNG.1 (2.6 nm), NNG.4 (5.2 nm) and NNG.6 (6.07 and 1.97 nm).***

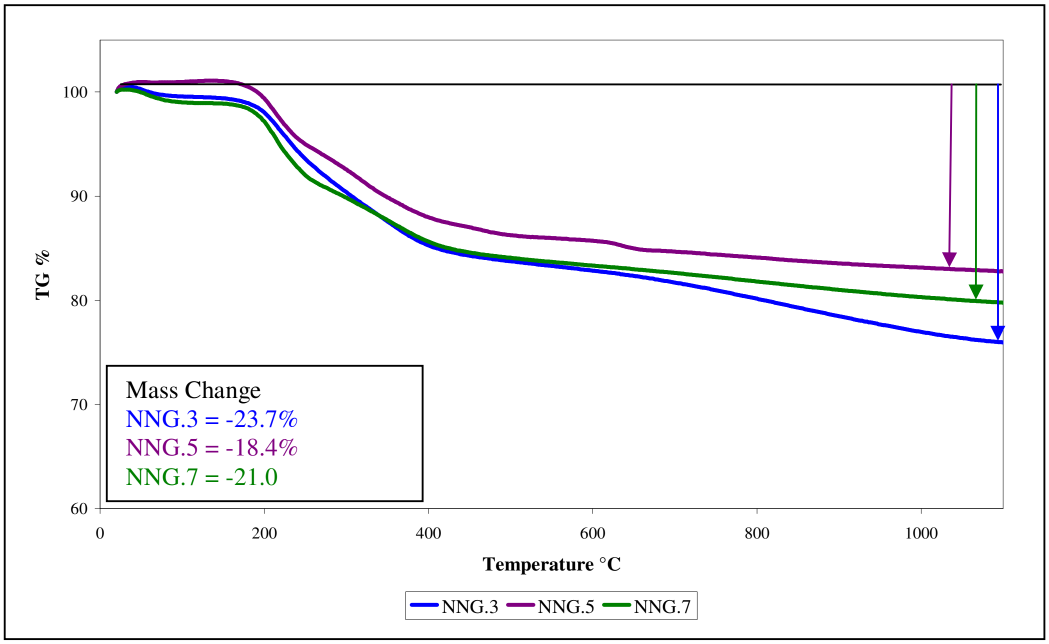

Figure 3-8 ***Thermal Gravimetric Analysis (TGA) of gold-glutathione-SnCe6 nanoparticles (Au-GS-SnCe6), NNG.3 (2.3 nm), NNG.5 (5.4 nm) and NNG.7 (6.24 and 1.73 nm).***

The residue from the TGA experiments from both the Au-GS and the Au-GS-SnCe6 sets of nanoparticles was shown by X-ray diffraction to be highly crystalline gold metal.

This is consistent with previous TGA work on alkanethiolate–gold nanoparticles.[137] An example of which (NNG.4) is shown in Figure 3-9.

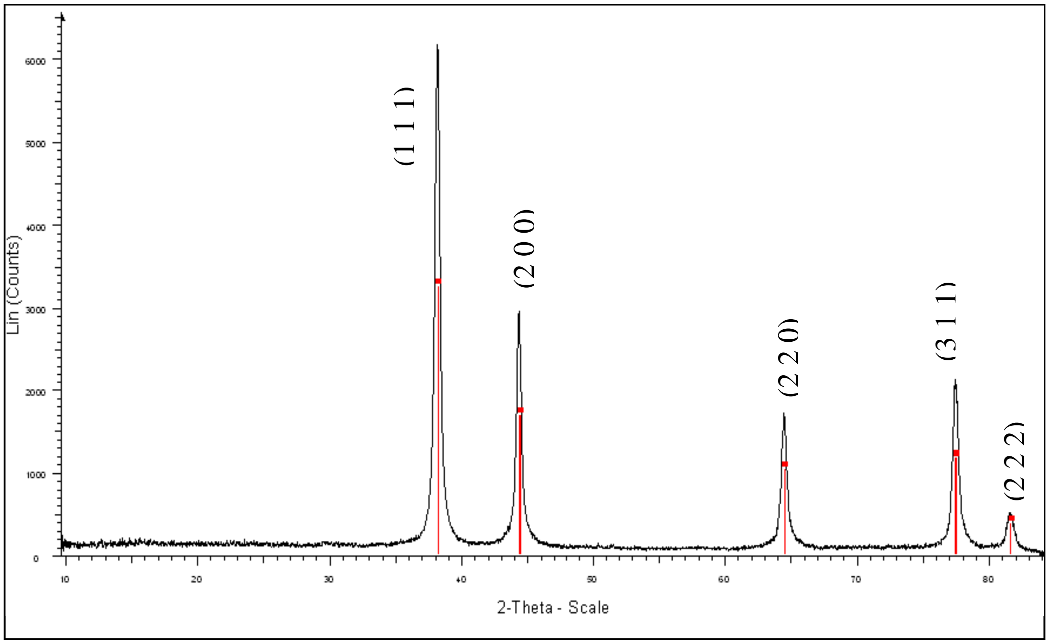

Figure 3-9 ***X-ray diffraction (XRD) pattern of the residue left in the pan after thermal gravimetric analysis, confirms presence of elemental gold in sample NNG.4. The pattern is indexed and shows the expected stick pattern (red) for gold metal.***

Infra-red spectroscopy of the Au-GS nanoparticles (NNG.1, NNG.4 and NNG.6) showed that the bands for glutathione were readily observed (Figure 3-10). However, the S-H vibration observed at 2524 cm^{-1} of the free glutathione ligand, was not observed for any of the subsequent samples. This is a clear indication that the glutathione was de-protonated and coordinated to the surface of the gold nanoparticle through the sulphur. The N–H vibration at 3250 cm^{-1} of free glutathione was not clearly observed on all samples, although a shoulder at a lower frequency was observed indicating a change in hydrogen bonding.

The aromatic rings band at ~1600 cm^{-1} of the tin chlorin e6 was not observed in the Au–GS–SnCe6 nanoparticles (NNG.3, NNG.5 and NNG.7) spectra. This was because there was an overlap of peaks from the glutathione in this region. Analysis of the IR spectra provides some evidence for the formation of Au-GS particles. However, the coupling of SnCe6 to these particles could not be clearly observed, as there was significant overlap of peaks.

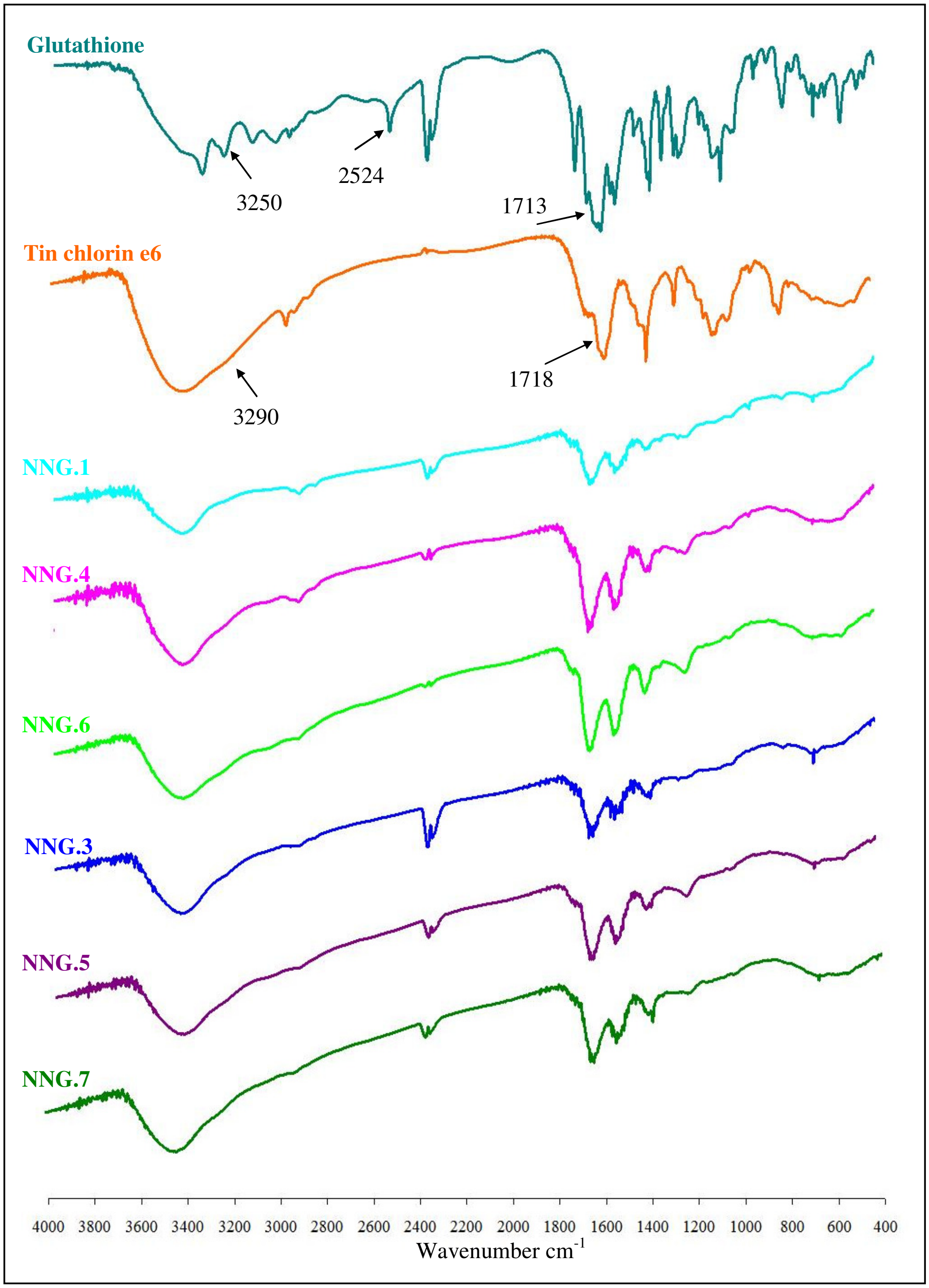

Figure 3-10 ***Transmission infra-red spectra of free glutathione, tin chlorin e6, glutathione-gold (Au-GS) particles, samples NNG.1 (2.6 nm), NNG.4 (5.2 nm) and NNG.6 (6.07 and 1.97 nm), and their conjugated products (Au-GS-SnCe6), NNG.3 (2.3 nm), NNG.5 (5.4 nm) and NNG.7 (6.24 and 1.73 nm) respectively.***

UV-visible absorption spectra were taken of all samples in deionised water and phosphate buffer solution. Particles in general dissolved more readily in phosphate buffer. For the Au-GS particles, only a slight surface plasmon was observed for NNG.1 and NNG.4 at around 550 nm in water (Figure 3-11). NNG.6 did not display any surface plasmon when dissolved in water. When the Au-GS nanoparticles (NNG.1, NNG.4 and NNG.6) were dissolved in phosphate buffer solution, surface plasmons were observed for all the samples around 525 nm.

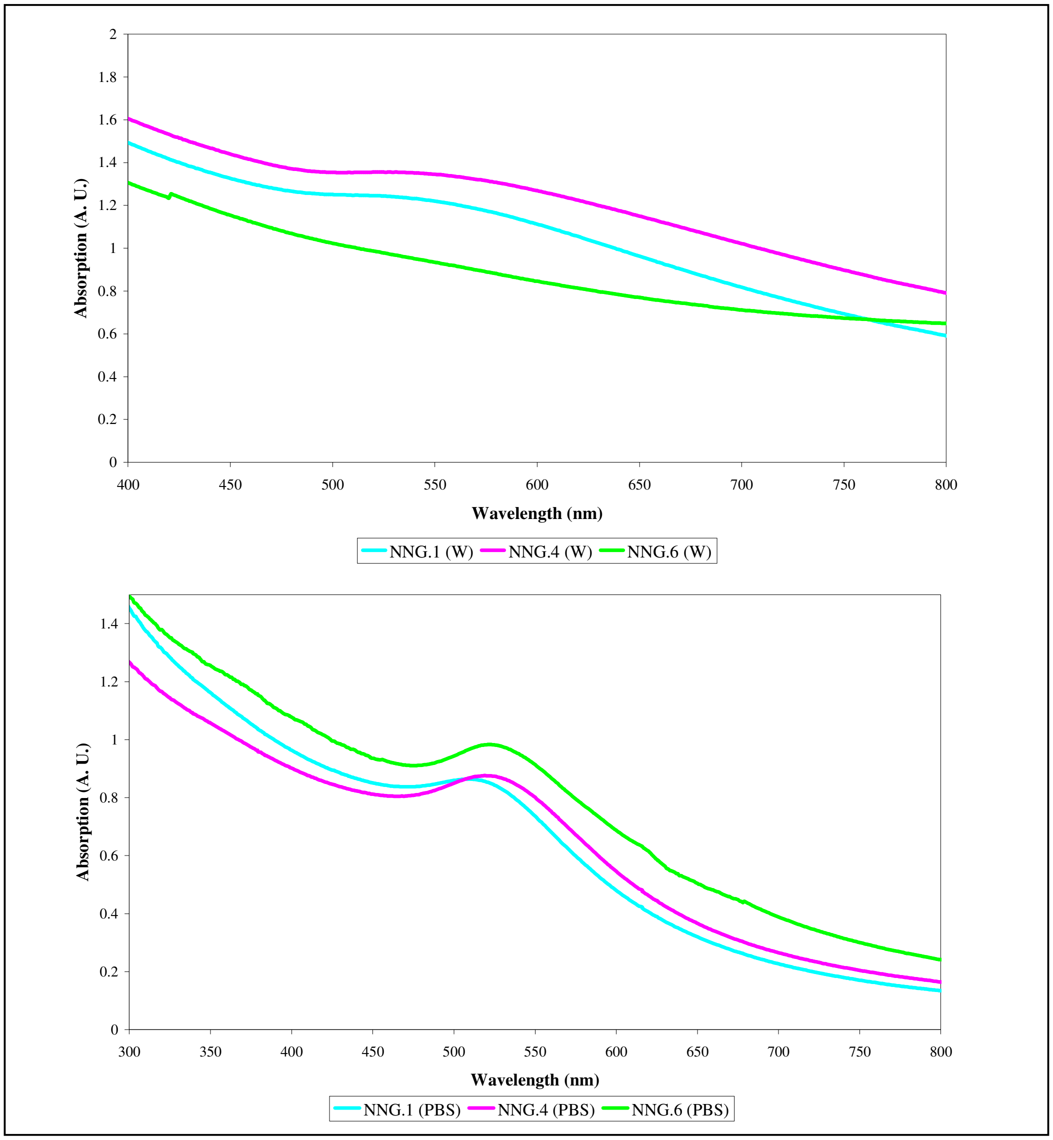

Figure 3-11 ***UV-visible absorption spectra of glutathione-gold (Au-GS) nanoparticles, samples NNG.1 (2.6 nm), NNG.4 (5.2 nm) and NNG.6 (6.07 and 1.97 nm) in water (top) and phosphate buffer solution (bottom).***

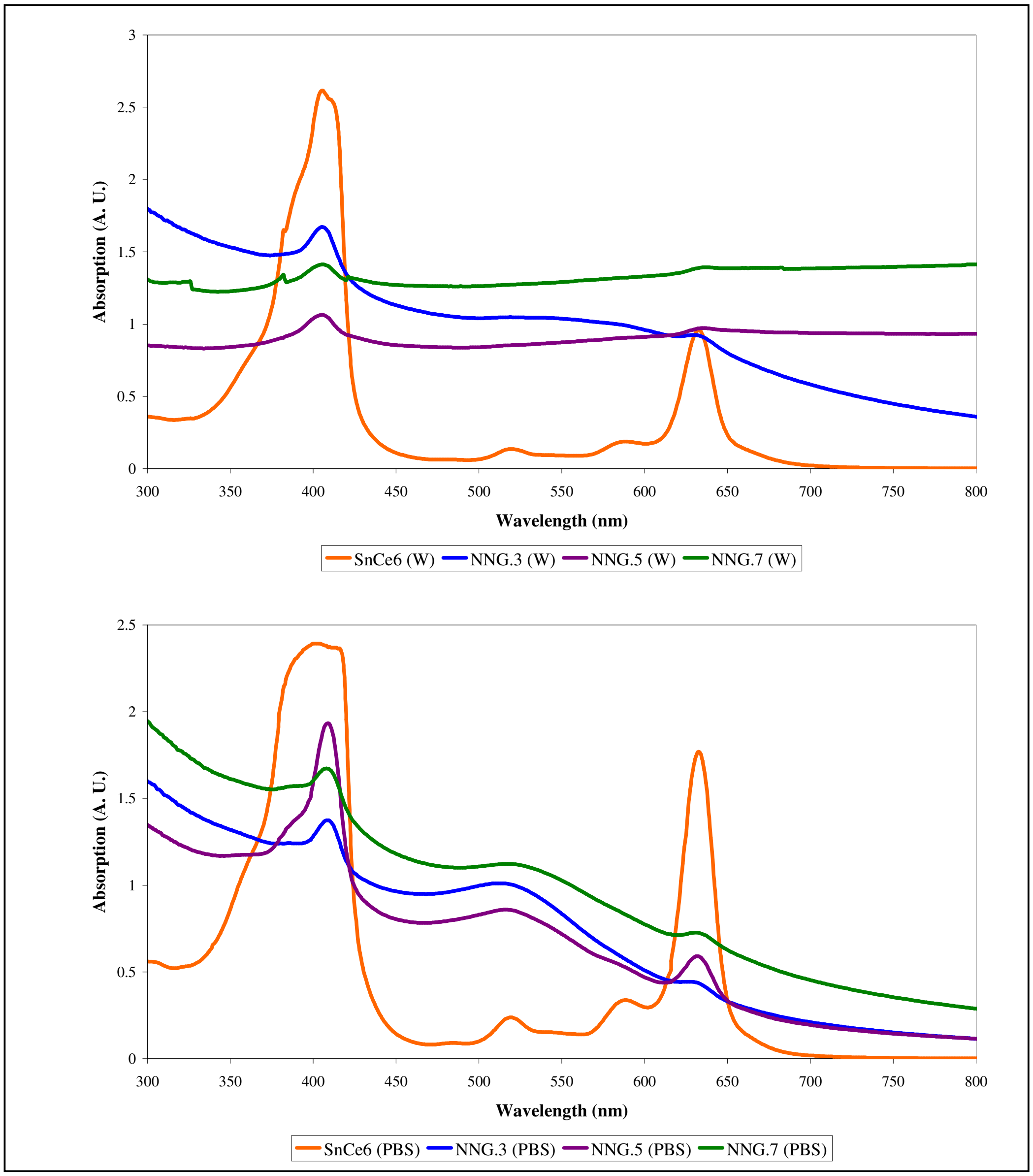

Figure 3-12 ***UV-visible absorption spectra of gold-glutathione-tin chlorin e6 (Au-GS-SnCe6) nanoparticles, NNG.3 (2.3 nm), NNG.5 (5.4 nm) and NNG.7 (6.24 and 1.73 nm) in water (top) and phosphate buffer solution (bottom).***

The presence of tin chlorin e6 was observed in the UV-visible absorption spectra (Figure 3-12) of Au-GS-SnCe6 particles (NNG.3, NNG.5, NNG.7) in water, indicating some solubility in water of these particles. The UV-visible absorption spectra of the same particles when taken in phosphate buffer are clearer. The Soret peak[138] at approximately 400 nm is clearly visible and can not be any other entity other than tin chlorin e6. The other dominant peak at approximately 630 nm is also observed in water, but is more pronounced in the UV-visible absorption spectra in phosphate buffer.

As the presence of the photosensitiser tin chlorin e6 was confirmed in samples NNG.3 NNG.5 and NNG.7, lethal photosensitisation microbiology experiments were carried out at the Eastman Dental Institute in collaboration with Linda Dekker. Figure 3-13 displays the antimicrobial kills achieved by the Au-GS-SnCe6 nanoparticles (samples NNG.5 and NNG.7). NNG.5 had the highest antibacterial kill at a 16 µM concentration. The antibacterial kill was concentration dependant.

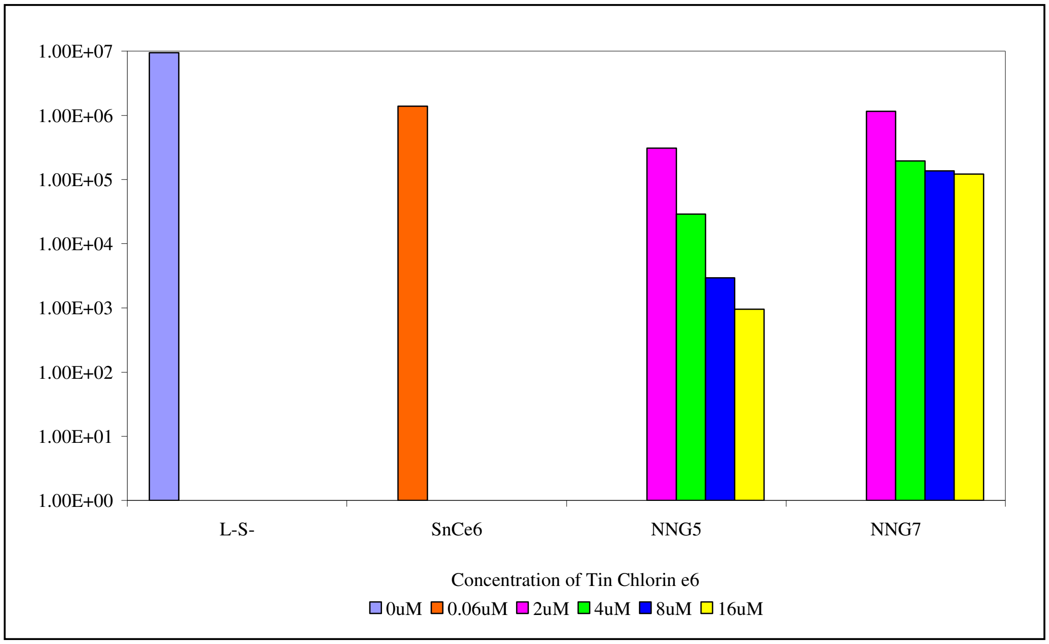

Figure 3-13 ***Lethal photosensitisation of S. aureus 8325-4 using a SnCe6-GS-Au nanoparticle conjugate and 30 min white light exposure. L-= no light, S-=no sensitiser***

3.4 Discussion

Gold-glutathione (Au-GS) nanoparticles were synthesised in acidified methanol, purified, and isolated as a solid. These nanoparticles were further functionalised in the second step of the reaction. The synthesis of Gold-glutathione-tin chlorin e6 (Au-GS-SnCe6) nanoparticles was successfully achieved in aqueous solution, purified, and isolated as a green / black solid. The coupling of tin chlorin e6 to the amino end of glutathione *via* a condensation reaction has proved to be a very reliable method for the functionalisation of applicable thiol coated gold nanoparticles.

In this study the core size of the gold nanoparticles were modified.[137,139] Murray *et al.*[137] found that by increasing the Au:thiol ratio larger particles are obtained. This is plausible as smaller particles have a larger total surface area, hence require more coverage. Therefore by increasing the amount of thiol in the reaction mixture smaller particles should be obtained. This was mostly in agreement with the results obtained in the study. In the synthesis experiments the total gold concentration was kept constant and thiol concentration was lowered for samples through samples NNG.1, NNG.4 and NNG.6 respectively. This did increase the average particle size from 2.6 ± 0.6 nm to 6.07 ± 1.4 nm. However, in sample NNG.6 where the gold thiol ratio was 1:0.25 two distinct size distributions were observed, 6.07 ± 1.4 nm and 1.97 ± 0.8. Since the preparation methods are based on nucleation of gold cores, the sizes of the resulting nanoparticles are inevitably distributed to statistical fluctuations in the nucleation process. Additionally, Whetten *et al.*[127] found one dominant size of Au-GS clusters when using a very similar approach. They separated their Au clusters by polyacrylamide gel electrophoresis (PAGE) and found the most abundant species as $Au_{28}(GS)_{16}$ by mass spectrometry.

Recently Pradeep *et al.*[140] found that small clusters (0.7 nm) of $Au_{25}(GS)_{18}$ prepared in a similar method are susceptible to electron beam damage in a TEM microscope. Upon exposure to the electron beam the cores coalesce to form larger particles. In this study, during TEM sessions this was also observed, as particles became more evident the longer a section of a TEM grid was studied. Therefore it is possible that the second size smaller size distribution observed in sample NNG.6 is an artefact of the coalescence of much smaller, more stable clusters of Au(GS). Unfortunately the image resolution on the TEM used is not high enough to detect any clusters before they coalesce.

In this study, the second step in the procedure to make gold-glutathione-tin chlorin e6 (Au-GS-SnCe6) nanoparticles was the coupling of a photosensitiser to the amine end of the glutathione on Au(GS) nanoparticles. This was achieved *via* a condensation reaction between a carboxylic acid group on the photosensitiser (tin chlorin e6) and amine group on the protecting thiol (glutathione). This was in contrast to the protocol used in the previous chapter where the carboxylic acid group was on the protecting thiol (tiopronin) and amine was on the photosensitiser (toluidine blue). This coupling method has been successful in using both approaches, and is versatile enough to allow many more synthetic combinations.

The elemental analysis data was primarily used to calculate the concentration of tin chlorin e6 on each of the samples. Ideally, a similar approach to Murray *et al.*[137] would have been adopted, where the TGA data was employed. However, the TGA data were inconsistent. For example sample NNG.1 which has motif Au-GS had a total mass loss of 31.64% for the organic fragments. Upon addition of the tin chlorin e6 to obtain NNG.3 (Au-GS-SnCe6) the total mass loss from the organic fragment was only 23.72%. The residue left in the pan for each of the samples was consistently found to be elemental, crystalline gold by X-ray diffraction. The peaks observed correspond to the (111), (200), (220), (311) and (222) facets of the fcc crystal structure of elemental gold.

The infra red (IR) spectroscopy suggested the presence of glutathione on the gold nanoparticles. The absence of the characteristic SH vibration at 2524 cm^{-1} is absent from the samples synthesised with both motifs of Au-GS and Au-GS-SnCe6. This implies that the glutathione was successfully de-protonated and that the sulphur formed a covalent bond with the gold on the surface of the nanoparticle, however the IR resolution was too poor to detect this directly. Studies by Basu *et al.*[119] found that glutathione binds to gold surfaces through the sulphur, along with further stabilisation by the amine groups which anchor the glutathione to the surface of the gold nanoparticle. They found that this was dependant on the pH of the reaction medium. Lower pH values favour the thiol of the cystine and the primary amine of glutamic acid of the tripeptide glutathione, to bind effectively to gold surfaces. As the synthesis conditions of Au-GS nanoparticles used in this study require low pH it can be assumed that fewer amine groups were available for further functionalisation, such as the attachment of the photosensitiser tin chlorin e6. This is evident from the IR spectra of the samples with the motif Au-GS-SnCe6 (NNG.3, NNG.5 and NNG.7) where the detection of tin chlorin e6 was not possible. This maybe because the concentration of tin chlorin e6 in the KBr pellets was below the detection threshold limit. Additionally, the glutathione which is present in higher concentrations would help mask any tin chlorin e6 peaks as they have many common functional groups.

The presence of tin chlorin e6 on nanoparticles with motif Au-GS-SnCe6 (NNG.3, NNG.5 and NNG.7) was confirmed by UV-visible absorption spectroscopy. UV-visible absorption spectra were taken in deionised water and phosphate buffer solution. The Soret peak appears in spectra taken in both deionised water and phosphate buffer solution at approximately 400 nm. The other dominant peak appears at 630 nm and was observed in both deionised water and phosphate buffer solution. The surface plasmon absorption usually observed at approximately 535 nm, was very weak in all samples dissolved in water. This indicates that although nanoparticles with motifs Au-GS-SnCe6 and Au-GS are soluble in water, higher solubility is achieved in solutions with higher ionic strengths such as phosphate buffer solutions. Surface charge, due to adsorbed species on gold nanoparticles affect the overall stability of the solution from aggregation. The ionic strength of a solution determines the Debye length around the nanoparticle. Therefore, by using ionic strength, it is possible to adjust the mean encounter distance between the gold nanoparticles.[141] The adjustment in the ionic strength of the medium in which the nanoparticles are dissolved in is a particle independent method of altering the repulsion distance between charged particles. Increasing the ionic strength of a solution decreases the Debye length. Consequently, the average distance of closest approach between particles decreases. This would increase the surface plasmon communication between particles. As particles aggregate in solutions of higher ionic strength the surface plasmon absorption becomes more evident.

Samples with motifs Au-GS-SnCe6 displayed antimicrobial properties. Bacterial kills were observed, and they were in accordance with the concentration of tin chlorin e6 present. NNG.5 was the most effective at lethal photosensitisation of bacteria. This is unsurprising as NNG.5 had the highest concentration of tin chlorin e6 with 7.68 mg of SnCe6 per 100 mg of sample. Although all the samples had lethal photosensitisation properties, the kill was not significantly enhanced. This was a surprising result as chapter 2 showed that the attachment of a photosensitiser to gold nanoparticles enhances the bacterial kill observed. This may be the result of the medium the nanoparticles were dissolved in. The microbiology experiments were carried out in phosphate buffer solution, which whilst increasing solubility also increased aggregation of the nanoparticles, that may have hindered singlet oxygen production by the photosensitiser. Additionally, if there was more of the sample left after the microbiology experiments, the TGA and elemental analysis would have been repeated in order to obtain a more accurate values so that the Murray *et al.*[137] analysis of calculating the amount of ligand per nanoparticle could be performed. Another method of confirming the amount of tin chlorin e6 per nanoparticle would have been to use UV-visible spectroscopy. This could not be performed due to insufficient mass of sample.

3.5 Conclusion

Nanoparticles with motifs of Au-GS-SnCe6, in different diameters ranging from 1.73 to 6.24 nm were synthesised in a two step reaction. The attachment of the photosensitiser tin chlorin e6 to glutathione protected gold nanoparticles was confirmed by UV-visible absorption spectroscopy. The expected enhanced bacterial kill for nanoparticles with such motifs was not observed. However, this study has established that the synthetic route is robust enough for many different combinations of Gold-thiol-photosensitiser to be explored.

The next chapter describes experiments conducted with charge stabilised nanoparticles and photosensitisers. These experiments investigated the mechanism by which enhanced kill by lethal photosensitisation of bacteria was achieved when photosensitisers are brought in close proximity to gold nanoparticles.

Chapter 4 Charge Stabilised Gold Nanoparticles and Photosensitisers

This chapter describes the synthesis and chemical interactions of charge stabilised gold nanoparticles with dyes. The nanoparticles were synthesised by the citrate reduction method.[28] *Factors which affect the synthesis of the nanoparticles and their interaction with various light activated antimicrobial dyes have been examined. It was found that when a solution of thiazine dye is titrated against gold hydrosol, at a critical concentration (ca.* 3×10^{-6} *M) there is an enhanced maximum absorption in the dye. The extinction coefficient is increased by a factor of* $1\log_{10}$. *This was observed for all the family of thiazine dyes, of which methylene blue and toluidine blue are established light activated antimicrobial agents. The same enhancement was not observed for anionic, acidic dyes such as rose bengal. It was found that mixing these charge stabilised gold nanoparticles with thiazine dyes enhanced the kill of bacteria.*

4.1 Introduction

In this study, charge stabilised gold nanoparticles synthesised by a modified Turkevich synthesis[28] were mixed with light activated antimicrobial agents, for experiments in determining the lethal photosensitisation of bacteria. In this introduction key aspects of the synthesis are reviewed. Furthermore, the application of thiazine dyes in lethal photosensitisation of bacteria is discussed.

Turkevich's citrate reduction remains popular for the synthesis of gold nanoparticles. The reaction is rapid and results in very stable sols. Ferns[17] reported, by varying the amount of citrate added the size of nanoparticles obtained can be modified. Colloids obtained are typically 12 – 70 nm in diameter. The gold nanoparticle solutions used for these experiments were synthesised using a modified Turkevitch synthesis[28] and the colloids produced are discussed in further detail.

The Turkevich synthesis[28,142] is a redox reaction where the oxidation of citrate produces acetone dicarboxylic acid, which in turn reduces Au(III) to Au(0). The formation of acetone dicarboxylic acid creates an induction period in the reaction. This induction period decreased with temperature, the required activation energy was *ca.* 15 kcal/mol. This was then followed by a nucleation step, resulting in rapid formation of a solution, super saturated with nuclei. The nuclei had a diameter of 1-2 nm and occurred approximately 5 seconds after the addition of the citrate. This was indicated by the colourless solution and absence of plasmon absorbance in the range of 500-900 nm. The synthesis of acetone dicarboxylic acid is the limiting factor for the reaction:

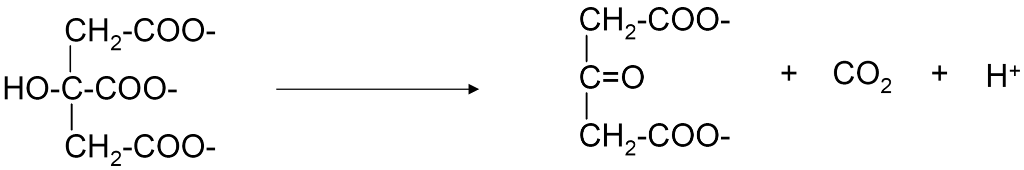

$$\mathrm{HO\text{-}}\overset{\mathrm{CH_2\text{-}COO\text{-}}}{\underset{\mathrm{CH_2\text{-}COO\text{-}}}{\mathrm{C}}}\mathrm{\text{-}COO\text{-}} \longrightarrow \overset{\mathrm{CH_2\text{-}COO\text{-}}}{\underset{\mathrm{CH_2\text{-}COO\text{-}}}{\mathrm{C{=}O}}} + \mathrm{CO_2} + \mathrm{H^+}$$

4-1

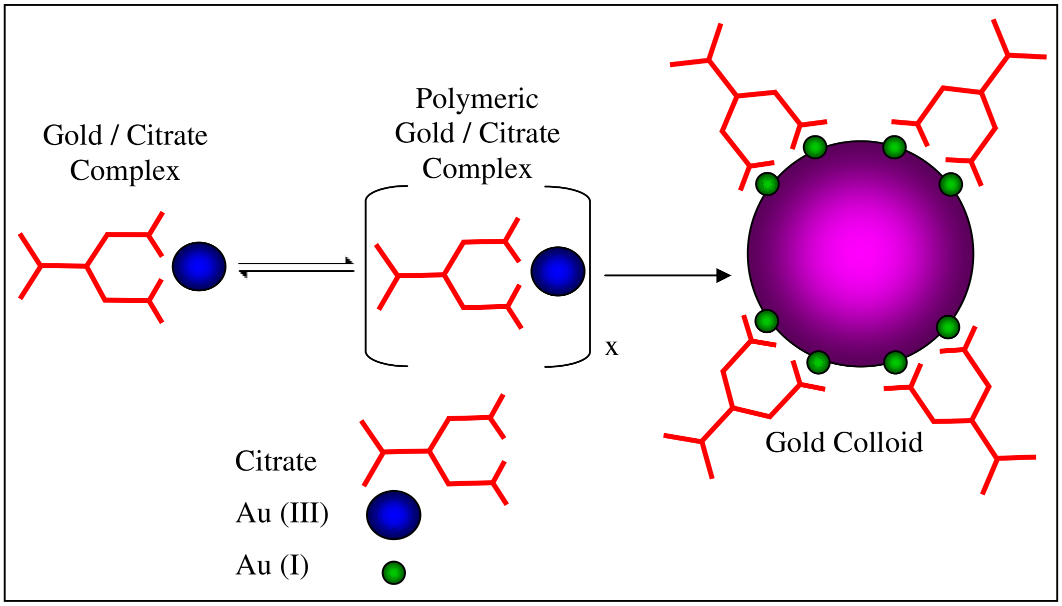

Figure 4-1 ***Schematic diagram adapted from Sandroff and Herschbach[44] which represents colloidal gold in the citrate complex. The citrate is strongly bound at sites where oxidation states of the gold +1.***

Sandroff and Herschbach[44] expanded on Turkevich's work. They concluded that the citrate ion remained strongly bound to the surface of the gold nanoparticle, providing a negative charge on the surface. The results were rationalised by the assumption that there were molecular donor and acceptor sites on the surface, which acted as either a Lewis acceptor or donor site. The Lewis acceptor surface sites comprised of a gold complex in a high oxidation state, and were readily reduced by electron donors with low ionisation potentials. The donor, or Lewis base, sites behaved like neutral metal and donated charge to electron acceptors with high electron affinity (Figure 4-1).

Geuze and Slot[29] reported the formation of colloidal gold by three independent processes:

1. Reduction step. Au^{3+} is reduced to form a supersaturated solution.
   $AuCl_{4(aq)}^{-} + 3e^{-} \rightarrow Au_{(s)} + 4Cl_{(aq)}^{-}$
2. Nucleation step. Gold atoms start to associate and begin to form seeds.
3. Growth step. This occurs due to gold condensation on the surface of the nuclei.

This is in general agreement with Turkevich's conclusions.[142]

Chow and Zukoski[43] showed that at the beginning of the reaction, however, large branched particles of high porosity were formed. As the reaction proceeded, the nanoparticle size decreased by splitting because of instability. This conclusion was reached using several analytical techniques such as TEM, UV-visible spectroscopy and light scattering. The results were visible during the reaction as the colours changed from colourless to black to blue to purple to red.

The dependence of the surface plasmon resonance absorption wavelength on the size of the particle was reviewed by Liz-Marzan.[143] From calculated data (Figure 4-2) by Khlebtsov *et al.*[144] it can be seen that particle size affects the position of the surface plasmon band in an absorption spectra. Furthermore, it was found by Link and El-Sayed[14] that the bandwidth of the surface plasmon resonance absorption peak strongly depends on particle size (Figure 4-2). From their plot it can be observed that the width first decreases with increasing particle size reaching a minimum at 22 nm particles, and then increases again.

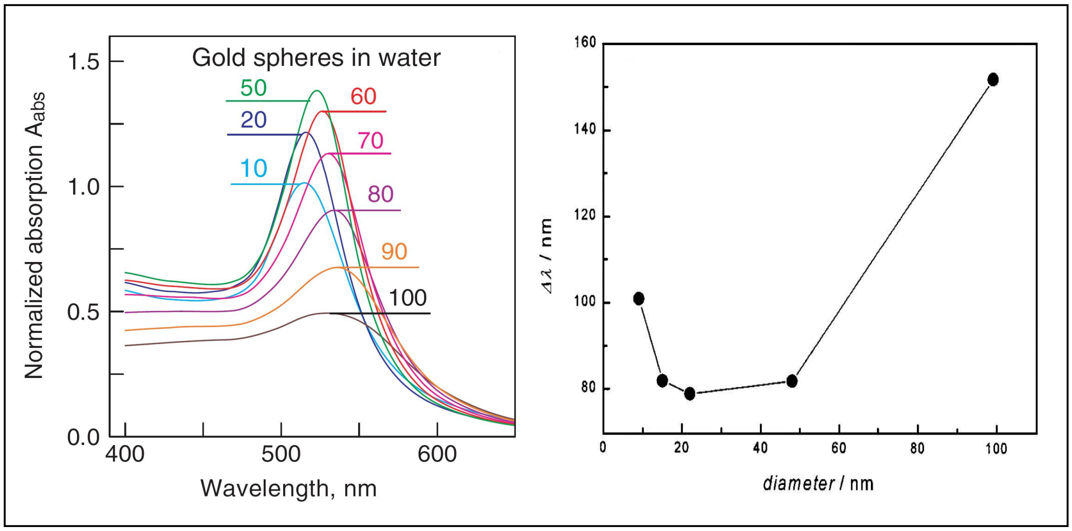

Figure 4-2 ***Normalized absorption spectra $A_{abs}(\lambda)$ of gold spheres with diameters of 10–100 nm in water[144] (left). Surface plasmon bandwidth as a function of particle diameter[14] (right).***

From calculated data collected by Liz Marzan[143] it was found that an increase in diameter from 10 up to 100 nm leads to a red shift of 47 nm. However an increase in aspect ratio for prolate ellipsoids, from 2.5 to 3.5 (smaller size variation) promotes a red shift of the longitudinal surface plasmon band by 92 nm, almost double that of the size effect. The shift in surface plasmon resonance has been used for the detection of DNA.[55] The peak position after the attachment of small proteins to the surface of charge stabilised gold nanoparticles has been modelled by Khelbtsov *et al.*[145] and the data are shown to be in excellent agreement with experimental data.

The world-wide increase of antibiotic-resistant strains of some bacterial species highlights the urgent need to develop novel, alternative therapeutic approaches for infectious diseases. PDT involves the combination of a light-activated agent (photosensitiser) and light of a specific wavelength to achieve lethal photosensitisation of the target organism.[74] The photosensitiser absorbs a photon of light and undergoes an energy state transition from the ground state to a higher energy triplet state. The activated triplet state can interact with molecular oxygen, generating singlet oxygen. Singlet oxygen is highly reactive and can diffuse up to 100 nm from the site of generation, damaging cell walls, plasma membranes and DNA, leading to death of the microbial cells.[146] The singlet oxygen generated can also interact with solvent and substrate molecules producing free radicals and radical ions.

Thiazine dyes absorb between 550-700 nm, and have a characteristic blue colour. Toluidine blue is used in staining of various cells, and in conjunction with malachite green for the staining of lipids. Both toluidine blue and methylene blue are used in the diagnosis of cancerous tissue. It was found by Bellin *et al.*[81] that tumour cells were susceptible to killing by light, when treated with methylene blue. These light activated antimicrobial agents are promising alternatives for the treatment of topical infections. The use of these antimicrobial agents in conjunction with nanoparticles and a bacterial recognition moiety is advantageous. They are more effective at killing bacteria since the oxygen produced is concentrated at the bacterial cell wall. Also, there is selective killing, since binding of the photosensitiser is in close proximity to the target organism, and this reduces the collateral damage to neighbouring healthy cells.[92]

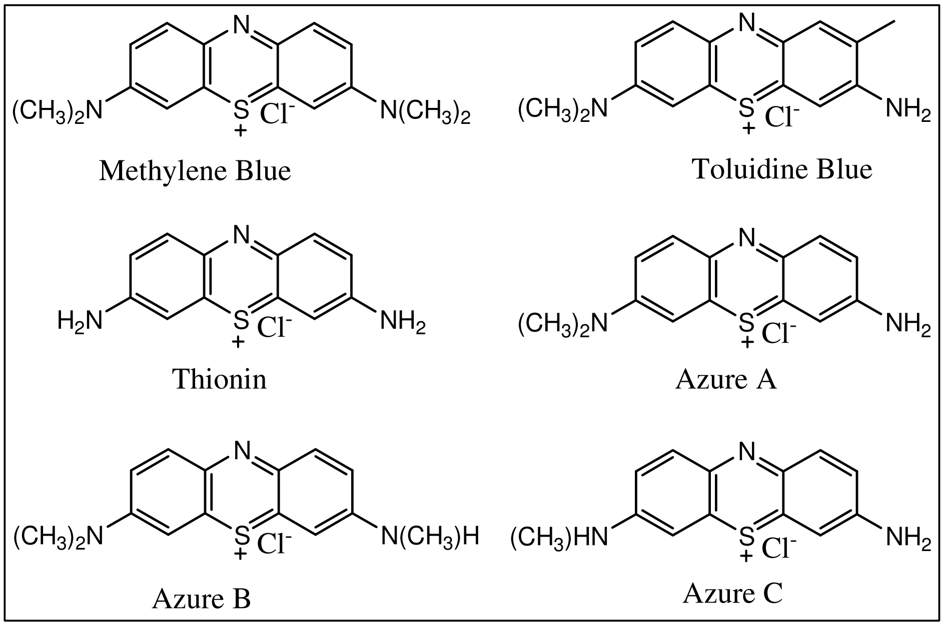

Figure 4-3 ***Structures of the thiazine family of dyes***

Some of the emerging light activated antimicrobial agents are dyes, more frequently used in bacterial staining. Methylene blue is a metachromatic dye commonly used in the staining of nuclei. Oxidation of methylene blue produces Azure A, B and C. Other closely related dyes are toluidine blue and thionin which all comprise the group of thiazine dyes (Figure 4-3).

Gold nanoparticles have nonspecific adsorption properties, which have allowed their use as tracers for proteins. However, full characteristics at a molecular level of the gold particle suspension and the adsorption of proteins have not yet been subject to a full study.[147] Factors affecting adsorption of dyes onto gold nanoparticles include: particle size, relative molecular weight of the dye and the pH.

When proteins, such as bovine serum albumin, are adsorbed onto the surface of gold nanoparticles, the maximum number of molecules that can be associated with a single particle is linearly related to the average projection area of the particle. The size of the particle would therefore affect the adsorption of dyes onto a surface. If it is assumed that the area occupied by the dye will be equal to its projection onto the gold particle surface, a monomolecular shell of dye covering the nanoparticle would result. Therefore, large dye molecules, have a lower number of molecules in contact with the gold nanoparticle surface. The effect of pH has not been investigated thoroughly in protein adsorption. However, since charge stabilised nanoparticles aggregate when electrolytes are added, the small increase in ionic strength causes aggregation of the particles.

Antimicrobial PDT has great potential as a therapeutic approach to eradicating microbial infections. Therefore enhancing the efficacy of known photosensitising agents of this therapeutic approach is highly desirable. The work presented here shows that gold nanoparticles enhance the effectiveness of an established photosensitiser: toluidine blue (TBO), against the important human pathogen *Staphylococcus aureus*.

4.2 Experimental

Synthesis of charge stabilised gold nanoparticles: All glassware was washed with aqua regia (3HCl:1HNO_3), followed by rinsing with copious amounts of water. All water used in the experiments is double distilled water (except where stated).

Stock Solutions: $HAuCl_4.3H_2O$ (42 mg, 0.11 mmol) was dissolved in deionised water (25 mL) to form solution A (~5 mM). $Na_3C_6H_5O_7.2H_2O$ (125 mg, 0.43 mmol) was dissolved in deionised water (25 mL) to give solution B (~20 mM).

Solution A (1 mL) was stirred with deionised water (18 mL) and boiled for 2 min. Then solution B (1 mL) was added drop wise over a period of approximately 50 sec. causing the colour change from clear to blue to pink/purple. After a further 1 min. of heating, the solution was left to cool to room temperature.

Titration experiments: dye solution (1 mL) was added to the nanoparticle solution (16 mL). This was stirred and a cuvette was filled to take a UV-visible absorption spectrum. The solution was not discarded but added back to the original mixture. Another 1 mL of dye solution was added etc. This was repeated 10, 15 or 20 times depending on the experiment.

Concentrations of Dyes:

Dye	Concentration (µM)
Toluidine Blue	5
Methylene Blue	5
Thionin	10
Azure A	10
Azure B	10
Azure C	10
Tin Chlorin E6	200
Rose Bengal	50
Rhodamine B	50

Table 4-1 ***Dyes and concentrations used for the titration experiments.***

Bactericidal assays: The bacterial assays were carried out at the Eastman Institute in collaboration with Sarah Tubby.

S. aureus (NCTC 6571) was maintained by weekly sub-culture on blood agar base (Oxoid Ltd, Basingstoke, UK) supplemented with 5% (v/v) horse blood. For experimental purposes, a few colonies of the organism were inoculated into nutrient broth No. 2 (Oxoid) and grown aerobically for 16 h at 37 °C. Cells were then harvested by centrifugation and re-suspended in sterile phosphate buffered saline (PBS) to an OD-$_{600}$ of 0.05 which corresponded to approximately 10^7 – 10^8 colony-forming units (cfu)/mL.

The light source used in this study was a General Electric® 28W Biax 2D compact fluorescent lamp which emits light across the visible spectrum. Prominent peaks were present at 435, 495, 545, 588 and 610 nm. The lamp was fitted into a refrigerated incubator (LTE Scientific Ltd, Oldham, UK) which maintained the temperature at a constant 22°C. The light intensity was measured using a digital luxmeter (Hagner Photometric Instruments Ltd, Bosham, UK) and was 3500-3700 lux. The photosensitiser, TBO, was purchased from Sigma-Aldrich (Dorset, UK).

Aqueous suspensions of gold nanoparticles were mixed with an equal volume of aqueous TBO and left at room temperature for 15 minutes. TBO was used at a final concentration of 1, 5, 10, 20 or 50 μM. The TBO-nanoparticle mixture (100 μL) was added to a suspension of *S. aureus* NCTC 6571 in phosphate buffered saline (PBS) (100 μL) and samples were irradiated with white light for 10 minutes (L+S+G+). *S. aureus* + PBS without photosensitiser or gold nanoparticles and which was not irradiated (L-S-G-) and irradiated samples of *S. aureus* + TBO only (L+S+G-) and *S. aureus* + PBS, without photosensitiser or gold nanoparticles (L+S-G-) were used as controls. The final concentration of nanoparticles used was 1 × 10^{15} particles/mL. The light intensity at the surface of the microtitre plate was 3,700 ± 20 lux. After irradiation, the number of surviving bacteria were determined by viable counting. The experiments were carried out in duplicate and on two separate occasions.

Singlet oxygen measurements: Singlet oxygen measurements employed the second harmonic (l_{ex} = 532 nm) of a Q-switched Spectra Physics GCR-150.10 Nd:YAG laser as the excitation source (~1 mJ per pulse, ~5 ns full-width at half-maximum); a tungsten-halogen lamp was used as the probe source. Detection was achieved using a monochromator (instruments SA Triax 320) coupled to a photomultiplier tube (Hamatsu R928). The phosphorescence from the sample was collected at 90º, was centred at 1270 nm (Infra Red Engineering Ltd., Essex UK) and then focused onto the active area of a liquid nitrogen-cooled germanium photodiode (North Coast EO-817P). The output from this device was AC coupled to a digital oscilloscope (Tektronix TDS-320), which digitized and averaged transients. Typically 20 laser shots were used for each sample. The transmitted light was monitored by a tektronix TDS-320 digital oscilloscope and the transferred to a personal computer (PC) for storage and analysis. The emission was measured for the toluidine blue/ gold nanoparticles solutions in D_2O.

Particle size measurements: Photon correlation spectroscopy (PCS), using a Zetasizer 3000 (Malvern, UK) was used to measure the hydrodynamic diameter of the gold nanoparticles in different concentrations of methylene blue. The measurements were conducted in plastic cuvette in distilled water at 25°C, and a z-average diameter of the particles was reported.

Fluorescence measurements: The measurement of fluorescence from the TBO and gold nanoparticle mixtures was determined on a Perkin Elmer LS50B spectrometer, with an excitation wavelength of 600 nm. The emission spectra were measured in 1 cm quartz luminescence cuvettes containing the TBO and gold nanoparticle solutions.

UV-visible absorption measurements: UV-visible absorption spectra (200–1100 nm, 1 nm resolution) of aqueous solutions in 1 cm quartz cells were recorded with a ThermoSpectronic, Heλios-λ UV-visible absorption spectrometer.

High resolution transmission electron microscopy (HRTEM): Samples were prepared by evaporating the required specimen on a carbon coated copper grid. Bright field TEM images were acquired using with an electron microscope operated at 100 kV (Joel 100CX). Typical magnification of the images was 100 000×. Analysis of the images was performed using the software program Image J.[116]

4.3 Results

Titration Experiments with Thiazine Dyes:

Thiazine dyes of specific concentrations (Table 4-1) were added in 1 mL aliquots to 16 mL of gold nanoparticle solution, which had been synthesised by a citrate reduction of aqueous hydrogen tetrachloroaurate. Immediately, after each addition a UV-visible absorption spectrum was taken. The same procedure was carried out for the anionic dyes tested.

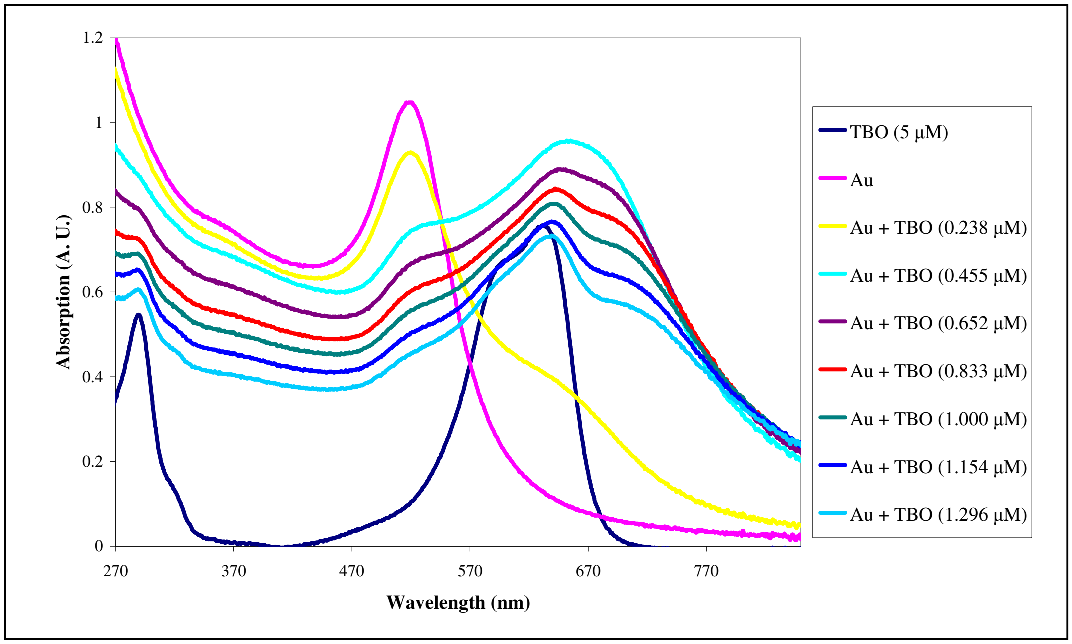

Figure 4-4 ***UV-visible absorption spectra showing the effect of increasing the concentration of toluidine blue (TBO) in a gold nanoparticle solution. The total toluidine blue concentration of 0.238 μM (yellow line) was obtained by the addition of 1 mL of toluidine blue (5 μM) to 16 mL of gold nanoparticle solution.***

A maximum enhancement of the dye absorption was observed after 2 additions of toluidine blue (5 μM), where there was a total toluidine blue concentration of 0.455 μM in the reaction mixture. The maximum enhanced absorption was observed at 652 nm to 655 nm. A gradual decrease in the nanoparticle surface plasmon resonance absorption was observed at 530 nm, which can be attributed to the increase in total volume; hence decrease in gold nanoparticle concentration. After the initial 2 additions of toluidine blue there was a gradual decrease in the maximum absorption of the gold nanoparticles and dye (Figure 4-4).

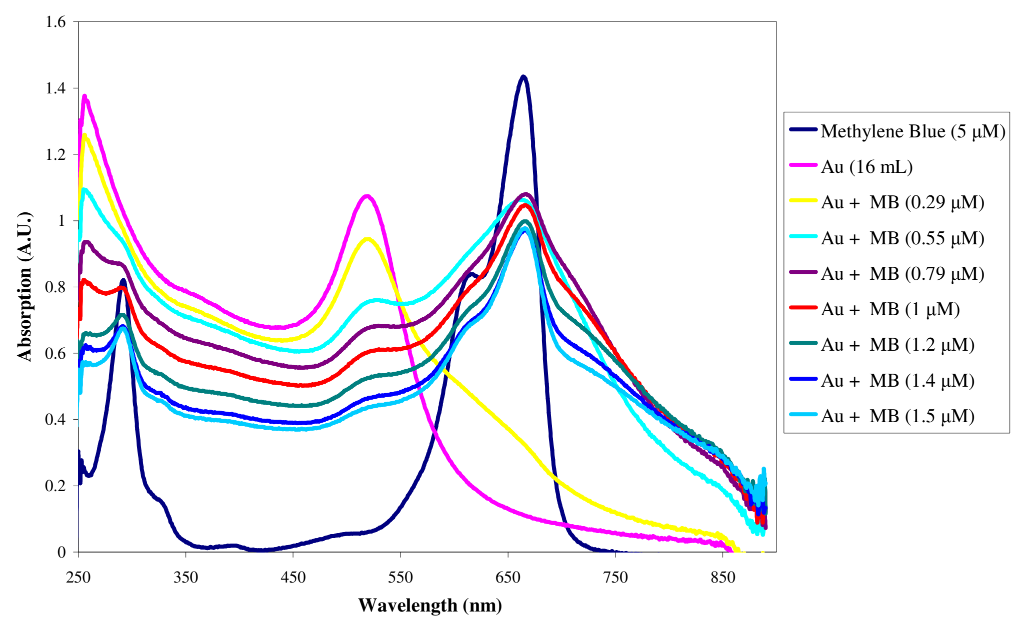

Figure 4-5 ***UV-visible absorption spectra showing the effect of increasing the concentration of methylene blue (MB) on a gold nanoparticle solution. The total methylene blue concentration of 0.29 µM (yellow line) was obtained by the addition of 1 mL of methylene blue (5 µM) to 16 mL of gold nanoparticle solution.***

After the third 1 mL addition of methylene blue (5 µM) to a gold nanoparticle solution (16 mL), a total methylene blue concentration of 0.79 µM was obtained. At this concentration an enhancement of the dye absorption in the gold nanoparticle solution was observed. The maximum enhanced absorption was observed at 667 nm. There was a gradual decrease in the nanoparticle surface plasmon resonance absorption at around 530 nm, which can be attributed to the increase in total volume, hence decrease in gold nanoparticle concentration. After the initial 3 additions of methylene blue there was a gradual decrease in the maximum absorption of the gold nanoparticles and dye (Figure 4-5).

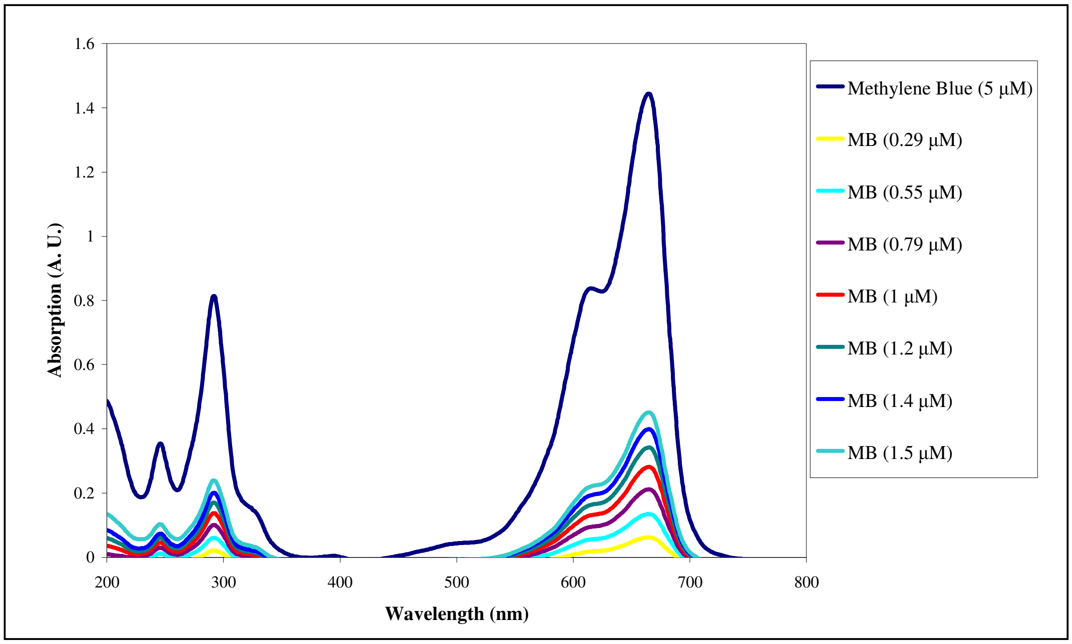

Figure 4-6 ***UV-visible absorption spectra showing the effect of increasing the concentration of methylene blue (MB) an aqueous solution. The total methylene blue concentration of 0.29 µM (yellow line) was obtained by the addition of 1 mL of methylene blue (5 µM) to 16 mL of deionised water.***

As predicted by the Beer-Lambert law[46] the effect of increasing the concentration of a dye increases its absorption. The effect of increasing concentration of methylene blue in aqueous solution is shown in Figure 4-6. At a methylene blue concentration of 0.79 µM in a gold nanoparticle solution the absorbance is greater than 1 (Figure 4-5). However, at the same methylene blue concentration in water the absorbance is around 0.2. The same trend was observed for all thiazine dyes. The thiazine dyes tested were Thionin (Figure 4-7), Azure A (Figure 4-8), Azure B (Figure 4-9), and Azure C (Figure 4-10). The enhanced absorptions in gold nanoparticle solutions for thionin, azure A, azure B and azure C were not as significant as methylene blue and toluidine blue. Additionally, a much higher concentration was required for this enhanced absorption to be observed.

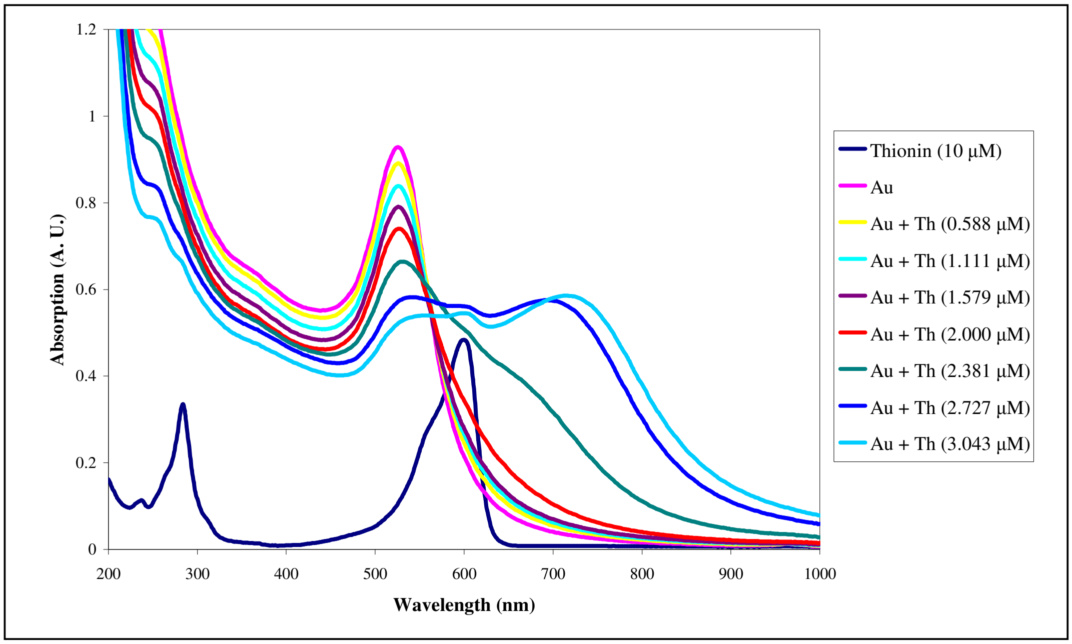

Figure 4-7 ***UV-visible absorption spectra of thionin (Th) in a gold nanoparticle solution. The total thionin concentration of 0.588 µM (yellow line) was obtained by the addition of 1 mL of thionin (10 µM) to 16 mL of gold nanoparticle solution. The maximum absorption at 604 nm was observed after 6, 1 mL additions of thionin (10 µM), where the final concentrations was 2.727 µM.***

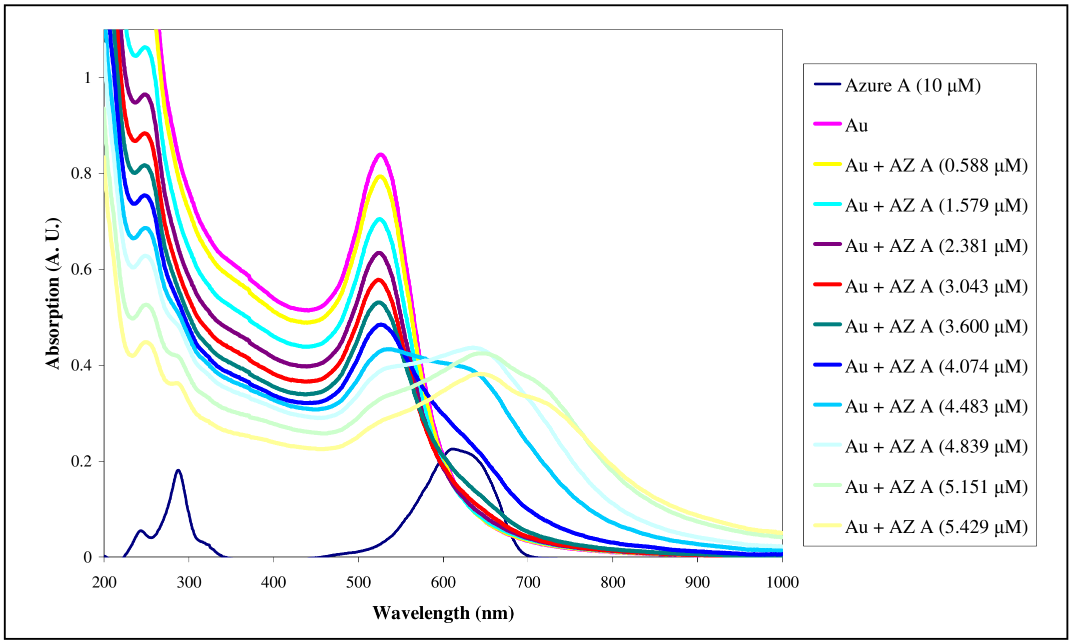

Figure 4-8 ***UV-visible absorption spectra of azure A (Az A) in a gold nanoparticle solution. The total azure A concentration of 0.588 µM (yellow line) was obtained by the addition of 1 mL of azure A (10 µM) to 16 mL of gold nanoparticle solution. The maximum absorption at 635 nm was observed after 15 additions of 1 mL azure A (10 µM) where the final concentration was 4.839 µM.***

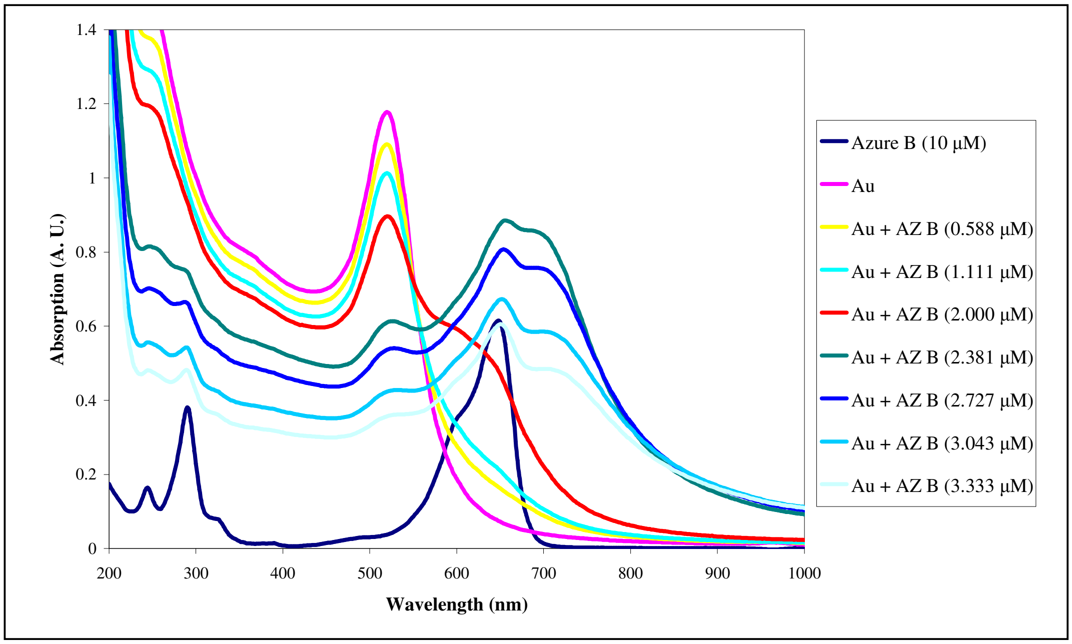

Figure 4-9 ***UV-visible absorption spectra of azure B (Az B) in a gold nanoparticle solution. The total azure B concentration of 0.588 µM (yellow line) was obtained by the addition of 1 mL of azure B (10 µM) to 16 mL of gold nanoparticle solution. The maximum absorption at 656 nm was observed after 4 additions of 1 mL azure B (10 µM) where the final concentration was 2.381 µM.***

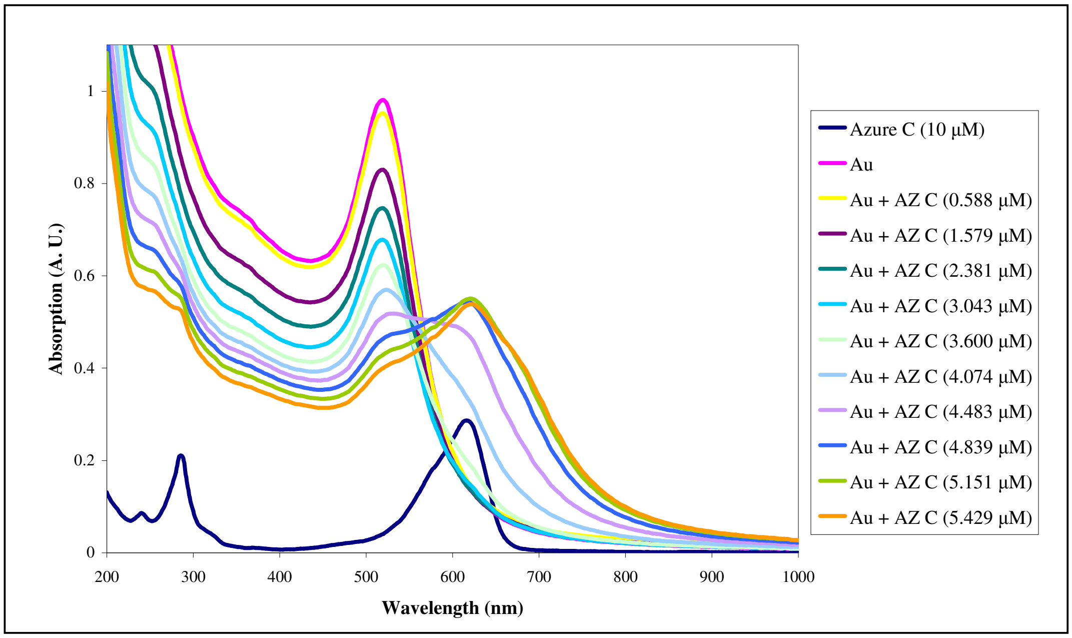

Figure 4-10 ***UV-visible absorption spectra of azure C (Az C) in a gold nanoparticle solution. The total azure C concentration of 0.588 µM (yellow line) was obtained by the addition of 1 mL of azure C (10 µM) to 16 mL of gold nanoparticle solution. The maximum absorption at 620 nm was observed after 17 additions of 1 mL Azure C (10 µM) where the final concentration was 2.381 µM.***

Dye	e (M^{-1} cm^{-1})	λ_{max}	Enhanced e (M^{-1} cm^{-1})	Enhanced λ_{max}	Enhanced Absorbance (A.U.)	Absorbance if no enhancement (A. U.)
Methylene Blue	2.9×10^{5}	664	1.1×10^{6}	667	1.08-0.23	0.23
Toluidine Blue	1.5×10^{5}	631	1.6×10^{6}	652	0.96-0.23	0.08
Thionin	4.8×10^{4}	600	1.2×10^{5}	714	0.59-0.27	0.15
Azure A	2.3×10^{4}	611	5.4×10^{4}	638	0.44-0.18	0.11
Azure B	6.1×10^{4}	648	2.7×10^{5}	656	0.89-0.25	0.15
Azure C	2.9×10^{4}	616	1.6×10^{5}	620	0.55-0.18	0.15

Table 4-2 ***Summary of extinction coefficients and absorption data for thiazine dyes in solution and adsorbed on to gold nanoparticles in solution.***

Table 4-2 summarises the extinction coefficients along with the enhanced extinction coefficients for all of the thiazine dyes. There was an average of around 1 log maximum enhancement when these dyes were titrated against gold nanoparticles compared to when they were titrated against water. By evaluating the various absorbance values of the thiazine dyes in the presence and absence of gold nanoparticle solution, there was an obvious increased absorption when the gold nanoparticles were present at specific concentrations. At a toluidine blue concentration of 0.455 μM, when mixed with gold nanoparticle solution the extinction coefficient of the dye was 1.6 x 10^{6} $M^{-1}cm^{-1}$ at 631 nm. A solution of toluidine blue in water at the same concentration had an extinction coefficient of 1.5 x 10^{5} $M^{-1}cm^{-1}$ at 631 nm. There is, therefore, an enhancement of more than one order of magnitude in the extinction coefficient at 631 nm when gold nanoparticles are present at low concentrations of toluidine blue. At higher concentrations, the increase in the maximum absorption at 631 nm becomes less with each addition. This corresponds best with saturation of the gold nanoparticle surface by the dye and further addition of the dye (> 100 μM) induces precipitation.

Example of how the values in Table 4-2 were calculated.
Extinction coefficient of methylene blue *e:*
Max absorption of methylene blue at 664 nm is 1.434
The concentration methylene blue was 5×10^{-6} M
$A = C \times l \times e$

$e = A \div (C \times l)$ $e = 1.434 \div (5 \times 10^{-6} \times 1)$ $e = 2.8 \times 10^{5}\ M^{-1}cm^{-1}$

Maximum enhanced absorption was observed after 3 additions of methylene blue (5×10^{-6}).

Moles of methylene blue in 3 mL:

$(3 \times 10^{-3}) \times (5 \times 10^{-6}) = 1.5 \times 10^{-8}$ mol.

Total volume where maximum enhanced absorption was observed:

16 mL (gold nanoparticles) + 3 mL (methylene blue) = 19 mL.

Concentration of methylene blue in the reaction mixture:

1.5×10^{-8} mol $\div\ 19 \times 10^{-3}$ L = 7.89×10^{-7} M.

Extinction coefficient of methylene blue (7.89×10^{-7} M) when gold nanoparticles are present.

Maximum enhanced absorption of methylene blue at 667 nm:

1.08 – 0.23(background) = 0.85,

$e = 0.85 \div (7.89 \times 10^{-7} \times 1)$, $e = 1.1 \times 10^{6}\ M^{-1}cm^{-1}$

Absorbance of methylene blue at concentration 7.89×10^{-7} M, when gold nanoparticles are not present:

$A = 7.89 \times 10^{-7} \times 1 \times 2.9 \times 10^{5}$. $A = 0.23$

A buffer solution was introduced into the titration experiments in order to investigate the effect of induced aggregation on the enhanced dye absorption. The addition of a buffer did not appear to affect the titration with methylene blue (Figure 4-11). However, there is an additional absorbance broad peak just below 800 nm, which was not present in the methylene blue titration alone with gold nanoparticles (Figure 4-5). This additional shoulder was probably an artefact of the aggregation induced by KCl. The enhanced absorbance peak of the methylene blue was present along with the additional aggregation shoulder. Therefore the absorbance associated with the dye was enhanced, and was not the result of aggregation of the gold nanoparticles because this peak occurs at a higher wavelength in this case.

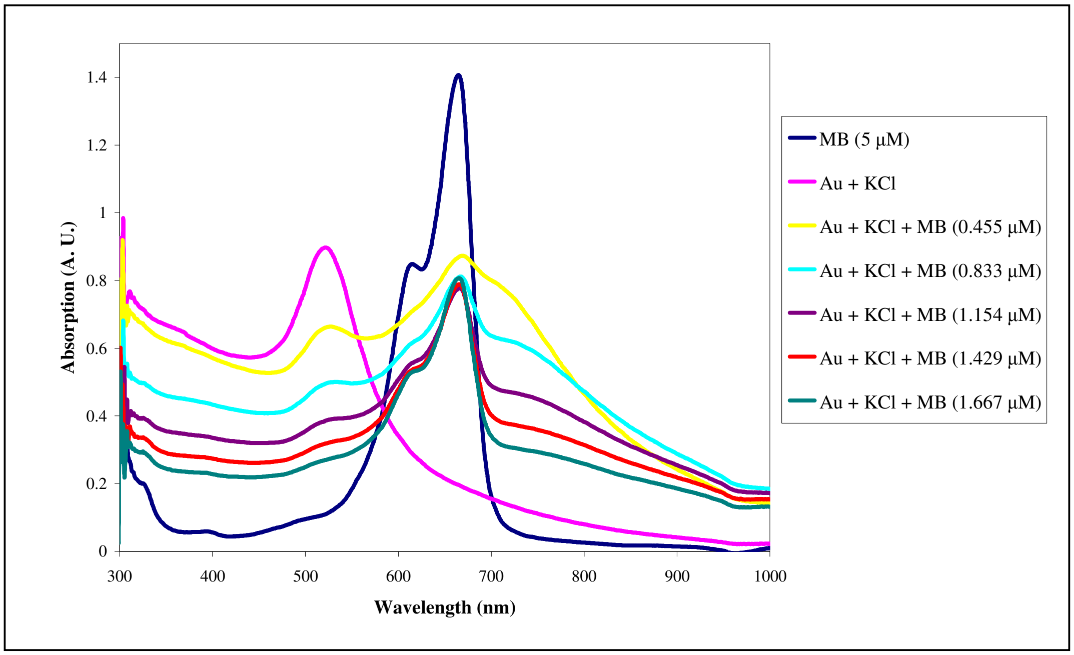

Figure 4-11 ***UV-visible absorption spectra of gold nanoparticles with increasing concentrations of methylene blue in the presence of KCl (1×10^{-3} M). The total methylene blue concentration of 0.29 µM (yellow line) was obtained by the addition of 1 mL of methylene blue (5 µM) to 16 mL of gold nanoparticle solution with KCl (1×10-3M). An enhanced absorption peak is observed at ca. 680 nm and an aggregation peak is observed at just below 800 nm.***

The point at which aggregation occurs by the addition of methylene blue was further investigated using photon correlation spectroscopy (PCS) with a Zetasizer 3000. This was used to measure the hydrodynamic diameter of the gold nanoparticles as the concentration of methylene blue increased. The experiments were carried out by performing the same titration experiments as before, but data were collected on a Zetasizer instead of a UV-visible absorption spectrometer. The measurements were conducted in plastic cuvette in distilled water at 25 °C, and a z-average diameter of particles was reported.

As illustrated by Figure 4-12, there was no appreciable aggregation of the nanoparticles at the methylene blue concentration of 0.79 µM. There was no significant aggregation of the nanoparticles until the concentration of methylene blue reached 2.1 µM, much higher than the concentrations at which enhanced UV-visible absorption of the dye was observed.

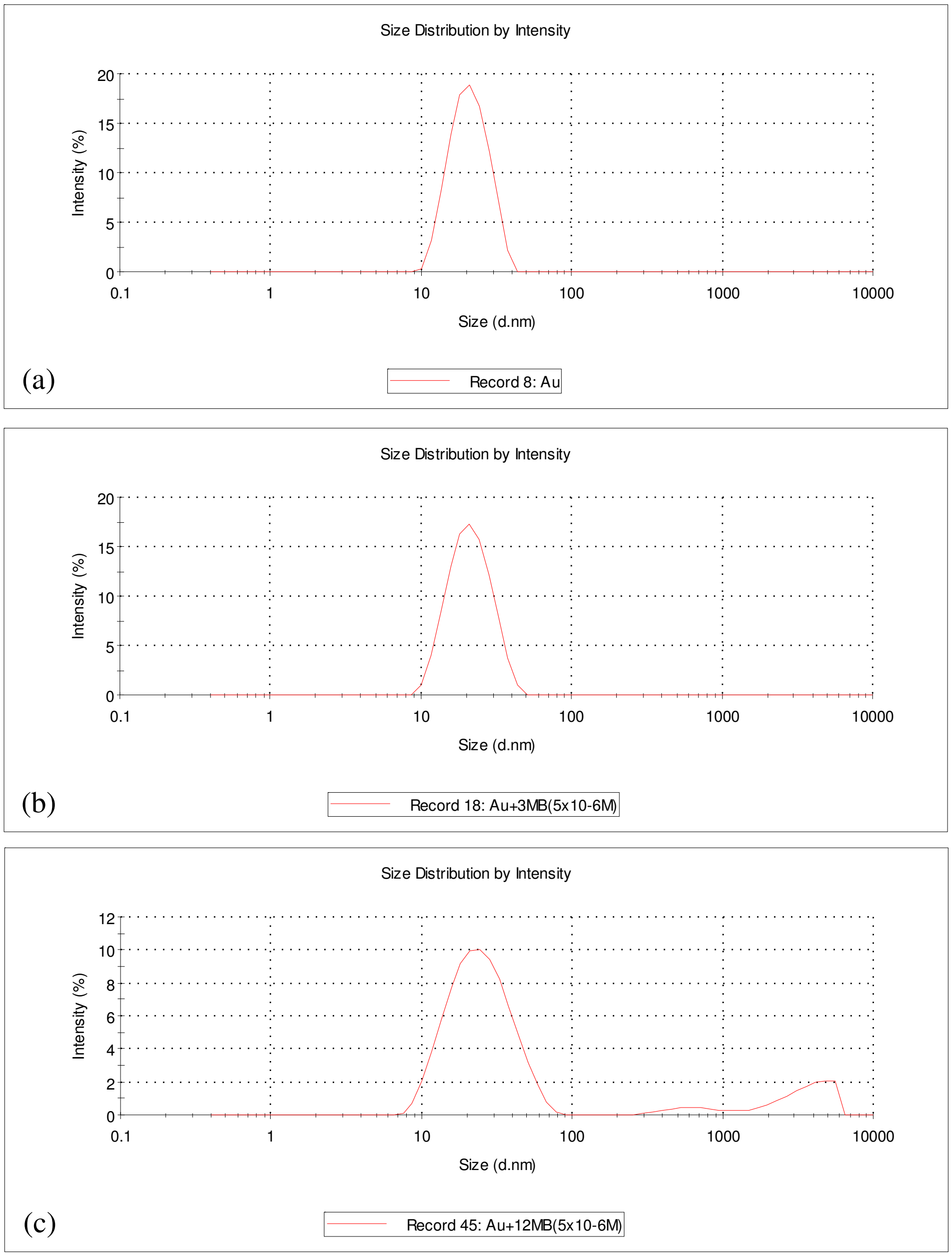

	Au (a)	Au + MB (0.79 µM) (b)	Au + MB (2.1 µM) (c)		
Peak	1	1	1	2	3
Size (nm)	21.4	21.9	26.3	693	3740
Intensity	100%	100%	84.2	3.2	12.6
Width (nm)	6.78	4.51	12.2	1240	1240

Figure 4-12 *The results from photon correlation spectroscopy (PCS) with a Zetasizer 3000 to measure the size distribution of (a) gold nanoparticle solution, (b) gold nanoparticle solution with methylene blue (0.79 µM) and (c) gold nanoparticle solution with methylene blue (2.1 µM).*

Titration Experiments with Anionic Dyes:

The same titration experiments were performed using anionic dyes. Tin chlorin e6 has been investigated as a possible LAAA.[91] It has higher yields of singlet oxygen when compared to other related chlorins, and has reactive carboxylic groups on the side chains outside the polycyclic core, where antibody targeting moieties can be conjugated.

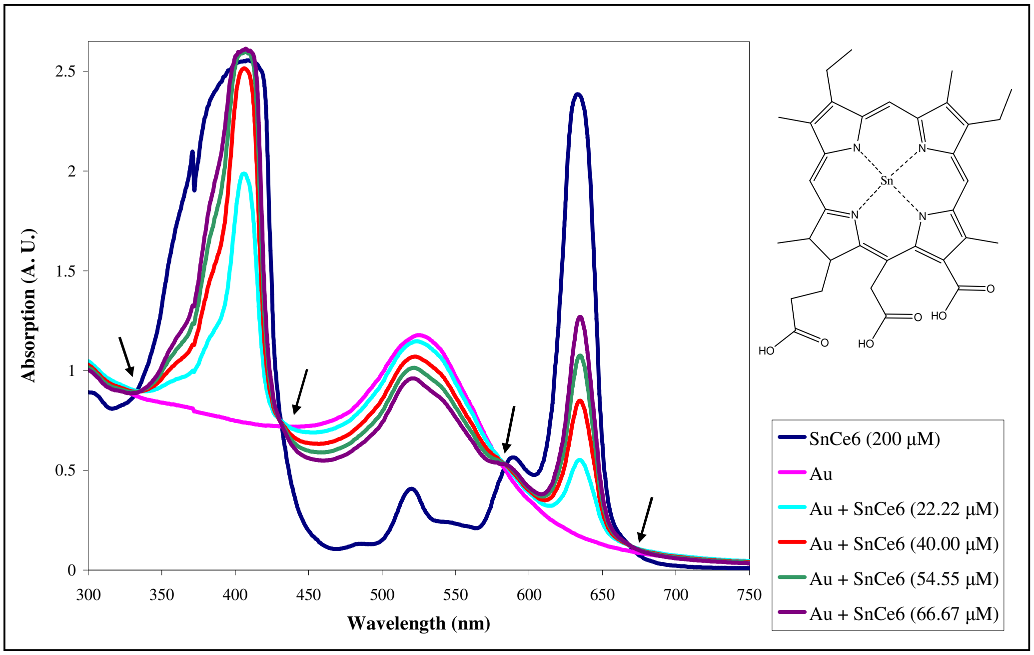

Figure 4-13 ***UV-visible absorption spectra tin chlorin e6 (SnCe6) in a gold nanoparticle solution. The total tin chlorin e6 concentration of 22.22 μM (turquoise line) was obtained by the addition of 2 mL of tin chlorin e6 (200 μM) to 16 mL of gold nanoparticle solution. The structure of structure of tin (IV) chlorine e6 is displayed at the top right of the figure. The four isosbestic points are indicated with the black arrows.***

Unlike the thiazine dyes there was no enhancement of the dye peak (Figure 4-13). There was a linear increase in the dye peaks of the absorption at approximately 400 nm and 625 nm, which corresponds to the increase in concentration. There was a familiar decrease in the nanoparticle peak which was a dilution effect. There were four isosbestic points on the UV spectra (372 nm, 422 nm, 612nm, 655 nm), which correspond to the wavelength at which the dye and the gold nanoparticle had the same extinction coefficients. The isosbestic points occur because the nanoparticle solution and the dye solution absorb light of that specific wavelength to the same extent regardless of the relative concentrations. There was no electronic communication between the dye and nanoparticle, hence isosbestic points were observed in the UV spectra. If there was electronic communication between the dye and nanoparticle, there would be an enhanced or shifted absorption (due to nanoparticle aggregation), and therefore no isosbestic would points appear.

As mentioned in Chapter 1, rose bengal is a red acidic anionic dye which has also been investigated as a LAA agent[82] and was titrated against gold nanoparticle solution in this investigation.

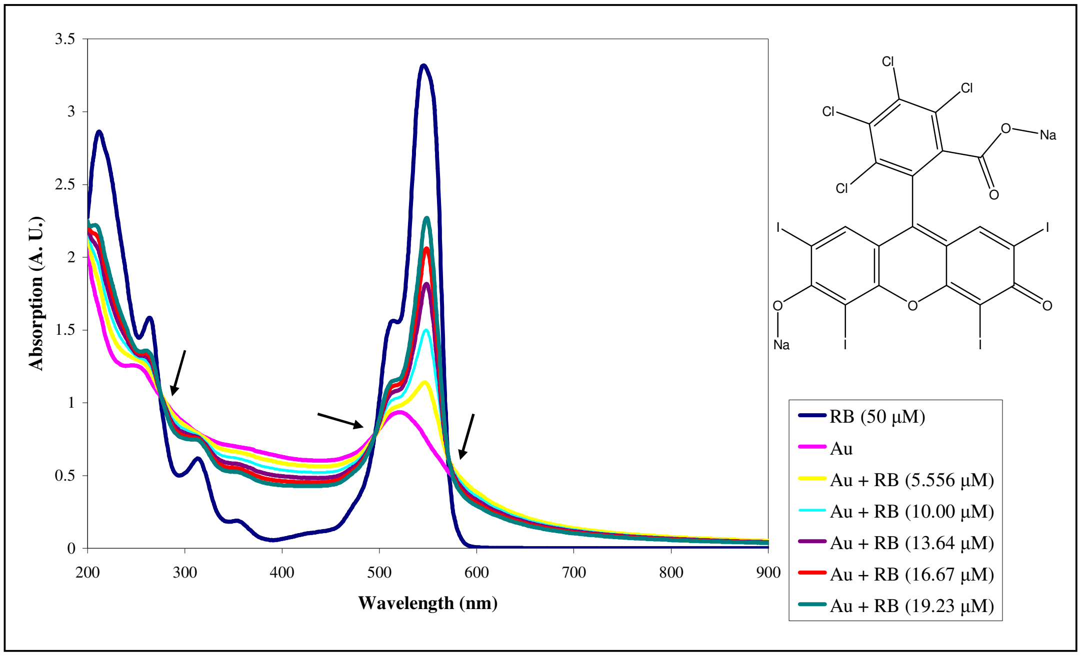

Figure 4-14 ***UV-visible absorption spectra of rose bengal (RB) in a gold nanoparticle solution. The total rose bengal concentration of 5.556 µM (yellow line) was obtained by the addition of 2 mL of rose bengal (50 µM) to 16 mL of gold nanoparticle solution. The structure of rose bengal is displayed at the top right of the figure. The three isosbestic points are indicated with the black arrows.***

The dilution effect of the gold nanoparticle solution was not observed in the rose bengal titration (Figure 4-14) as the gold nanoparticle surface plasmon absorption peak is overlapped by the rose bengal absorption peak. Again there was no enhancement of the maximum absorption of the rose bengal which would then be followed by a gradual decrease. There was an increase in the maximum absorption peak of the rose bengal which corresponds to the increase in concentration of rose bengal. There were three isosbestic points on the UV-visible absorption spectrum (270 nm, 497 nm, 574 nm) where the extinction coefficients of the dye and gold nanoparticle solution were equal.

Rhodamine B is an amphoteric dye which is either acidic or basic depending on the pH of the medium, which defines the overall charge on the molecule. In the slightly acidic medium of the gold nanoparticle solution it is assumed that the dye is in its anionic form.

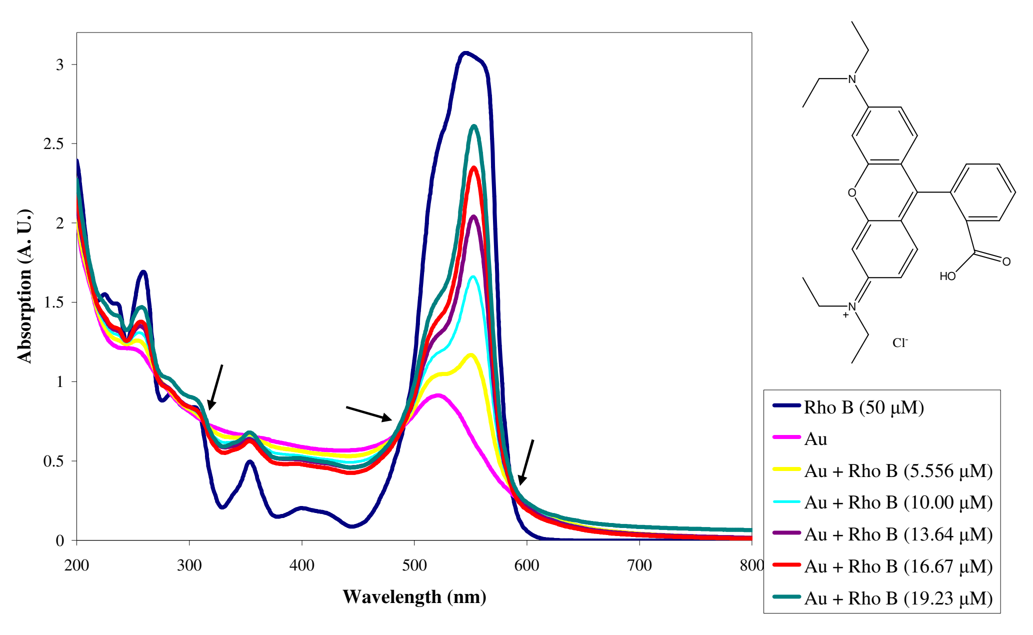

Figure 4-15 ***UV-visible absorption spectra of rhodamine B (Rho B) in a gold nanoparticle solution. The total rhodamine B concentration of 5.556 µM (yellow line) was obtained by the addition of 2 mL of rhodamine B (50 µM) to 16 mL of gold nanoparticle solution. The structure of structure of rhodamine B is displayed at the top right of the figure. The three isosbestic points are indicated with the arrows.***

There was no enhancement of the maximum absorption of the dye rhodamine B (Figure 4-15). Additionally, the nanoparticle surface plasmon resonance absorption peak falls below the dye peak so the dilution effect of the maximum absorption in the nanoparticle peak was not observed. However, the increase maximum absorption of the rhodamine dye peak which corresponds to the increase in concentration was observed. There were three isosbestic points on the UV-visible absorption spectra (310 nm, 487 nm, 594 nm) where the extinction coefficients of the dye and gold nanoparticle solution were equal.

Lethal Photosensitisation of Bacteria Experiments:

As previously discussed (chapters 2 & 3), it has long been known that microbes can be killed by white light in the presence of a photosensitiser such as toluidine blue (TBO).[148] The results from this work have demonstrated that the efficacy of lethal photosensitisation of bacteria can be enhanced by the addition of gold nanoparticles. The gold nanoparticles used in these experiments were synthesised by the same method as those used in the titration experiments, and had a diameter of 21.4 nm (Figure 4-12).

There was an enhancement of lethal photosensitisation of *S. aureus* when the TBO was used in conjunction with gold nanoparticle solution. This enhancement was concentration dependant (Figure 4-16). Some enhancement was observed at 1 µM whereas; significant enhancement was evident using higher TBO concentrations of 5, 10 and 20 µM. Enhancement was greatest using 10 and 20 µM TBO (Figure 4-17). Enhancement appeared to be dependent on the ratio of TBO to nanoparticles. The optimum final concentration of toluidine blue for the lethal photosensitisation of bacteria was found to be 20 µM as higher concentrations appeared to give less effective kills (Figure 4-17).

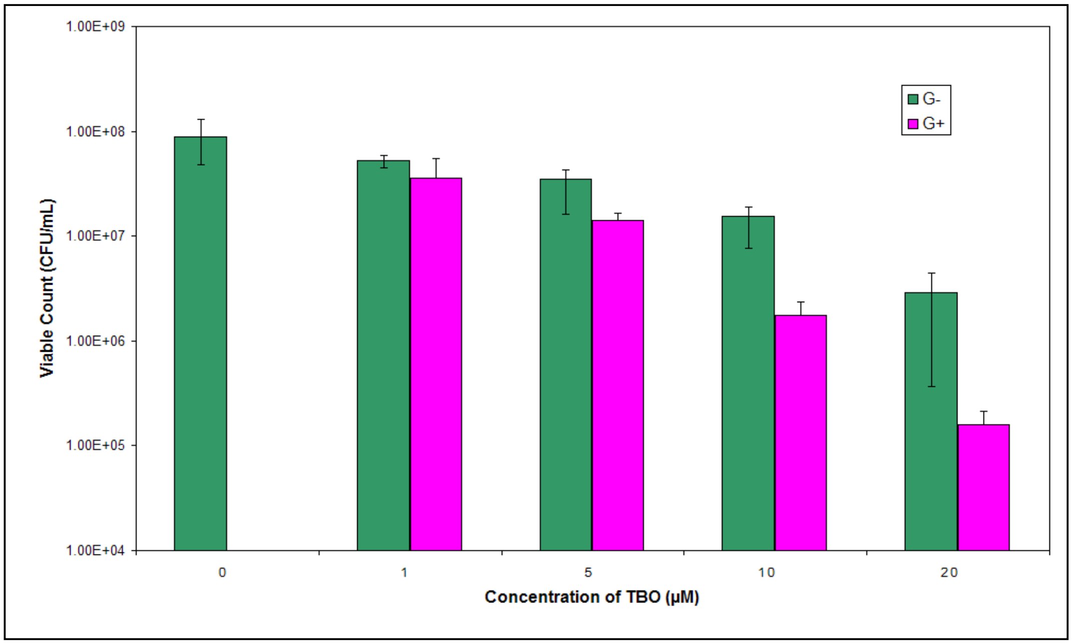

Figure 4-16 ***Lethal photosensitisation of S. aureus by TBO (1 µM, 5 µ, 10 µM and 20 µM) in the absence (green, G-) and presence (pink, G+) of gold nanoparticles.***

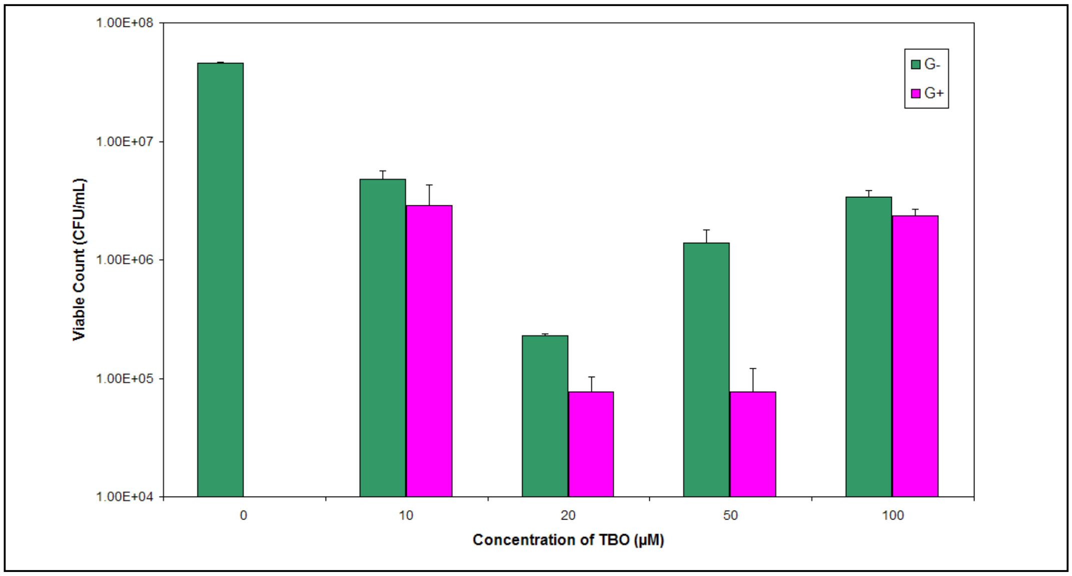

Figure 4-17 ***Lethal photosensitisation of S. aureus by TBO (10 µM, 20 µM, 50 µM and 100 µM) in the absence (green, G-) and presence (pink, G+) of gold nanoparticles.***

The UV-visible absorption spectra at a final toluidine blue concentration of 20 µM, with water and gold nanoparticle solution is shown in Figure 4-18. An enhanced absorption is observed for the toluidine blue in the presence of gold nanoparticles. Additionally, an aggregation shoulder at approximately 700 nm is also observed.

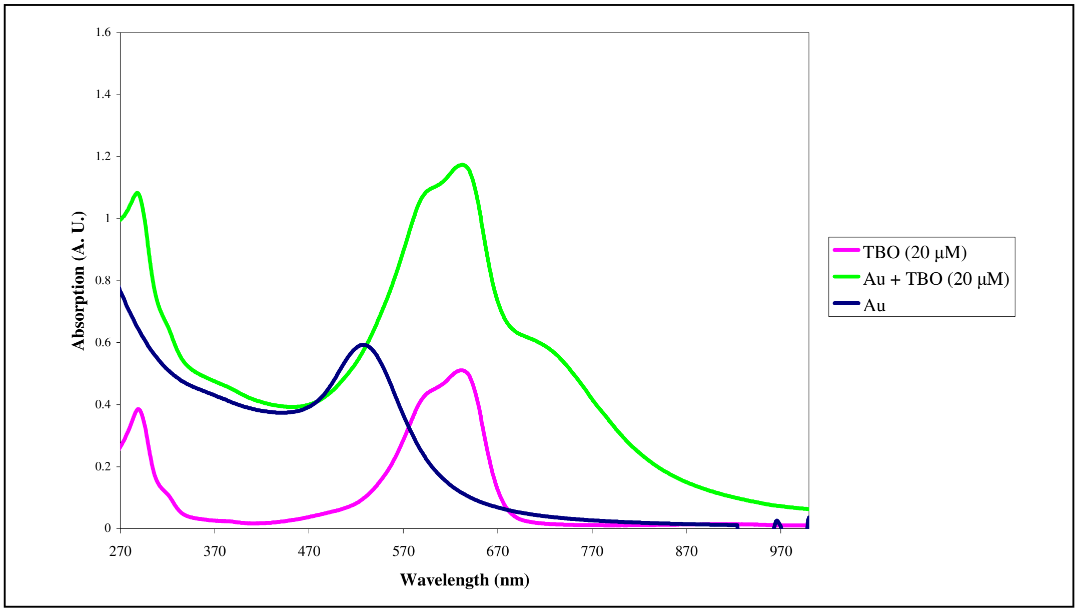

Figure 4-18 ***UV-visible absorption spectra of toluidine blue (TBO) (20 µM), TBO (20 µM) + gold nanoparticle solution and only gold nanoparticle solution. An enhanced absorption is observed for the TBO when gold nanoparticles and TBO are mixed.***

A series of experiments were conducted to measure the quantity of singlet oxygen produced from the toluidine blue at different concentrations when mixed with gold nanoparticles, an example of which is shown (Figure 4-19). All of the experiments were conducted at the same gold nanoparticle concentration and size but at different toluidine blue concentrations and are summarised in Figure 4-20. These experiments were conducted by measuring the emission associated with the singlet oxygen to triplet oxygen conversion at 1260 nm. The amount of singlet oxygen was determined by measuring the area of the singlet oxygen fluorescence peak which is proportional to the singlet to triplet oxygen conversion. The data showed that the amount of singlet oxygen produced was directly linked to the TBO concentration.

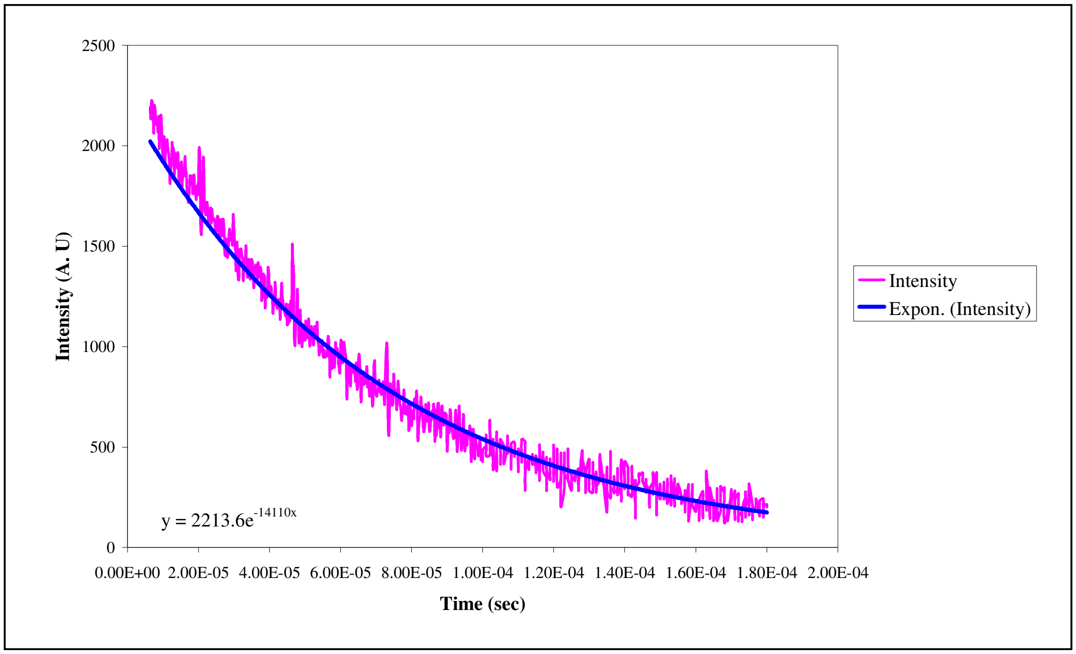

Figure 4-19 ***Emission against time plot at 1260 nm after photoirradiation (532 nm) of a sample of gold nanoparticles and TBO (4.7 μM). The plot shows the fluorescence emitted by singlet-triplet oxygen conversion, the area under the curve is proportional to the amount of singlet oxygen generated.***

Data were collected at various toluidine blue concentrations ranging from 2.5 μM to 12.5 μM, whilst keeping the gold nanoparticle concentration constant (Figure 4-20). Obvious trends can be extracted form the data; increasing the concentration of toluidine blue increases the amount of singlet oxygen produced and addition of gold nanoparticle solution significantly decreases the amount of singlet oxygen produced, which is almost proportional at each concentration.

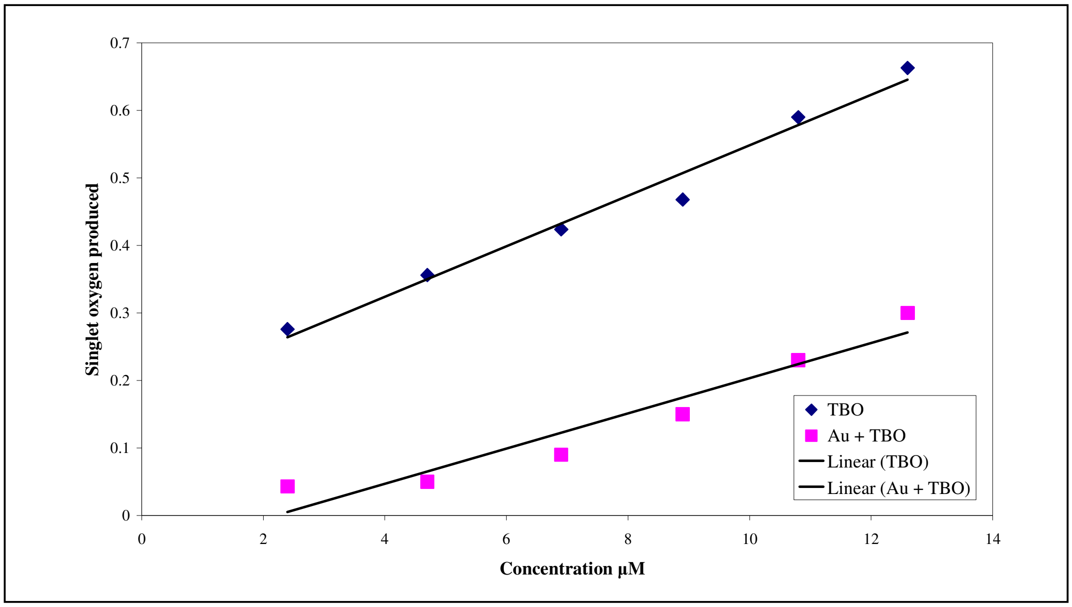

Figure 4-20 ***Relative amounts of singlet oxygen produced for TBO and TBO + gold nanoparticle solutions at different TBO concentrations. The concentration of singlet oxygen produced is dependant on the concentration of toluidine blue present.***

Toluidine blue has fluorescence at approximately 670 nm (Figure 4-21). This fluorescence is quenched in the presence of the gold nanoparticles. The peaks observed at 600 nm are a harmonic of the excitation source of the excitation light inputted.

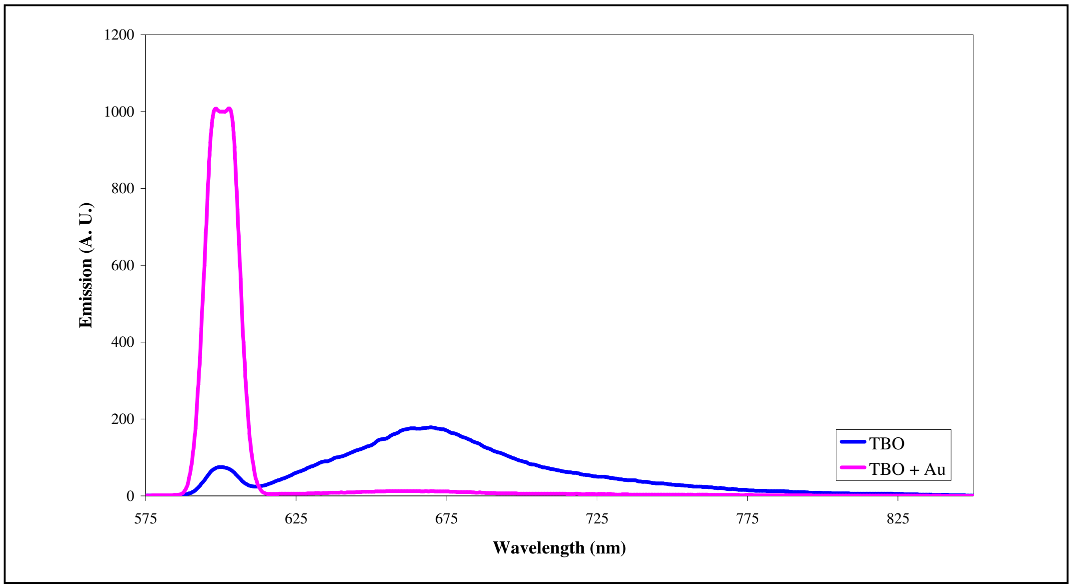

Figure 4-21 ***Fluorescence spectra of toluidine blue (TBO) (5.5 µM) and TBO-Au nanoparticle mixture, where the final concentration of toluidine blue is 5.5 µM. The fluorescence of TBO is quenched in the presence of gold nanoparticles.***

The gold nanoparticles used in all of the studies were synthesised using a modified Turkevich citrate reduction.[142] The sample synthesised NN1.2, displayed the enhanced kill of bacteria. However, many of the samples subsequently synthesised did not enhance the lethal photosensitisation of bacteria. Therefore, it was concluded that there were more factors affecting the synthesis reaction than first observed.

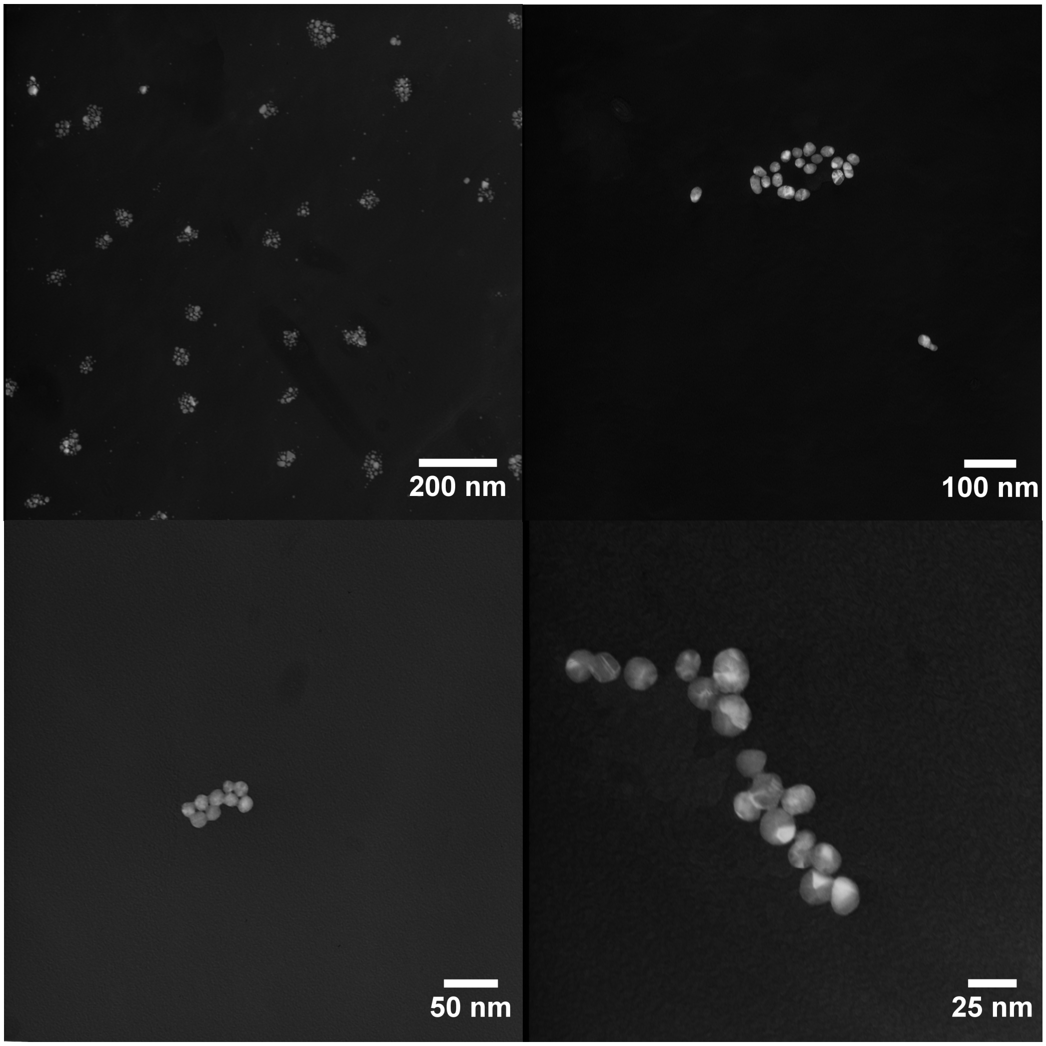

Figure 4-22 ***Transmission electron microscopy images of citrate stabilised gold nanoparticles (Sample NN1.2) at various magnifications.***

Different sized nanoparticles were tested at the Eastman Dental Institute for enhanced lethal photosensitisation of bacteria. These were synthesised by the Turkevich method as modified by Fren.[18] The final average size of these nanoparticle solutions were 16 nm, 25 nm, 40 nm, 70 nm, 100 nm and 150 nm (from Ferns analysis[18]). Again none of these showed any enhancement in the lethal photosensitisation of bacteria.

Sample NN1.2 had an average diameter of 18 nm ± 3.5 (Figure 4-22). This sample enhanced the kill of bacteria and many attempts were made to reproduce this sample. Although in each case nanoparticles were produced, none enhanced the lethal photosensitisation of bacteria. Also none of these samples fit the UV-visible absorption profile of NN1.2, or had the same pH. Attempts were made to regulate the reaction to determine where the inconsistency was being introduced (same beakers, syringes, needles, heating time etc). It was discovered that the rate of addition of the reducing agent, was an important factor in determining the final size of nanoparticle. Whereas the amount of citrate added varies the size between 16-150 nm (Fren[18]), the rate of addition can vary the range between 15-25 nm (Table 4-3).

Sample	Time Taken For 20 ml of Water to Boil	Time Taken To Add Citrate	Time Left Boiling After Citrate is added	$\lambda_{(max)}$(nm)
NN1	120 sec	60 sec	60 sec	522
NN2	120 sec	120 sec	60 sec	524
NN3	120 sec	30 sec	60 sec	521
NN5	120 sec	50 sec	60 sec	522-523
NN6	120 sec	40 sec	60 sec	522

Table 4-3 ***The rates of addition of sodium citrate, to a solution of auric acid for the synthesis of gold nanoparticles.***

Increasing the rate of addition of the sodium citrate reductant, whilst synthesising gold nanoparticle solutions, resulted in a decrease in the wavelength of maximum absorbance of the surface plasmon resonance (Table 4-3). Therefore, by adding the reducing agent at a faster rate smaller nanoparticles were obtained. The synthetic protocol was adjusted so that the particle size could be closely monitored and further gold nanoparticle solutions which had similar UV-visible absorption profiles to NN1.2 were synthesised for testing for photodynamic action at the Eastman Dental Institute (Figure 4-23).

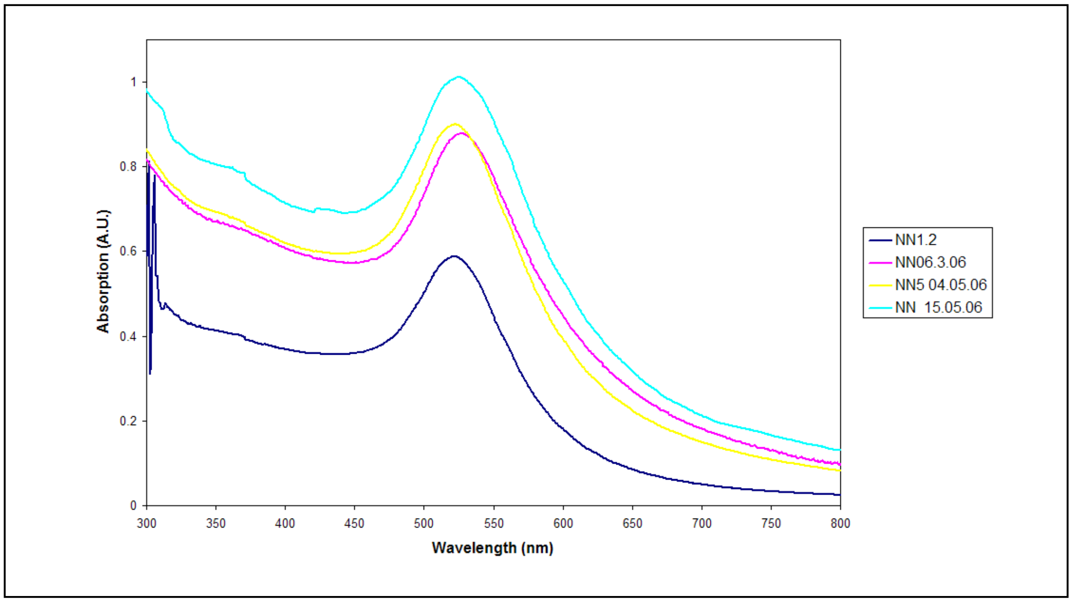

Figure 4-23 ***UV-visible absorption spectra of samples that have been found to enhance the kill of bacteria (NN 1.2, NN 06.03.06) and samples that were predicted to enhance the kill of bacteria (NN5 04. 05.06, NN 15.05.06)***

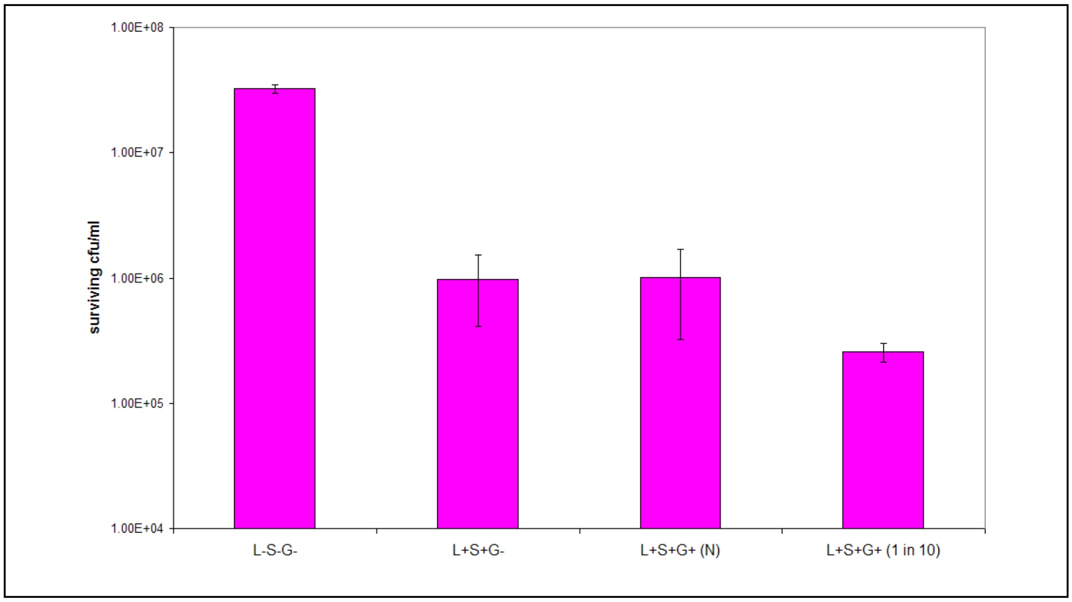

Figure 4-24 ***Viable counts of S. aureus, when 20 µM toluidine blue and sample NN06.03.06 are present. When the sample NN06.03.06 is diluted (1 in 10), toluidine blue added then irradiated with white light for 30 secs there is a statistically significant enhance of kill of bacteria of approximately 2 log_{10}.***

It was found that sample NN(06.03.06) also promoted the lethal photosensitisation of bacteria (Figure 4-24). However, this sample had to be diluted so that the UV-visible absorption profile matched sample NN1.2 more accurately, which indicates a critical ratio between the photosensitiser and gold nanoparticles is needed for effective lethal photosensitisation of bacteria.

Sample	$\lambda_{(max)}$(nm)
NN1.2	522
NN06.03.06	527
NN5 04.05.06	523
NN15.05.06	526

Table 4-4 ***Maximum absorbance wavelengths in UV-visible absorption spectra of samples which enhance the kill of bacteria (NN 1.2, NN 06.03.06) and samples that were predicted to enhance the kill of bacteria (NN5 04. 05.06, NN 15.05.06)***

Samples NN5 04.05.06 and NN15.05.06 had a maximum wavelength absorption fall in-between the two samples NN1.2 and NN06.03.06 which were known to enhance the kill of bacteria (Table 4-1).

4.4 Discussion

The optical response of gold metallic colloids arises from the ease at which electromagnetic fields excite electrons at the surface of particles. This photo-excitation induces charge density oscillations, a collective movement of electrons, the surface plasmon, gives rise to the intense colour of the solution, and absorption at around 530 nm.

The electronic excitation leads to electronic field redistribution near the metal surface. Therefore molecules which are in the vicinity of this surface experience an intense electric field, which may give rise to the enhancement in the maximum absorption of some dyes in the visible region. Dyes absorb light in the visible region and have a characteristic spectrum. This spectrum changes when a dye is adsorbed onto the surface of gold nanoparticles. This is indicative of electronic communication between the dye and the gold nanoparticle surface.

Increasing the dye concentration increases the maximum absorption, as defined by the Beer Lambert law: $A = C \times l \times e$. Where the path length (l) and extinction coefficient (*e*) are constant and the absorption (A) is proportional to the concentration (C).

All of the thiazine dyes have a similar structure (Figure 4-3) and hence, displayed comparable enhancement after the dye is added to a gold nanoparticle solution (Figure 4-4, Figure 4-5, Figure 4-7, Figure 4-8, Figure 4-9, Figure 4-10). There was a gradual decrease in maximum nanoparticle absorption, where as the dye peak reached a maximum and then decreased. This indicates that large loadings of dye molecules on gold nanoparticles have detrimental effects on the maximum absorption. It is possible that the surface of the gold nanoparticle may be covered by the maximum number of dye molecules possible, and the additional dye molecules may not be affected by the charge on the nanoparticles. As the inter chromophore distance decreased flocculation of the nanoparticles occurred. After the methylene blue titration experiment was completed and left to stand for a week, a black solid was observed. However trying to isolate such a small mass of solid was extremely difficult. EDAX was performed on some that were isolated but the results were inconclusive.

The enhanced maximum observed in the UV-visible absorption spectra of thiazine dyes also resembles that of particle aggregation which was reported by Turkevich in the 700 nm region.[149] Therefore a control titration experiment was carried out. This involved the same titration experiment with a gold nanoparticle solution and addition of a methylene blue solution. The added component of this titration was KCl which induced aggregation. Adsorbed anionic citrate on the gold nanoparticle forms a layer of electrostatic repulsion, which prevents the aggregation of the nanoparticles. Electrolytes (solution of KCl) screen the repulsive electrostatic forces of the citrate layer and induce aggregation. Aggregation was observed at around 710 nm and the maximum enhancement in the methylene blue was observed at around 680 nm. This indicates that although KCl induced aggregation on the gold nanoparticles, the dye still exhibited an enhanced adsorption.

In the absence of KCl the point at which methylene blue induced aggregation of gold nanoparticles was investigated using a zetasizer. For this system aggregation of gold nanoparticles and an increase in particle size was not observed until the concentration of methylene blue reached 2.1 μM. This concentration is higher than 0.79 μM which was the concentration observed to give the maximum enhanced absorption. This adds to the argument that dye molecules in close proximity to the gold nanoparticle surface experience an intense electrical field and this has an antenna effect on the absorption of these dyes.[150]

Generally, the UV-visible absorption spectrum of the thiazine dyes when titrated against gold nanoparticle solutions, showed an enhancement of the absorption of the dye, at the wavelength of the normal dye maxima. There was a gradual decrease in maximum surface plasmon resonance absorption of the nanoparticle peak, which was attributed to the continuing increase in total volume to the reaction mixture hence decrease in relative concentration. The absorption peak for the thiazine dyes generally increases until a critical concentration is reached. This critical concentration gives the maximum enhancement. Once reached, the maximum absorption then gradually declined, indicating that large loadings of dye molecules on gold nanoparticles have detrimental effects on maximum absorption. The surface of the nanoparticle may be covered by the maximum number of dye molecules possible and therefore, the additional dye molecules would not be affected by the charge on the nanoparticles. As the inter-chromophore distance decreases flocculation of the gold nanoparticles occurs.

The enhancement in UV-visible absorption spectra was not observed for acidic, anionic dyes. This implied that a basic, cationic dye which was able to adsorb onto the surface of gold nanoparticles was required for enhancement of the absorption properties of the dye. Acidic, anionic dyes display isosbestic points, which suggest that there is no communication between the dye and nanoparticle. The anionic dyes investigated were tin chlorin e6, rose bengal and rhodamine B.

Rhodamine 6C has a similar structure to rhodamine B and is another zwitter ion. Rhodamine 6G has a strong absorption in the visible and a high fluorescence yield, and its well characterised properties has allowed the dye to be used as a probe for aggregation effects on surfaces.[151] Hu *et al.*[152] studied the aggregation effects of rhodamine 6G on the surface of gold nanoparticles. The 2-3 nm gold nanoparticles used for their experiments were synthesised using SCN^- as the reductant. The pH of the final gold sol was increased by the addition of K_2CO_3. Therefore, when rhodamine 6G was added it was in the cationic form and could adsorb onto the surface of the gold nanoparticle. Their similar titration experiment involved keeping the concentration of rhodamine G constant followed by addition of gold nanoparticle solution. The study found the disappearance of the sharp absorption band in the visible region at 525 nm and the appearance of two new bands at 507 and 537 nm. They have attributed this to the close packing of the cationic dye molecules around the surface.

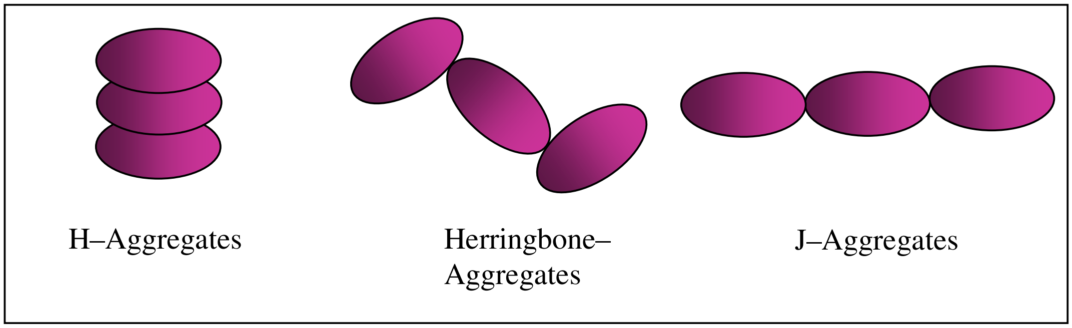

Figure 4-25 ***Types of aggregates formed by dyes in solution***

There are a number ways that dye molecules could aggregate on the surface (Figure 4-25). Hu *et al*[152] have suggested that the dye form herringbone type aggregates. This would account for the appearance of the two new absorption bands at 507 and 537 nm. Herringbone aggregates have two associated absorption bands corresponding to the two different transitions that are polarised along perpendicular directions.[114] However aggregates of 2 nm gold nanoparticles could account for the absorption band at 537 nm as they would be large enough to exhibit a surface plasmon. The absorption band at 507 nm would be associated with H–aggregates of the dye rhodamine 6G. H–aggregates consist of a parallel arrangement of dye molecules to form a vertical stack and correspond to a blue shift in the absorption band,[114] which is consistent with their study. The other type of dye aggregates that could form are J–aggregates which have a head to tail arrangement of dye molecules and are associated with a red shift.[114] The slight shift in the absorption bands of the dyes, in the titration experiments discussed in this chapter are possibly a result of dye aggregates on the surface of gold nanoparticles.

Toluidine blue is a positively charged molecule with a chloride counter ion. Therefore it would be electrostatically attracted to the gold nanoparticle surface which is negatively charged. The toluidine blue could co-ordinate to the surface of the gold nanoparticle through the sulphur atom of the dye as it is extremely aurophillic. Also, in aqueous solution the toluidine blue molecules are likely to form a shell around the gold nanoparticles.

The maximum enhancement in bacterial kill was observed at a toluidine blue concentration of 20 μM. The UV-visible absorption spectra of TBO (20 μM), the gold nanoparticles and a mixture of both are displayed in Figure 4-18. The gold nanoparticles displayed a plasmon resonance peak at approximately 530 nm. A significant enhancement of approximately 240% in the maximum absorption of toluidine blue at 620 nm was observed in the presence gold nanoparticles. The additional shoulder at approximately 710 nm was due to the aggregation of the gold nanoparticles. As previously reported in this chapter this was studied using a zetasizer, this showed that the main size of the gold nanoparticles was 20 nm and that this increased to approximately 100 nm at higher TBO concentrations due to aggregation.

Addition of toluidine blue to a gold nanoparticle solution, so that the final concentration of TBO is 20 μM in the reaction mixture, results in an enhanced UV-visible absorption profile analogous to the results previously reported. Additionally, the disappearance of the plasmon resonance peak but a broadening of the absorbance peak of the resulting mixture compared with that of the TBO alone was displayed (Figure 4-18).

Photosensitisers have been covalently linked to gold nanoparticles to increase their efficacy.[99] Wieder *et al.* [99] have shown that covalently linking phthalocyanine to gold nanoparticles results in the enhanced killing of human cells when irradiated. The results presented here demonstrate that light activated antimicrobial activity of toluidine blue can be enhanced by gold nanoparticles even when they are not covalently linked. The presence of gold nanoparticles resulted in a 2 $\log_{10}$ increase in the number of colony forming units (CFU) killed, following short periods of irradiation (10 min) with a domestic light source. It has been suggested that irradiating gold nanoparticles covalently linked to phthalocyanine, induces an energy transfer between phthalocyanine and gold, which leads to an enhanced singlet oxygen production and enhanced kill of human cells.[99] This was attributed to increased triplet energy transfer from the phthalocyanine–gold conjugate to molecular oxygen.[153] It was concluded that the photosensitisation efficacy of the conjugate was dependant on the presence of monomeric phthalocyanine on the nanoparticle surface. The results presented in this chapter suggest that covalent linkage of the photosensitiser is not essential to achieve enhanced photodynamic action.

Nanoparticles can act as acceptor (quencher) or donor units.[154] Gold nanoparticles can act as efficient quenchers of fluorophores, and is the basis by which DNA sensing using gold nanoparticles operates.[55] It has been suggested that quenching of the fluorophore by the gold surface results from both non-radiative energy transfer from the dye to the metal and from the collision of the dye against the gold surface (dynamic quenching).[155] It was found in this study that the weak fluorescence of toluidine blue at 670 nm is quenched in the presence of gold nanoparticles (Figure 4-21)

The fluorescence of the dye 'nile red' has been investigated in experiments by Chen *et al.*[156] Nile red was adsorbed onto the surface of gold nanoparticles, and was used in the detection of thiols. Nile red is a hydrophobic, highly fluorescent dye that undergoes intensity or wavelength shifts upon changes in the polarity of its environment.[157] Chen *et al.*[156] found the fluorescence of nile red to be weak when adsorbed onto the surface of gold nanoparticles. When the adsorbed nile red was displaced in the presence of thiols the fluorescence of the nile red was restored. Interestingly when the desorbed nile red was examined, it was found to have changed structure suggesting a chemical reaction at the surface of the gold nanoparticle. Chen *et al.*[156] attributed the quenched fluorescence to Förster resonance energy transfer (FRET) where a donor chromophore (nile red), in its excited state transfers its energy by a non-radiative, long-range dipole-dipole coupling mechanism to an acceptor (gold nanoparticle) in close proximity (typically <10 nm). The results from their study correlate with the fluorescence experiments presented in this chapter.

The fluorescence experiments, UV-visible absorption and singlet oxygen experiments were performed in order to try and determine the mechanism by which the enhanced lethal photosensitisation of bacteria is observed. The results are summarised below;

- In the presence of gold nanoparticles there is a marked increase in the extinction coefficient at 631 nm of toluidine blue.
- At a 20 μM concentration of toluidine blue, where the maximum bacterial kill was observed this enhancement of the extinction coefficient was still present.
- There is a significant decrease in the amount of singlet oxygen produced by the toluidine blue when mixed with gold nanoparticles.
- The presence of gold nanoparticles quenches the weak fluorescence of toluidine blue at 670 nm
- Aggregation of nanoparticles is induced at high loadings of dye molecules.

There was an abrupt increase in the extinction coefficient of toluidine blue in the presence of gold nanoparticles. This was attributed to the adsorption of the toluidine blue molecules onto the surface of the gold nanoparticle through the sulphur atom on the TBO. This altered the profile of the UV-visible absorption spectra. This was characteristic of all thiazine dyes when mixed with gold nanoparticles. Although the mixing of gold nanoparticles with the dye significantly increases the extinction coefficient of the dye, it did not lead to more singlet oxygen being produced. In fact, the opposite effect was observed and significantly less singlet oxygen was formed. Furthermore, the fluorescence of the TBO was completely quenched in the presence of gold nanoparticles. This implied other radical species such as hydroxyls and superoxides may have been produced when gold nanoparticles were mixed with toluidine blue. These hydroxyl radicals and super oxide species are toxic to bacteria; hence mixtures of gold nanoparticles with toluidine blue exhibit enhanced kill of bacteria.

Considering all the data from these studies, it can be argued that the presence of gold nanoparticles on TBO can harvest more incident light per molecule. This produces an excited state of the dye. The excited state decays through a non-radiative process- as no dye-fluorescence is observed. However the non-radiative process is not dominated by formation of singlet oxygen, which is significantly depressed in the presence of the gold nanoparticles. In the presence of gold nanoparticles, TBO relaxes to the ground state by a non-radiative decay and this process is primarily through formation of other reactive oxygen species- such as hydroxyl radicals. It is the formation of these reactive species that are responsible for the increased bacterial kills observed. Hence, the gold nanoparticles have two roles- firstly they enhance the light capture of the dye, by having absorbed dye on the surface of the particles, and secondly they help direct the decay pathway for the dye encouraging a non-radiative process through formation of excess bactericidal radical species.

Chow and Zukoski[43] reported that the wavelength of maximum absorbance of a gold nanoparticle solution can be related to the diameter of the colloidal gold particle. A longer wavelength corresponds to a larger particle. Fren[18] described the particle size obtained as a function of the number of nuclei over which the available gold is divided and is not a result of a reduction of a different percentage of the available gold. This is valid when examining particle size over a wide range. The colloid solution produced by the citrate reduction of hydrogen tetrachloroaurate is dependant on the statistical fluctuations in the nucleation process. Repeated attempts failed to produce nanoparticles with identical UV-visible absorption profiles and pH. However a correlation was observed between the rate of addition of sodium citrate and the diameter of diameter of nanoparticles produced. Faster rates of addition favoured smaller particles. The results obtained were in agreement with Sariva *et al.*[158] The addition of citrate at a higher flow rate results in a higher concentration of nuclei being produced near the start of the reaction and that the growth period begins once all of the citrate is added. In general, when there is a slower rate of addition larger particles are produced and there is an increase in maximum wavelength absorption.

Summary of results:

Synthesis of gold nanoparticles was investigated using a modified Turkevich citrate reduction.[142] By varying the citrate rate of addition different sized nanoparticles were obtained. Fast addition of the citrate produced smaller nanoparticles in the range of 16 nm. Adding the citrate over 50 seconds yielded nanoparticles of approximately 20 nm.

The adsorption of dye molecules onto the surface of the nanoparticle was investigated. The collective movement of electrons (surface plasmon) gives rise to the intense colour of gold nanoparticles. This electronic redistribution near the surface of the gold nanoparticle effects molecules in close proximity to the surface. An enhanced absorption has been observed for the dyes in the thiazine group when the dye is titrated against the nanoparticle solution.

Generally in the UV-visible absorption spectrum of the thiazine dyes, there is a gradual decrease in maximum nanoparticle absorption, where as the dye peak reaches a maximum. The decrease in the nanoparticle intensity in the UV-visible absorption spectrum corresponds to the decrease in concentration. The absorption peak for the thiazine dyes generally increase until a critical concentration is reached. This critical concentration gives the maximum enhancement. The maximum absorption then gradually declines, indicating that large loadings of dye molecules on gold nanoparticles have detrimental effects on maximum absorption. The surface of the nanoparticle may be covered by the maximum number of dye molecules possible and the additional dye molecules may not be affected by the charge on the nanoparticles. As the inter chromophore distance decreases it may cause flocculation of the nanoparticles.

An enhancement of approximately one $\log_{10}$ in the extinction coefficient was displayed in the UV-visible absorption spectra for all of the thiazine dyes, in the presence of gold nanoparticles (16 nm) at a dye concentration of approximately 3×10^{-6} M. There is an average enhancement of an average of 0.65 absorption units in the maximum absorption of the dye, which indicates a direct communication between the nanoparticle and the dye.

The enhancement in extinction coefficient was not observed for acidic, anionic dyes. Acidic, anionic dyes display isosbestic points, which suggest that there is no communication between the dye and nanoparticle, and that they do not adsorb onto the surface of gold nanoparticles. Flocculation is observed when KCl is added to the gold nanoparticles and dyes. However an enhancement is still observed.

Gold nanoparticles which absorb wavelengths of light between 522 and 527 nm, enhance the lethal photosensitisation of bacteria when used in conjunction with methylene or toluidine blue. These nanoparticles were 18 nm in diameter. Although there was an enhancement in the lethal photosensitisation of bacteria, increased amounts of singlet oxygen were not detected. Additionally the fluorescence of the dye was quenched in the presence of gold nanoparticles at 670 nm. This implies that the other pathways such as the formation of hydroxyl radicals are important to enhance the lethal photosensitisation of bacteria.

It is thought that in the presence of gold nanoparticles with TBO makes it relax to the ground state by a non-radiative decay. This process is primarily through formation of other reactive oxygen species- such as hydroxyl radicals. The formation of these reactive species is responsible for the increased bacterial kills observed. The gold nanoparticles enhance the light capture of the dye, by having absorbed dye on the surface of the particles, and direct the decay pathway for the dye encouraging a non-radiative process through formation of excess bactericidal radical species.

4.5 Conclusion

It was found that the mixing of gold nanoparticles with basic cationic dyes of the thiazine family enhance the extinction coefficient of the dye. This was not observed for the acidic anionic dyes investigated. The fluorescence of the thiazine dye toluidine blue is quenched in the presence of gold nanoparticles. Additionally, the production of singlet oxygen by toluidine blue decreases in the presence of gold nanoparticles. It was discovered that the covalent attachment of a light activated antimicrobial such as toluidine blue is not required for an enhancement in bacterial kill to be observed. It is thought that the enhanced bacterial kill is a result of reactive oxygen species other than singlet oxygen, such as hydroxyl radicals being produced.

In order to further investigate the relationship between nanoparticles and photosensitisers the nature of the nanoparticle was changed from gold to semi-conductor (CdSe) quantum dots. Similar experiments, involving the mixing of photosensitisers with quantum dots were performed and will be discussed in the next chapter.

Chapter 5 Quantum Dots and Toluidine Blue

The purpose of this study was to determine whether CdSe quantum dots (QD) could enhance the antibacterial activity of the LAAA, Toluidine Blue (TBO). Suspensions of Staphylococcus aureus (5.47 × 10^7 *cfu/ml) were exposed to white light and TBO in the presence and absence of 25 nm diameter CdSe/ZnS quantum dots (which had an emission maximum at 627 nm). When the ratio of TBO:quantum dots were 2667:1 (quantum dot concentration of 0.0075 µM), killing of S. aureus was enhanced by 1.72* $\log_{10}$ *units. In the case of Strep. pyogenes an enhanced kill of 1.55* $\log_{10}$ *units was achieved using TBO and quantum dots in the ratio 267:1. It was determined from fluorescence quenching and singlet oxygen measurements that the quantum dots enhanced the ability of toluidine blue to increase the formation of singlet oxygen, especially at high TBO:QD ratios. The process was shown mechanistically to operate by a non-FRET mechanism, where the quantum dot converted part of the light source to the absorption maximum for toluidine blue. If such enhanced killing can be achieved in vivo, quantum dots may be useful in improving the efficacy of antimicrobial photodynamic therapy.*

5.1 Introduction

Quantum dots (QDs) are nanometer scale semiconductor crystals of types II–VI, III–V or IV, dependant on the elements position in the periodic table.[159] Cadmium selenide quantum dots are from group II–VI have been well characterised[160] and were the focus of this study, hence are the quantum dots referred to in the rest of this chapter.

Semi-conductor quantum dots have physical dimensions smaller than the excitation Bohr radius.[161] When a photon of visible light hits a semiconductor quantum dot, static electrons from the valence band become mobile and are excited into a higher conduction band within a semiconductor matrix. As the electron becomes mobile it leaves behind a hole. After a certain period of time, usually in nano seconds, the electrons and holes recombine. In quantum dots this recombination causes the emission of a photon at a frequency characteristic of the material. The amount of energy required to induce the electrons to become mobile and produce the quantum dot emission is called the bandgap energy.[162] The band gap energy is related to the size, shape and composition of the quantum dot. This dependence is due to the quantization of discrete energy levels, as the quantum dots size is in the same order as the excitation Bohr radius.[163]

Quantum dots have a number of attractive optical properties. For example, monodispersed quantum dots have narrow size tuneable photoluminescence with full width half maxima (FWHM) in the range of 25 – 40 nm.[164] The absorption spectra of quantum dots are broad, often ranging from the visible region towards and into the ultraviolet. Like the photoluminescence emission, the absorption spectrum also scales with the size of the quantum dot.[164] The combination of broad absorption and narrow symmetric emission has made quantum dots very attractive for multiplexing. Multiplexing is where different sized quantum dots are excited with the same wavelength of light to produce emission of different wavelengths, and thus yielding different colours.[165]

The size dependant photoluminescence colours of quantum dots are distributed through out the visible region of the electromagnetic spectrum (Figure 5-1). As the size of the particle decreases the bandgap increases, and the photoluminescence has a blue shift. The size dependant photoluminescence colour has been exploited in various applications including lasers, light emitting diodes and imaging.[161]

The quantum dots used for the experiments in this chapter have a coating of ZnS. This acts as a physical barrier, whereby the often more soluble CdSe cannot come in contact with the surrounding medium and dissolve through ionisation. The ZnS shell has larger bandgap energy than CdSe, eliminating the cores defects states and passivates the surfaces non radiative recombination sites.[159] This results in an increased quantum yield. Also, the Zn-S bond lengths are similar to Cd-Se bond lengths, minimising crystal lattice strain and facilitating Zn-S epitaxial growth.[162]

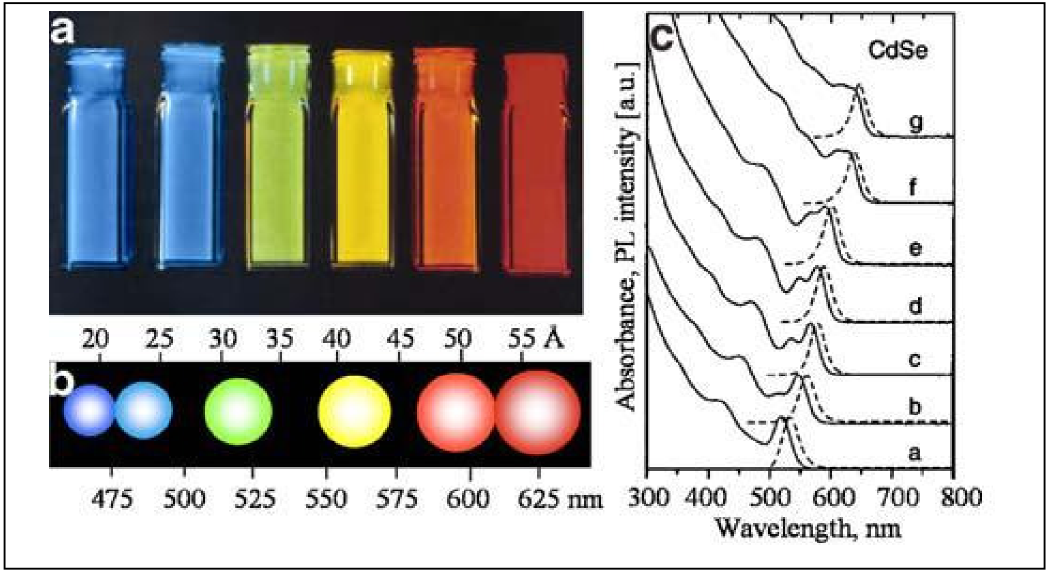

Figure 5-1 ***(a) Size-dependent photoluminescence colour and (b) schematic presentation of size, colour, and photoluminescence wavelength of CdSe–ZnS QDs. (c) Absorption (solid lines) and photoluminescence (broken lines) spectra of CdSe QDs with various sizes taken from reference [161].***

Although the quantum dots used in this study were bought from Evident Technologies, they can be synthesised by the following procedure. Dimethylcadmium and selenium are initially dissolved in the organic solvent tri-*n*-octylphosphine at defined ratios (usually a molar ratio of 1.4:1.0) and injected into a hot (350 °C) co-ordinating solvent of tri-n-octylphosphine oxide (TOPO) under argon gas. A decrease in temperature and change in colour of the solution from colourless to light yellow to orange to red, indicates the nucleation and growth of the quantum dots. The growth of the quantum dots is dependant on Ostwald ripening and a reduction of the temperature can lead to smaller particles being obtained. To produce a capping layer of ZnS a solution of dimethylzinc and hexamethydisilathiane in tri-*n*-octylphosphine can be slowly dripped into the reaction vessel after isolating or obtaining CdSe quantum dots of the desired size.[162] The quantum dots bought from Evident Technologies also had a surface coating of polyethylene glycol to aid solubilisation in water. A table summarising the various synthesis methods, capping materials and biofunctionalisation has been presented by Iga *et al.*[159]

Quantum dots have been used in a variety of applications including; gene technology, fluorescent labelling, cell tracking, pathogen and toxin detection, in *vivo* animal imaging and Förster resonance energy transfer analysis (FRET).[165,166] FRET occurs when the electronic excitation of a fluorophore, such as a quantum dot, is transferred to a nearby acceptor molecule (dye) without exchanging light (non-radiative), which may relax to its ground state by the emission of a photon. The process results from dipole – dipole interactions, and is dependant on the separation distance between donor and acceptor. FRET operates efficiently over donor-acceptor distances ranging from 1 to 10 nm.[167] The transfer efficiency increases with increasing spectral overlap between the donor emission and acceptor absorption. FRET leads to the reduction of the donor's emission and excited state lifetimes and an increase in the acceptor's emission intensities.[165] FRET is suited to measuring differences in distance making it appropriate for detecting conformational change of ligand bound assays.[168]

Quantum dots are extremely attractive for FRET analysis assays because conventional fluorescence assays have problems associated with cross-talk. Cross-talk occurs when there is direct excitation of the acceptor and there is spectral overlap between the donor and acceptor emissions which produces background emission, limiting the systems sensitivity.[168] As quantum dots have a broad absorption spectrum an appropriate excitation wavelength can be chosen so that absorption by the acceptor is not possible. Quantum dots have a narrow symmetric emission which allows for easy recognition from acceptor emission profiles.[166] Conventional fluorescence assays which measure fluorescence of bound dye require the separation from free dye before extent of binding can be measured. FRET simplifies these assays as binding can be measured directly. One drawback to quantum dot labelling is the difficulty in producing stable quantum dot biomolecule complexes in which, the number and orientation of the dyes and biomolecules on the surface of the quantum dots is well characterised, and the synthesis reproducible.[168] For the experiments discussed in this chapter the quantum dots were used in conjunction with a light activated antimicrobial (toluidine blue) to enhance the lethal photosensitisation of bacteria by photodynamic action through a non-FRET mechanism.

As detailed in previous chapters, photodynamic therapy is a local, repeatable and non-invasive technique that has the potential to be an effective alternative to antibiotic therapy in the treatment of local infections.[74,169] Photodynamic action involves the killing of target microbes via the formation of oxygen-derived cytotoxic species produced by the interaction of a photosensitising compound with light of an appropriate wavelength.[84,170] Targeting of the infecting microbes can be achieved by chemical modification of the photosensitiser and/or by choosing appropriate light energy doses that do not damage host cells.[171,172] The production of reactive oxygen species at the microbial target results in rapid oxidative damage and cell death *via* a range of mechanisms, depending on the nature of the target which include; the bacterial cell wall/membrane, viral nucleic acids, and enzymes.[173] A wide variety of photosensitisers are available and toluidine blue (TBO) has been used successfully by a number of investigators as an effective photosensitiser of antibiotic-resistant microbes.[174,175]

Samia *et al*.[176] used quantum dots and covalently attached a phathalocyanine dye (Pc4) through an alkyl amino group on the photosensitisers' axial substituent. They found that Pc4 has an absorption that spans wavelengths *ca*. 550 and 630 nm. However quantum dots were needed as a primary donor between the wavelengths of 400 and 500 nm. Conjugation of the photosensitiser to the quantum dot resulted in the indirect excitation of Pc4 using 488 nm light (at which Pc4 does not absorb). They attributed this to a FRET type mechanism from the quantum dot to Pc4 as the emission of this dye was observed at 680 nm. This combination of photosensitiser and quantum dot allows the use of an excitation wavelength where the photosensitiser alone does not absorb. The emission spectral properties of the quantum dots can be adjusted to match the absorption profile of any dye by modifying the size of the quantum dots. Interestingly, in the study of Samia *et al*.[8] the photosensitising ability of the quantum dots in the absence of a photosensitiser was discovered, through the detection of singlet oxygen. Although the amount of singlet oxygen produced was very low (*ca*. 5%) in comparison to the photosensitiser (43%), it was still a significant result.[176] However, their experiments were conducted in toluene which would not be suited to biological systems. Additionally there have been some issues concerning the toxicity of certain quantum dots through the leaching of cadmium ions.[177]

Quantum dots are highly selective energy donors as clearly demonstrated by several groups.[167,168,178-180] Due to the ability of quantum dots to harvest light over a broad range of wavelengths and emit this at a wavelength absorbed by TBO, the antimicrobial effectiveness of TBO should increase when white light was used as the irradiating source. To test this hypothesis a series of fluorescence absorption and singlet oxygen experiments were conducted.

The experiments in this chapter were concerned with improving the effectiveness of TBO in the lethal photosensitisation of bacteria using quantum dots. It was found that quantum dots enhance the effectiveness of TBO. An investigation using UV-visible absorption, and fluorescence spectroscopy along with singlet oxygen measurements were carried out in order to uncover information on the mechanism by which this occurs.

5.2 Experimental

Target organisms: *Staphylococcus aureus* NCTC 6571 and *Streptococcus pyogenes* NCTC 12202. *Staph. aureus* was maintained by weekly transfer on nutrient agar while *Strep. pyogenes* was sub-cultured on blood agar

Light source: The light source used was for the microbiology experiments was a General electric 28-watts Biax 2D compact fluorescent lamp that emits light across the visible spectrum. Prominent peaks were present at 435, 495, 545, 588 and 610 nm (Figure 1). The lamp was fitted into a refrigerated incubator (LTE scientific ltd., Oldham, U.K) that maintained the temperature at a constant 22°C. The light intensity at the surface of the microtitre plates was measured using a digital luxmeter (Hagner photometric instruments limited; Bosham, U.K) and was found to be 3,600 lux.

Photosensitiser: The photosensitiser used in this study was toluidine blue O (C.I. 52040; Sigma-Aldrich Ltd, Poole, UK). The required concentration of the dye was prepared by dissolving measured dye powder in sterilised distilled water and diluted further to a required final concentration. The final concentration of TBO used in this study was 20 μM.

Quantum dots: The quantum dots used were 25 nm diameter CdSe/ZnS nanoparticles with a polyethylene glycol surface coating (T2-MP Maple Red-Orange EviTags; Evident Technologies, New York, USA). These exhibited high absorbance below 550 nm and had an emission maximum at 627 nm.

Lethal photosensitisation of bacteria: *Staph. aureus* was grown in nutrient broth overnight in a shaking incubator at 37 °C while *Strep. pyogenes* was grown overnight at 37 °C in air supplemented with 5% CO_2. The cells were then harvested by centrifugation and re-suspended in an equal volume of phosphate buffered saline (PBS) and then diluted to an optical density of 0.05 at 600 nm, which was approximately equal to 106 colony-forming units (cfu)/mL. In all experimental setups, the light source was fitted vertically into a refrigerated incubator at a distance of 41 cm to the 96-well flat bottom microtitre plate containing the bacterial suspensions.

A range of different concentrations of quantum dots were prepared in sterile distilled water. To each test well, 20 µL of bacterial suspension, 10 µL of 80 µM TBO and 10 µL of suspension of quantum dots were added. The final concentration of TBO in each well was 20 µM, and the concentration of the quantum dots ranged from 0.75 to 0.0075 µM. The ratio of TBO:quantum dots, therefore, ranged from 27:1 to 2667:1. Half of the wells (2 for each concentration of quantum dots) were exposed to white light for 5 or 10 minutes. Suspensions treated this way were designated L+T+Q+. The remaining wells were not exposed to light to determine the dark toxicity (L-T+Q+). Additional control wells were also prepared without the quantum dots and treated in the same way (L+T+Q-, L-T+Q-). Bacterial suspensions with quantum dots but without TBO were also prepared and treated in the same way (L+T-Q+). To determine the effect of white light alone, a further 4 wells were prepared and either exposed to white light (L+T-Q-) or kept in the dark (L-T-Q-). The number of viable bacteria in each well was enumerated by viable counting of serial dilutions of the microbial suspension. Serial dilutions were prepared in sterile PBS, and 20 µL of the aliquots were plated on nutrient agar plates (for *Staph. aureus*). All of the viable counts were performed in triplicate.

UV-visible absorbance of quantum dots (controls): The quantum dots had an initial concentration of 3 µM. This solution was serially diluted to give quantum dot solution concentrations of 0.3 µM, 0.15 µM, 0.06 µM and 0.03 µM. To a cuvette distilled water (1.5 mL) and quantum dots (0.5 mL, 0.15 µM) were added and the UV-visible absorption spectra recorded for each of the dilutions of quantum dots. The final quantum dot solution concentrations in the cuvette were 0.075 µM, 0.0375 µM, 0.015 µM and 0.0075 µM and the UV-visible spectra was measured at each dilution.

UV-visible absorbance of quantum dots with toluidine blue: A solution of toluidine blue was prepared of concentration 80 µM. The quantum dots had an initial concentration of 3 µM. This solution was serially diluted to give quantum dot solution concentrations of 0.3 µM, 0.15 µM, 0.06 µM, 0.03 µM. To a cuvette distilled water (1 mL), toluidine blue stock solution, (0.5 mL, 80 µM) and quantum dots (0.5 mL) were added and the UV- visible absorption spectra recorded. The quantum dot solution was serially diluted to give final quantum dot concentrations of 0.075 µM, 0.0375 µM, 0.015 µM and 0.0075 µM, these solutions contained toluidine blue of 20 µM. The UV-visible spectra were measured at each dilution.

Fluorescence of quantum dots (controls): The measurement of fluorescence from the quantum dots, TBO and quantum dot- TBO mixtures was determined on a Perkin Elmer LS50B spectrometer, with an excitation wavelength of 365 nm. The emission spectra were measured in a 1 cm quartz luminescence cuvettes containing quantum dot solution of set concentrations with and without the dye. To a cuvette H_2O (1.5 mL) and TBO (80 µM, 0.5 mL) were added and the fluorescence spectra recorded at a TBO concentration of 20 µM.

Fluorescence of quantum dots with toluidine blue: To a cuvette distilled water (1 mL), toluidine blue (0.5 mL, 80 µM) and quantum dots (0.5 mL) were added and fluorescence spectra recorded (500-800 nm), this provides a solution that is 0.75 µM in quantum dot and 20 µM in TBO. To water (1 mL) and an aqueous TBO solution (0.5 mL, 80 µM) the quantum dot solution which was serially diluted to give final quantum dot concentrations of 0.075 µM, 0.0375 µM, 0.015 µM and 0.0075 µM. The total concentration of TBO in each sample was 20 µM. The fluorescence spectra were measured for the initial and all serially diluted samples.

Determination of FRET: A 3 mm internal diameter NMR tube (4 cm long) was placed concentrically inside a 1 cm plastic cuvette and fixed in place with super glue. To quantum dot solutions 0.0125 µM in water was placed inside the N.M.R tube, TBO solutions of 80, 60, 40, and 0 µM were placed in the plastic cuvette. The fluorescence spectra from the QD were measured at each TBO concentration.

Measurement of singlet oxygen: Singlet oxygen measurements employed the second harmonic (l_{ex} = 532 nm) of a Q-switched Spectra Physics GCR-150.10 Nd:YAG laser as the excitation source (~1 mJ per pulse, ~5 ns full-width at half-maximum); The phosphorescence from the sample was collected at 90º, selected by an interference filter centered at 1270 nm (Infra Red Engineering Ltd., Essex UK) and then focused onto the active area of a liquid nitrogen-cooled germanium photodiode (North Coast EO-817P). The output from this device was AC coupled to a digital oscilloscope (Tektronix TDS-320), which digitized and averaged transients. Typically 20 laser shots were used for each sample. The emission was measured on the same toluidine blue/ quantum solutions as for the previous fluorescence experiments except that the toluidine blue and dilution experiments were carried out in D_2O.

5.3 Results

The effect on the viability of *Staph. aureus* sensitised with TBO, when exposure to white light for 10 minutes in the presence and absence of quantum dots is shown in Figure 5-2. In the absence of quantum dots, the TBO (20 µM) achieved a 1.75 $\log_{10}$ reduction in the viable count of a suspension of *Staph. aureus* containing 5.4×10^7 cfu/ml. When quantum dots were used with toluidine blue in the ratio TBO:quantum dots was 2667:1, where the concentration of toluidine blue was 20 µM and quantum dots was 0.0075 µM, there was a further 1.72 $\log_{10}$ decrease in the viable count of the bacteria. As the quantum dot concentration reduced, the extent of the enhanced kill increased - such that the greatest kill was achieved at the highest TBO-quantum dot ratio (lowest quantum dot concentration). None of the positive or negative controls showed any significant changes in the number of viable bacteria throughout the course of these experiments.

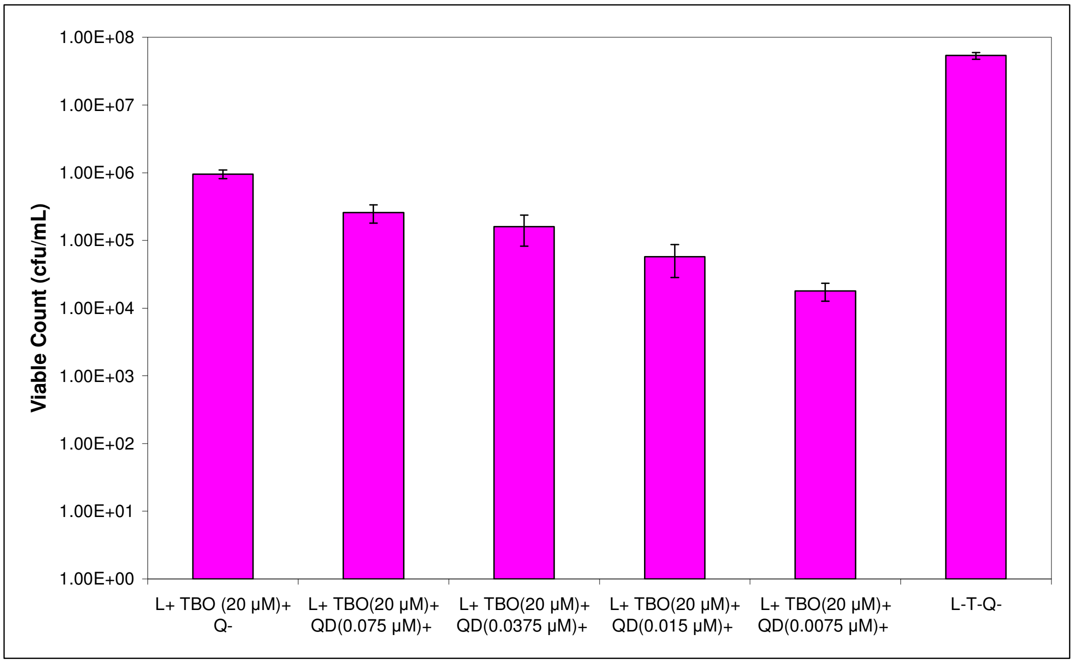

Figure 5-2 ***Lethal photosensitization of Staph. aureus by TBO in the absence and presence of various concentrations of 25 nm diameter CdSe/ZnS quantum dots. L = light; QD = quantum dots; TBO = toluidine blue.***

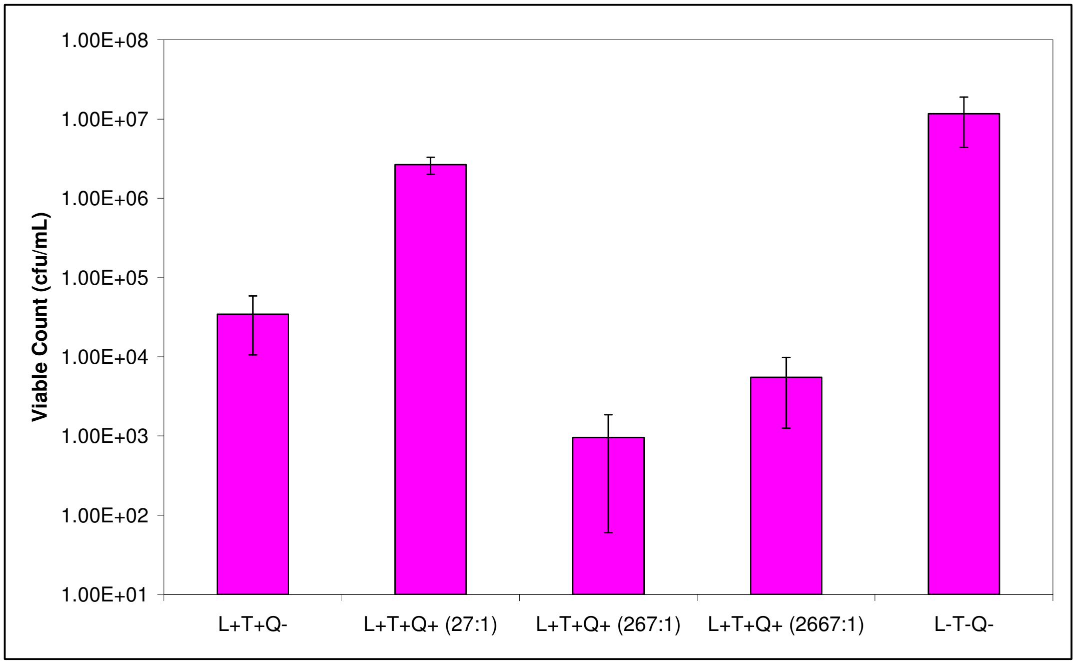

Figure 5-3 ***Lethal photosensitization of Strep. pyogenes by TBO in the absence and presence of various concentrations of 25 nm diameter CdSe/ZnS quantum dots.***

When used at certain concentrations, enhanced kills of *Strep. pyogenes* were also achieved (Figure 5-3). In the absence of the quantum dots, a 5 minute exposure of the organism (at a concentration of 1.16 x 10^7 cfu/mL) to light in the presence of TBO resulted in a 2.53 $\log_{10}$ reduction in the viable count. However, when quantum dots were included at a TBO:quantum dots ratio of 267:1, the reduction in viable count amounted to 4.08 $\log_{10}$ units, an enhanced kill of 1.55 $\log_{10}$ units. At TBO:quantum dots ratios of 2667:1 enhanced kills were also observed but the enhancement was not as great as that observed at a ratio of 267:1. As with the *S. aureus* experiments the highest quantum dot concentration of 0.75 μM (TBO:quantum dots (27:1)) resulted in kills that were lower than those achieved with TBO alone. Positive and negative controls showed no significant changes in cell numbers throughout the course of these experiments.

In order to unravel the cause of the enhancement in bacterial kill, four additional experiments were conducted. First an absorption experiment was carried out to measure the absorption characteristics of quantum dots when mixed with toluidine blue. Secondly, a direct measurement of the amount of singlet oxygen generated at different quantum dot-TBO ratios was taken. Thirdly, an experiment was carried out to measure the fluorescence quenching of the quantum dots in the presence of TBO at different concentrations. Finally, an investigation into the type of mechanism, whether it be a FRET or non-FRET was conducted.

The absorption at 625 nm in the UV-visible absorption spectra (Figure 5-4) of quantum dots increased with concentration. Quantum dots absorb at all wavelengths below 650 nm in the visible part of the spectrum. Mixtures of toluidine blue with quantum dots absorb wavelengths of less than 700 nm in the visible part of the spectrum.

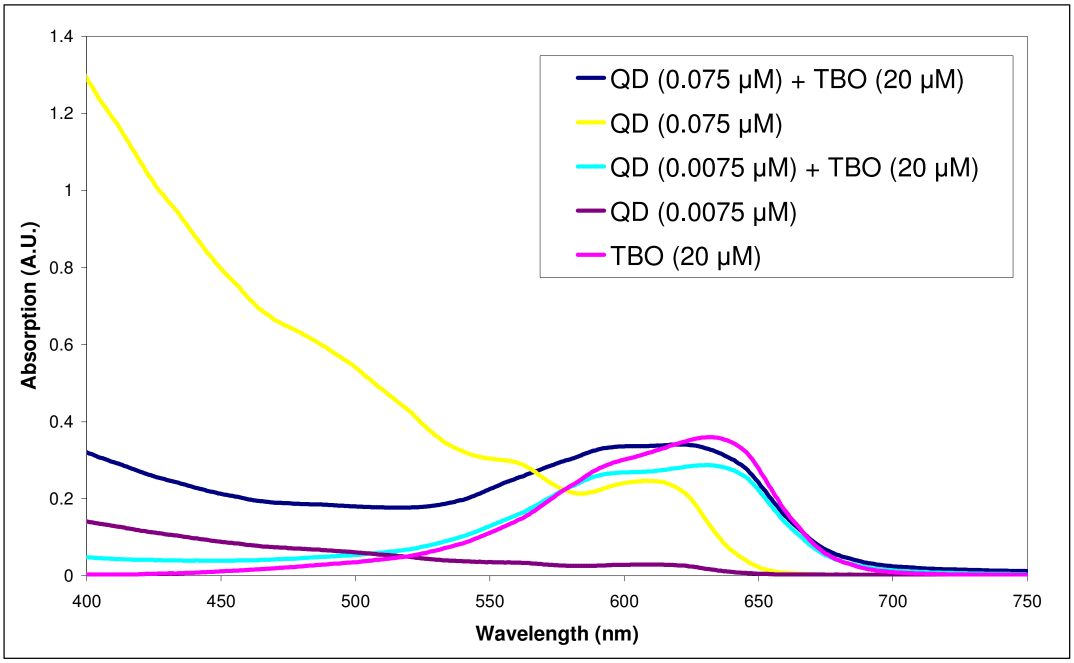

Figure 5-4 ***UV-visible absorption experiments at various concentrations of quantum dots with and without toluidine blue (20 µM).***

The second experiment was to measure the quantity of singlet oxygen produced from the different quantum dot concentrations when mixed with toluidine blue. This experiment measured the emission associated with the singlet oxygen to triplet oxygen conversion at 1260 nm. The amount of singlet oxygen was determined by measuring the area of the singlet oxygen fluorescence peak (measures singlet to triplet oxygen conversion), by integrating the area under the best fit exponential curve (Figure 5-5). These show that the amount of singlet oxygen produced is directly linked to the quantum dot:TBO ratio. All of the experiments were conducted at the same TBO concentration but at different quantum dot concentrations. At the lowest quantum dot concentration (0.0075 µM), the largest amount of singlet oxygen was generated - and this was more than twice the amount of singlet oxygen generated at the highest quantum dot concentration of 0.075 µM. Furthermore, singlet oxygen was produced in the absence of quantum dots – indeed the amount produced was greater than in the presence of quantum dots demonstrating that the latter suppressed singlet oxygen generation.

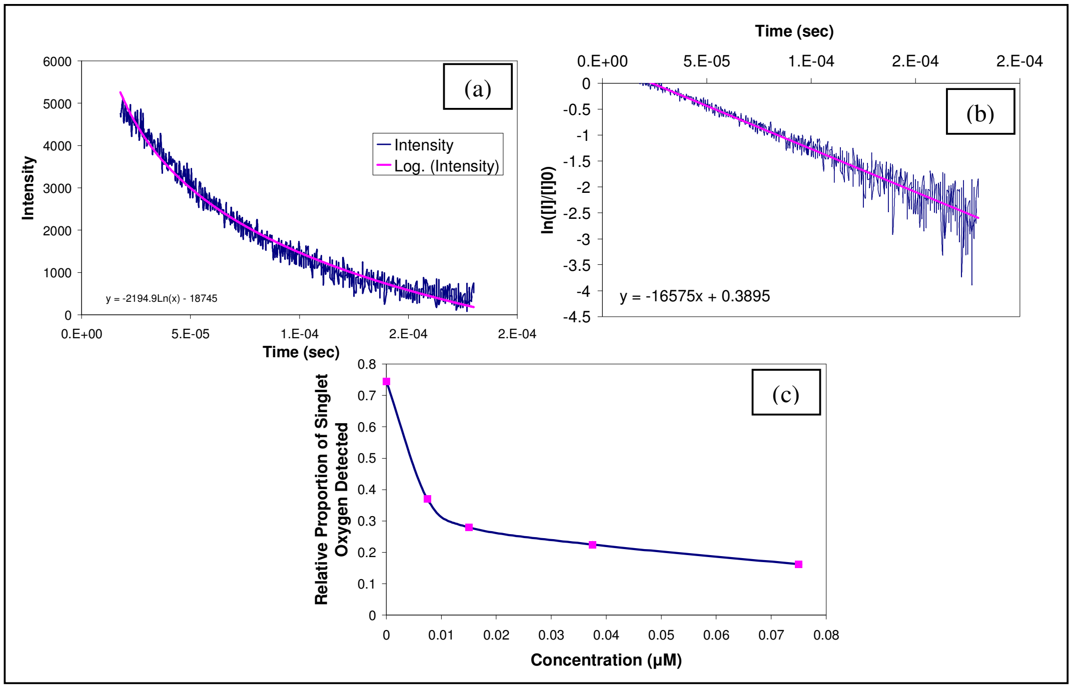

Figure 5-5 ***(a) Plot of intensity against time of the singlet oxygen decay produced from quantum dots at 0.015 μM and toluidine blue at 20 μM (area under the curve is proportional to singlet oxygen concentration). (b) Plot of ln[I]/[I]$_0$ transformation of the first order exponential decay of singlet oxygen. (c) Graph of the relative proportion of singlet oxygen produced as a function of the concentration of quantum dots whilst a constant concentration of toluidine blue (20 μM) was maintained.***

It was found that the emission peak of the quantum dots at 627 nm when mixed with TBO was significantly reduced (Figure 5-6). This indicates that the TBO and quantum dots were interacting with each other. Furthermore, this communication was concentration-dependent, with the greatest reduction in emission seen at the lowest quantum dot concentration (Figure 5-6 (d)). The evidence of emission adsorption was very strong because the peak associated with the emission was significantly reduced (up to ca. 90% absorption by TBO), whilst the second harmonic peak associated with the exciting wavelength seen at ca. 720 nm was largely unaffected by the process.

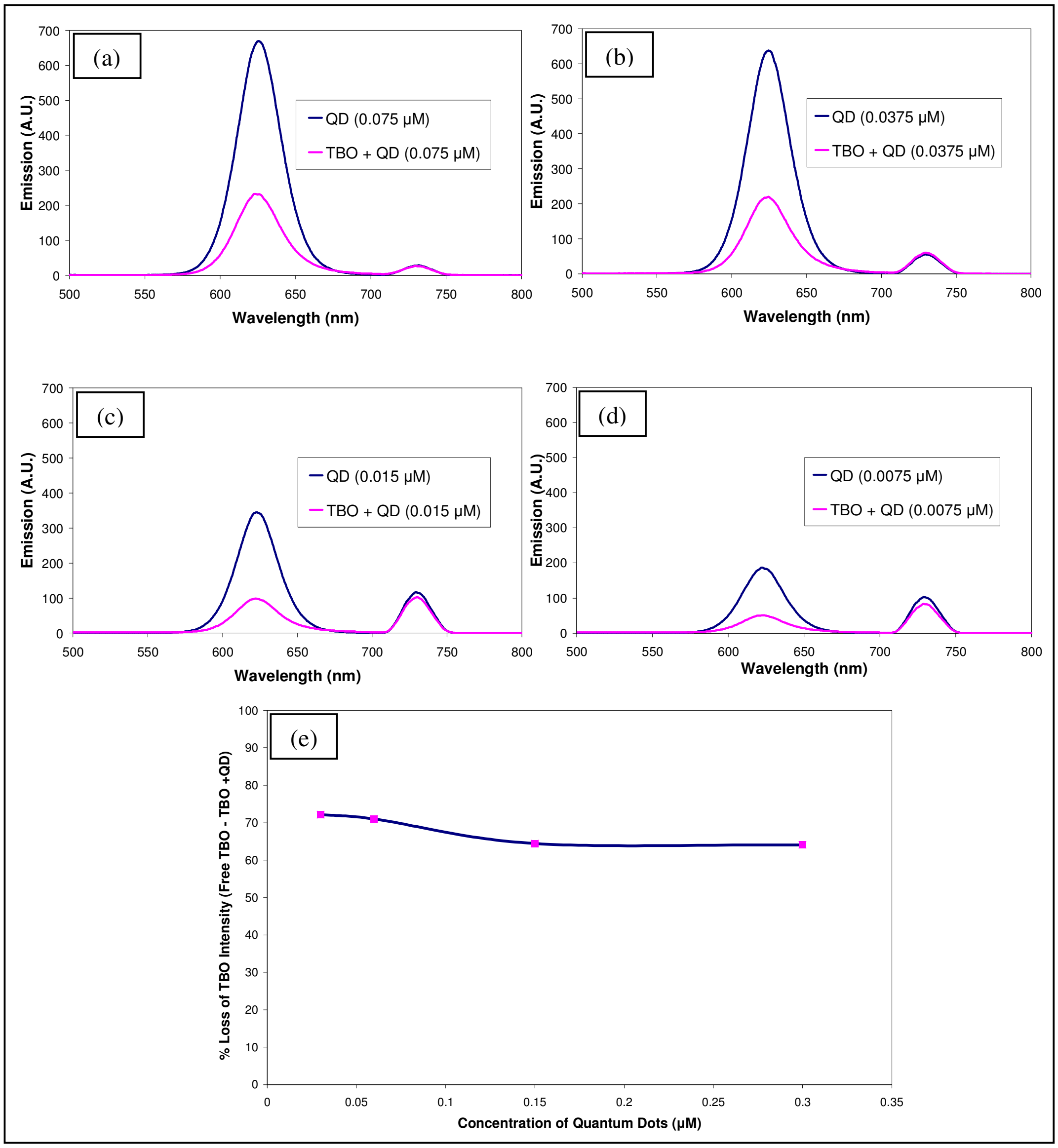

Figure 5-6 *(a) Fluorescence spectra of quantum dots at 0.075 µM concentration (blue) and a mixture of quantum dots (0.075 µM)with toluidine blue, 20 µM (pink). (b) Fluorescence spectra of quantum dots at 0.0375 µM concentration (blue) and a mixture of quantum dots (0.0375 µM) with toluidine blue, 20 µM (pink). (c) Fluorescence spectra of quantum dots at 0.015 µM concentration (blue) and quantum dots (0.015 µM) with toluidine blue, 20 µM (pink). (d) Fluorescence spectra of quantum dots at 0.0075 µM concentration (blue) and a mixture of quantum dots (0.0075 µM) with toluidine blue, 20 µM (pink). The fluorescence emission decreases as the concentration of quantum dots decreases. The fluorescence emission of the quantum dots is reduced when TBO (20 µM) is present. (e) The percentage fluorescence emission (expressed as fluorescence in the presence of TBO/ fluorescence without TBO × 100) as a function of quantum dot concentration in the presence of TBO 20 µM. The peaks between 700 and 750 nm in (a), (b), (c) and (d) are second order excitation peaks from the 365 nm excitation.*

An experiment to determine whether the quantum dots and toluidine blue could interact through a radiation-less energy exchange FRET mechanism or through an emission – re-absorption phenomenon was conducted (Figure 5-7). FRET mechanisms are reported to operate over very short distances (10 nm), by separating the TBO and QD in separate compartments of the same cell with an intervening wall separation of at least 100,000 nm it was demonstrated mechanistically that the process could be accounted for by a non-FRET mechanism.

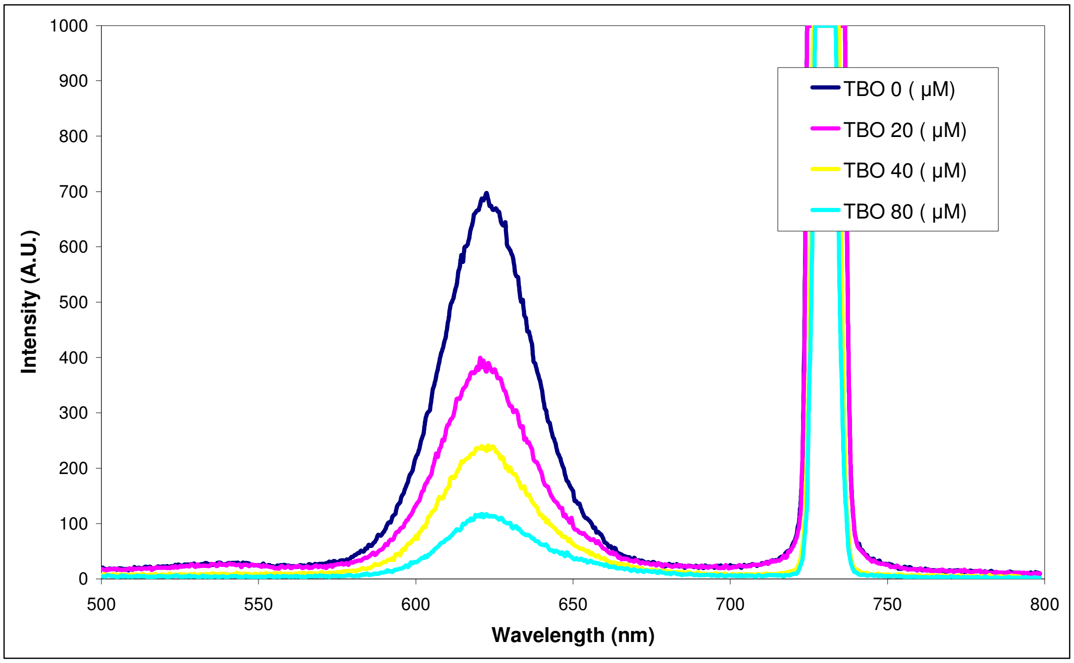

Figure 5-7 ***Quenched fluorescence of quantum dots (0.0125 μM) in the presence of various concentrations of TBO – the separation distance was in excess of 100,000 nm.***

5.4 Discussion

Toluidine blue has long been known to be an effective lethal photosensitiser of bacteria. Mathews[181] and MacMillan *et al.*[80] have reported the use of this dye to sensitise bacteria, killing by white light and light from a helium/neon laser, respectively. The results in this chapter have demonstrated that the addition of quantum dots with an emission maximum of 627 nm, which is close to the absorption maximum of 630 nm of

TBO, can significantly enhance the efficacy of TBO-mediated lethal photosensitisation of *Staph. aureus* and *Staph. pyrogenes*.

There is currently great interest in the potential use of quantum dots and other nanoparticles in photodynamic therapy.[8,182] In a study by Samia *et al.*[176], quantum dots have been shown to transfer energy directly to molecular oxygen to generate singlet oxygen.[176] CdSe/ZnS quantum dots with a diameter of 5 nm were used in the study and, on irradiation with light with a wavelength of 488 nm, singlet oxygen was generated with a quantum yield of approximately 5%. In contrast, the results in this chapter do not display any bactericidal effect when bacteria were irradiated in the presence of quantum dots and in the absence of TBO. This may be because either no singlet oxygen was generated by the quantum dots or else the yield was so low that the resulting bacterial kill was too small to be detectable. When quantum dots are covalently linked to a photosensitiser, singlet oxygen can be generated on irradiation with light of a wavelength not absorbed by the photosensitiser itself.[176] In this study, on irradiation with 488 nm light, CdSe/ZnS quantum dots linked to a silicon phthalocyanine photosensitiser were able to generate singlet oxygen by a "fluorescence" resonance energy transfer (Förster resonance energy transfer - FRET) mechanism. In this mechanism the excitation energy can be transferred by a radiationless process to a neighboring fluorophore when their energy level difference corresponds to the quantum of excitation energy. The conditions for this mechanism are: the fluorescent emission spectra of the energy donor must overlap the absorption spectrum of the energy acceptor. The two fluorophores need not necessarily be part of the same molecule. Energy transfer will take place between isolated molecules in solution as long as the concentration is high enough to bring the average intermolecular distance to less than a few nm.

The experiments conducted by Samia *et al.*[176] were performed in toluene, a solvent which would not be compatible with biological systems. Shi *et al.*[183] synthesised water miscible Cd/Te quantum dots organic dye nanocomposites which produced singlet oxygen. The organic dye used was *meso*-tetra(4-sulphonatophenyl)porphine dihydochloride (TSPP) and was electrostatically bound to the surface of the quantum dot. In their UV-visible absorption experiments they found the bound dye absorption had a slight blue shift when compared to the unbound dye. This is consistent with the results in this chapter and can be attributed to H-type aggregates of the dye on the quantum dot surface. H–aggregates consist of a parallel arrangement of dye molecules to form a vertical stack and correspond to a blue shift in the absorption band.[114] Shi *et al.*[183] also observed immediate aggregation on addition of dye which was not observed in the results presented here. This can be explained by comparing the concentration of dye used; the Shi *et al.* experiment uses a concentration an order of magnitude larger. In agreement with the results presented here, Shi *et al.*[183] found the emission from the quantum dots reduced greatly upon addition of dye. In contrast to the results presented by Samia *et al.*[176], Shi *et al.*[183] did not detect any singlet oxygen production in the absence of a dye, which is again consistent with the results presented here. The dye that Shi *et al.*[183] used (TSPP) had no appreciable absorption at the excitation wavelength (355 nm, Nd:YAG) that they used to irradiate the quantum dot/dye nanocomposite for the singlet oxygen detection experiments. A FRET type mechanism was proposed to account for the singlet oxygen produced. FRET is the non-radiative transfer from the quantum dot to the dye which subsequently produced singlet oxygen.

The experiments in this chapter were performed on quantum dots which were not covalently linked to the toluidine blue molecules. Irradiation with white light resulted in bacterial kills in considerable excess to those achieved when toluidine blue was used alone. Significantly, the greatest kills or enhancements were seen at the higher TBO:quantum dots ratios or lowest quantum dot concentrations. The CdSe/ZnS quantum dots exhibited high absorbance with a number of bands (440-550 nm and 610-620 nm) emitted by the white light source used. The emission band of the quantum dots (627 nm) corresponded closely with the main absorbance band of the TBO (630 nm). It is possible, therefore, that the TBO molecules were sufficiently close to the quantum dots (within 6 nm) to enable a FRET mechanism to take place resulting in the generation of cytotoxic species and, consequently, a bactericidal effect. It is also possible that the TBO interacts with the PEG coating of the quantum dot via a weak electrostatic/hydrogen bonding interaction.

The greatest interaction between the quantum dot and toluidine blue was observed at the lowest quantum dot concentration which is counter intuitive to a direct FRET mechanism. The ratio of TBO:QD was crucial for achieving an enhancement of the bactericidal effect. For *Staph. aureus*, enhancement occurred only when the ratio of TBO:quantum dots was between 133:1 and 2667:1 at quantum dot concentrations between 0.075 and 0.0075 μM. There have been many reports which conclude that quantum dots are not toxic to biological cells[177,184] from leaching of cadmium ions. However this did not affect the lethal photosensitisation results here as control experiments indicated that the quantum dots were toxic to the bacteria in the environment and for experimental time that they were in contact.

The fluorescence measurements of the TBO:QD mixture showed significant absorption of the quantum dot emission. This reduction in emission may be due to energy transfer from the quantum dot to the toluidine blue. By measuring the emission of a compartmentalised quantum dot and toluidine blue solution, it was evident that the quantum dot emission as measured by the instrument detector was directly proportional to the external toluidine blue concentration and followed the Beer-Lambert law. This indicates that the light emitted by the quantum dots is directly absorbed by the toluidine blue solution (Figure 5-7). This process can only be through a radiative process as the two compartments were separated by a distance far in excess of that required for a FRET pathway to operate. This experiment indicates that the observed pathway in fluorescence seen for intermixed QD-TBO solutions can be fully explained by a non-FRET mechanism in which the quantum dot absorbs radiation and emits at the maximum absorption of the toluidine blue dye.

In summary:-

- Mixtures of quantum dots and toluidine blue enhance bacterial kills in solution upon irradiation with white light at low quantum dot concentrations. Quantum dots have no direct toxic effect on the bacteria in the presence or absence of the white, light, and the observed bacterial kill did not scale with relative singlet oxygen concentration.
- Quantum dots suppress the formation of singlet oxygen from toluidine blue in water. The higher the quantum dot concentration in a solution, the lower the amount of singlet oxygen produced. Toluidine blue on its own produces more singlet oxygen on irradiation with white light than any TBO/QD solution.

- Quantum dot fluorescence is significantly absorbed in the presence of toluidine blue. The quantum dot fluorescence is quenched through absorption of the emitted light from the quantum dot and not through a FRET mechanism. The amount of emitted light from the quantum dot that is absorbed by the TBO is directly proportional to the TBO concentration.
- The emission spectrum of the light used in the experiments did not match very well with the TBO absorption maximum; however the QD emission and TBO absorption were closely matched.

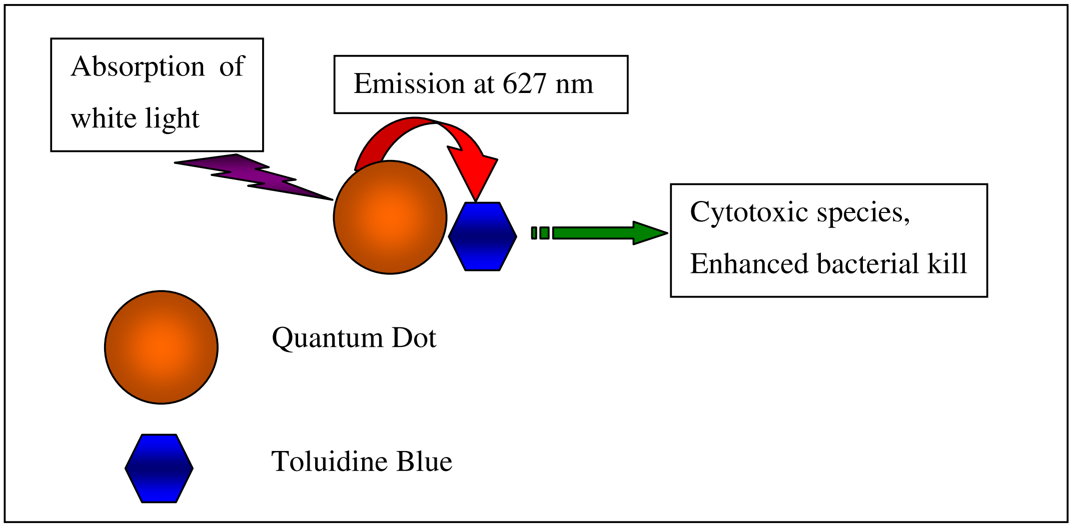

Figure 5-8 ***Absorption of white light by quantum dots and emission at 627, which is absorbed by toluidine blue. Toluidine blue is essential for the formation of singlet oxygen and cytotoxic species which are lethal to bacteria.***

It can be deduced that quantum dots synergistically enhance the ability of toluidine blue to kill bacteria. No bacterial kill was seen in the absence of toluidine blue and the quantum dots improve the photosensitising ability of toluidine blue by absorbing light with a wavelength less than 620 nm and up-shifting this *via* an emission process to approximately 627 nm which is close to the absorption maximum of the toluidine blue (Figure 5-8). The quantum dots also have a further role in the process, as they suppress the formation of singlet oxygen from the excited toluidine blue molecule. The QD-TBO interaction is a complicated one, in the presence of quantum dots more toluidine blue is found in the excited state. However, the toluidine blue relaxes to its ground state through the formation of cytotoxic molecular species other than singlet oxygen:

presumably other radicals such as the hydroxyl radical.[90] It is the formation of these activated radicals that are responsible for the enhanced bacterial kills observed.

5.5 Conclusion

In conclusion, quantum dots of CdSe/ZnS enhance the antimicrobial effect of the light-activated antimicrobial agent toluidine blue. The lethal photosensitisation of *Staph. aureus*, using toluidine blue and quantum dots is concentration-dependent. An excess of a 1.7 $\log_{10}$ enhancement was observed with the lowest quantum dot concentration (0.0075 μM), highest QD:TBO ratios. It was deduced that an emission- absorption process from the quantum dots to the toluidine blue occurs, especially at low quantum dot concentrations by fluorescence measurements. The enhanced bacterial kills observed in lethal photosensitisation experiments in the presence of quantum dots and toluidine blue are the result of light-induced production of greater quantities of reactive oxygen species (other than singlet oxygen) by toluidine blue. An energy transfer from the quantum dots to toluidine blue is induced at low quantum dot concentrations. Light was absorbed by the quantum dots and then re-emitted at the absorption maximum of TBO. The quantum dot, converts the incident white light to the frequency at which toluidine blue has a maximum absorption. Consequently a greater proportion of toxic species are formed and an enhanced bacterial kill is observed.

Chapter 6 Conclusion

This thesis reported on coupling light activated antimicrobial agents with gold nanoparticles to provide new nano bio-materials which displayed enhanced antimicrobial properties. The gold nanoparticle formed the central core of the nano-biomaterial. Organic molecules were adsorbed onto the surface or they were chemically attached. Light activated antimicrobial agents were mixed with gold nanoparticles so that they were adsorbed onto the surface. Additionally alkane thiol protected nanoparticles were synthesised, and the light activated antimicrobial was chemically attached to the monolayer. A mechanistic study was performed in order to uncover information on the relationship between quantum dots and toluidine blue.

6.1 Summary of Results

A novel highly effective and potent light activated antimicrobial was synthesised. The conjugation of toluidine blue to tiopronin–gold nanoparticles has proved to be exceptionally effective at killing *Staphylococcus aureus*. At 1 μM concentration and using white light for 30 minutes, the conjugate showed a reduction in colony forming units (cfu) of 4.5 $\log_{10}$ compared with 0.5 $\log_{10}$ for toluidine blue at the same concentration. The superior performance of the conjugate was attributed to the enhanced extinction coefficient of toluidine blue–tiopronin–gold nanoparticles, a result of the association to the gold core surface, when compared to free toluidine blue. In terms of their minimum bactericidal concentrations (MBCs), the covalently linked toluidine blue–tiopronin–gold nanoparticle conjugates are the most potent light-activated antimicrobial agents reported to date. This gold-thiol-photosensitiser motif was further investigated by using the thiol glutathione (GS) and photosensitiser tin chlorin e6. Nanoparticles with motifs of gold-glutathione-tin chlorin e6 (Au-GS-SnCe6), of different diameters ranging from 1.73 to 6.24 nm were synthesised in a two step reaction. The attachment of the photosensitiser tin chlorin e6 to glutathione protected gold nanoparticles was confirmed by UV-visible absorption spectroscopy. This study established that the synthetic route is robust enough for many different combinations of gold-thiol-photosensitiser to be explored.

The adsorption of basic cationic dyes of the thiazine family onto gold nanoparticles enhances the extinction coefficient of the dyes. This was not observed for the acidic anionic dyes investigated. The fluorescence of the thiazine dye toluidine blue is quenched in the presence of gold nanoparticles. Additionally, the production of singlet oxygen by toluidine blue decreases in the presence of gold nanoparticles. Importantly it was found that the covalent attachment of a light activated antimicrobial such as toluidine blue was not required for an enhancement in bacterial kill to be observed. The enhanced bacterial kill observed was attributed to reactive oxygen species other than singlet oxygen, such as hydroxyl radicals being production.

Quantum dots of CdSe/ZnS enhance the antimicrobial effect of the light-activated antimicrobial agent toluidine blue. It was found that the lethal photosensitisation of bacteria using toluidine blue and quantum dots was concentration-dependent. An excess of 1.7 $\log_{10}$ enhancement in bacterial kill was observed with the lowest quantum dot concentration (0.0075 µM). A mechanistic study revealed that an emission - absorption process from the quantum dots to the toluidine blue occurs, especially at low quantum dot concentrations. The enhanced bacterial kills observed in lethal photosensitisation experiments in the presence of quantum dots and toluidine blue, are attributed but not proven to be due to light-induced production of greater quantities of reactive oxygen species (other than singlet oxygen) by toluidine blue. Incoming light was absorbed by the quantum dots and then re-emitted at the absorption maximum of toluidine blue. The quantum dot, converts the incident white light to the frequency at which toluidine blue has a maximum absorption. Consequently a greater proportion of toxic species are formed and an enhanced bacterial kill is observed.

The investigations conducted in this work can be split into two areas; covalent attachment of photosensitisers to gold nanoparticles and mixing of photosensitisers with nanoparticles. The covalent attachment of photosensitisers to thiol protected gold nanoparticles was divided into a further two systems. The two systems investigated had motifs of gold-tiopronin-toluidine blue and gold-glutathione-tin chlorin e6. The synthesis of these particles has proven to be versatile and the coupling chemistry robust enough to be applied to different systems. The covalent attachment of photosensitisers to gold nanoparticles has antibacterial properties and nanoparticles with the motif gold-tiopronin-toluidine blue enhance the bacterial kill. This has been the first application of nanoparticles coupled with photosensitisers in the lethal photosensitisation of microbes.

The second area investigated was the mixing of nanoparticles and photosensitisers. This was split into a further two systems of gold and CdSe quantum dots. Both systems were found to enhance the kill of bacteria. The singlet oxygen experiments for both systems found that the relative proportion of singlet oxygen produced by the photosensitiser, in the presence of gold and CdSe nanoparticles was suppressed. This indicates that the mechanism by which bacterial kill is achieved is not solely due to the production of singlet oxygen and that other radical species such as hydroxyl radicals play an important role. It was found that the photoluminescence of toluidine blue was quenched by gold nanoparticles, whereas the photoluminescence of the quantum dots was absorbed by the toluidine blue, suggesting that the enhanced bacterial kill operates *via* different pathways. In the case of CdSe quantum dots and toluidine blue some evidence was found to suggest a non-FRET mechanism whereby, the quantum dots absorb light and re-emit the light at a wavelength optimum for the absorption by toluidine blue. In the case of charge stabilised gold nanoparticles it was found that mixing of these particles with certain basic cationic dyes achieved enhanced extinction coefficients by UV-visible absorption spectroscopy. This enhanced absorption is thought to be part of the reason behind the enhanced bacterial kills observed when gold nanoparticles are mixed with photosensitisers.

In general nanoparticles of gold and CdSe enhance the lethal photosensitisation of bacteria, and that covalent attachment of the photosensitiser to the surface of the nanoparticle is not necessary for this enhancement to be observed. The relationship between the nanoparticles and photosensitisers seems to be a complex one, where the nature of the nanoparticles and photosensitisers, the ratio between the two and size of the particles, all play a vital role. It appears that each system has its own mechanistic pathway by which enhanced lethal photosensitisation of bacteria occurs. However, enough evidence has been gathered in this investigation to suggest an antenna effect by the nanoparticle so that a higher concentration of toxic species (other than singlet oxygen) is produced.

6.2 Future perspectives

There many other aspects of chromophore functionalised gold nanoparticles that could be investigated. One of these is changing the linker tiopronin to other bioavailable molecules such as amines. The core size could be further increased and decreased to find an optimum, where the bacterial kill is highest. This could be achieved by decreasing the temperature at which the gold core was formed along with altering the coating : gold ratio. The gold–thiol nanoparticles acted as a supporting scaffold for attachment of the photosensitiser groups and also conferred water solubility. Other thiols which allow water solubility could be investigated. Additionally, the other photosensitisers could be placed in the gold-thiol-photosensitiser motif. It should be possible for the gold core to support further molecules. This could be utilised for the attachment of a specific targeting moiety such as an antibody or antibody fragment that is specific for a certain bacterial type, to obtain selective killing of bacteria.

In order to investigate the mechanism by which this enhanced bacterial kill operates EPR studies should be performed, to identify the triplet state of the photosensitiser when irradiated by light. This should be done in the presence and absence of gold nanoparticles to detect any differences.

References

1. M. B. Cortie, *The weird world of nanoscale gold.* Gold Bulletin, 2004. **37**(1-2): p. 12-19.
2. S. Eustis and M. A. El-Sayed, *Why gold nanoparticles are more precious than pretty gold: Noble metal surface plasmon resonance and its enhancement of the radiative and nonradiative properties of nanocrystals of different shapes.* Chemical Society Reviews, 2006. **35**(3): p. 209-217.
3. M. C. Daniel and D. Astruc, *Gold nanoparticles: Assembly, supramolecular chemistry, quantum-size-related properties, and applications toward biology, catalysis, and nanotechnology.* Chemical Reviews, 2004. **104**(1): p. 293-346.
4. L. F. Kozin and V. T. Melekhin, *Extraction of gold from ores and concentrates by leaching with the use of cyanides and alternative reagents.* Russian Journal of Applied Chemistry, 2004. **77**(10): p. 1573-1592.
5. R. H. Swendsen, *Statistical mechanics of colloids and Boltzmann's definition of the entropy.* American Journal of Physics, 2006. **74**(3): p. 187-190.
6. S. K. Ghosh and T. Pal, *Interparticle coupling effect on the surface plasmon resonance of gold nanoparticles: From theory to applications.* Chemical Reviews, 2007. **107**(11): p. 4797-4862.
7. L. A. Dykman and V. A. Bogatyrev, *Gold nanoparticles: Preparation, functionalisation, applications in biochemistry and immunochemistry.* Uspekhi Khimii, 2007. **76**(2): p. 199-213.
8. A. C. S. Samia, S. Dayal and C. Burda, *Quantum dot-based energy transfer: Perspectives and potential for applications in photodynamic therapy.* Photochemistry and Photobiology, 2006. **82**(3): p. 617-625.
9. A. K. Gupta and M. Gupta, *Synthesis and surface engineering of iron oxide nanoparticles for biomedical applications.* Biomaterials, 2005. **26**(18): p. 3995-4021.
10. G. Schmid, R. Pfeil, R. Boese, F. Bandermann, S. Meyer, G. H. M. Calis and W. A. Vandervelden, $Au_{55}[P(C_6H_5)_3]_{12}Cl_6$ *- a Gold Cluster of an Exceptional Size.* Chemische Berichte-Recueil, 1981. **114**(11): p. 3634-3642.
11. M. Giersig and P. Mulvaney, *Preparation of Ordered Colloid Monolayers by Electrophoretic Deposition.* Langmuir, 1993. **9**(12): p. 3408-3413.
12. U. Simon, G. Schon and G. Schmid, *The Application of Au-55 Clusters as Quantum Dots.* Angewandte Chemie-International Edition in English, 1993. **32**(2): p. 250-254.
13. H. J. Zhang, G. Schmid and U. Hartmann, *Reduced metallic properties of ligand-stabilized small metal clusters.* Nano Letters, 2003. **3**(3): p. 305-307.
14. S. Link and M. A. El-Sayed, *Size and temperature dependence of the plasmon absorption of colloidal gold nanoparticles.* Journal of Physical Chemistry B, 1999. **103**(21): p. 4212-4217.
15. A. I. Frenkel, C. W. Hills and R. G. Nuzzo, *A view from the inside: Complexity in the atomic scale ordering of supported metal nanoparticles.* Journal of Physical Chemistry B, 2001. **105**(51): p. 12689-12703.
16. J. W. Gentry, *The legacy of John Tyndall in aerosol science.* Journal of Aerosol Science, 1997. **28**(8): p. 1365-1372.

17. G. Frens, *Particle-Size and Sol Stability in Metal Colloids.* Kolloid-Zeitschrift and Zeitschrift Fur Polymere, 1972. **250**(7): p. 736-&.
18. G. Frens, *Controlled Nucleation for the Particle Size in Monodisperse Gold Suspensions.* Nature Physical Science, 1973. **241**: p. 20-22.
19. M. G. Blaber, M. D. Arnold, N. Harris, M. J. Ford and M. B. Cortie, *Plasmon absorption in nanospheres: A comparison of sodium, potassium, aluminium, silver and gold.* Physica B-Condensed Matter, 2007. **394**(2): p. 184-187.
20. L. E. Murillo, O. Viera, E. Vicuna, J. G. Briano, M. Castro, Y. Ishikawa, R. Irizarry and L. Sola, *Growth kinetics of gold nanoparticles.* 2006 International Conference on Computational Nanoscience and Nanotechnology - Iccn 2002, 2002: p. 435-438.
21. P. N. Njoki, I. I. S. Lim, D. Mott, H. Y. Park, B. Khan, S. Mishra, R. Sujakumar, J. Luo and C. J. Zhong, *Size correlation of optical and spectroscopic properties for gold nanoparticles.* Journal of Physical Chemistry C, 2007. **111**: p. 14664-14669.
22. T. Klar, M. Perner, S. Grosse, G. von Plessen, W. Spirkl and J. Feldmann, *Surface-plasmon resonances in single metallic nanoparticles.* Physical Review Letters, 1998. **80**(19): p. 4249-4252.
23. M. Faraday, *The Bakerian Lecture: Experimental Relations of Gold (and Other Metals) to Light.* Philosophical Transactions of the Royal Society of London, 1857. **147**: p. 145-181.
24. B. L. Cushing, V. L. Kolesnichenko and C. J. O'Connor, *Recent advances in the liquid-phase syntheses of inorganic nanoparticles.* Chemical Reviews, 2004. **104**: p. 3893-3946.
25. S. L. Barnholtz, J. D. Lydon, G. Huang, M. Venkatesh, C. L. Barnes, A. R. Ketring and S. S. Jurisson, *Syntheses and characterization of gold(III) tetradentate Schiff base complexes. X-ray crystal structures of [Au(sal(2)pn)]Cl center dot 2.5H(2)O and [Au(sal(2)en)]*PF_6. Inorganic Chemistry, 2001. **40**(5): p. 972-976.
26. W. Ostwald, *Practical Colloid Chemistry*. 4th ed. 1924, New York: Dutton. 1-11.
27. H. B. Weiser, *Inorganic Colloid Chemistry*. Vol. 1. 1933, New York: Wiley. 21-57.
28. J. Turkevich, P. C. Stevenson and J. Hillier, *A Study of the Nucleation and Growth Processes in the Synthesis of Colloidal Gold.* Discussions of the Faraday Society, 1951(11): p. 55-&.
29. J. W. Slot and H. J. Geuze, *A New Method of Preparing Gold Probes for Multiple-Labeling Cyto-Chemistry.* European Journal of Cell Biology, 1985. **38**(1): p. 87-93.
30. J. W. Slot and H. J. Geuze, *Sizing of Protein a-Colloidal Gold Probes for Immunoelectron Microscopy.* Journal of Cell Biology, 1981. **90**(2): p. 533-536.
31. M. Brust, M. Walker, D. Bethell, D. J. Schiffrin and R. Whyman, *Synthesis of Thiol-Derivatized Gold Nanoparticles in a 2-Phase Liquid-Liquid System.* Journal of the Chemical Society-Chemical Communications, 1994(7): p. 801-802.
32. R. G. Pearson and J. Songstad, *Application of Principle of Hard and Soft Acids and Bases to Organic Chemistry.* Journal of the American Chemical Society, 1967. **89**(8): p. 1827-&.

33. M. Brust, J. Fink, D. Bethell, D. J. Schiffrin and C. Kiely, *Synthesis and Reactions of Functionalized Gold Nanoparticles.* Journal of the Chemical Society-Chemical Communications, 1995(16): p. 1655-1656.
34. M. J. Hostetler, A. C. Templeton and R. W. Murray, *Dynamics of place-exchange reactions on monolayer-protected gold cluster molecules.* Langmuir, 1999. **15**(11): p. 3782-3789.
35. B. Nikoobakht and M. A. El-Sayed, *Preparation and growth mechanism of gold nanorods (NRs) using seed-mediated growth method.* Chemistry of Materials, 2003. **15**(10): p. 1957-1962.
36. K. R. Brown, D. G. Walter and M. J. Natan, *Seeding of colloidal Au nanoparticle solutions. 2. Improved control of particle size and shape.* Chemistry of Materials, 2000. **12**(2): p. 306-313.
37. K. R. Brown, L. A. Lyon, A. P. Fox, B. D. Reiss and M. J. Natan, *Hydroxylamine seeding of colloidal au nanoparticles. 3. Controlled formation of conductive Au films.* Chemistry of Materials, 2000. **12**(2): p. 314-323.
38. T. K. Sau, A. Pal, N. R. Jana, Z. L. Wang and T. Pal, *Size controlled synthesis of gold nanoparticles using photochemically prepared seed particles.* Journal of Nanoparticle Research, 2001. **3**(4): p. 257-261.
39. F. Chen, G.-Q. Xu and T. S. A. Hor, *Preparation and assembly of colloidal gold nanoparticles in CTAB-stabilized reverse microemulsion.* Materials Letters, 2003. **57**(21): p. 3282-3286.
40. H. Bonnemann and R. M. Richards, *Nanoscopic metal particles - Synthetic methods and potential applications.* European Journal of Inorganic Chemistry, 2001(10): p. 2455-2480.
41. V. K. Lamer and R. H. Dinegar, *Theory, Production and Mechanism of Formation of Monodispersed Hydrosols.* Journal of the American Chemical Society, 1950. **72**(11): p. 4847-4854.
42. E. J. Perry, *Extinctiometric Methods for Studying Protective Colloid Action and Ostwald Ripening of Silver Bromide Sols.* Journal of Physical Chemistry, 1958. **62**(5): p. 585-589.
43. M. K. Chow and C. F. Zukoski, *Gold Sol Formation Mechanisms - Role of Colloidal Stability.* Journal of Colloid and Interface Science, 1994. **165**(1): p. 97-109.
44. C. J. Sandroff and D. R. Herschbach, *Kinetics of Displacement and Charge-Transfer Reactions Probed by Sers - Evidence for Distinct Donor and Acceptor Sites on Colloidal Gold Surfaces.* Langmuir, 1985. **1**(1): p. 131-135.
45. M. Aslam, L. Fu, M. Su, K. Vijayamohanan and V. P. Dravid, *Novel one-step synthesis of amine-stabilized aqueous colloidal gold nanoparticles.* Journal of Materials Chemistry, 2004. **14**(12): p. 1795-1797.
46. E. A. K. J. E. Hughey, R. L. Keiter, *Principles of Structure and Reactivity*. 4th ed. Inorganic Chemistry. 1993, New York: Harper Collins College Publishers.
47. G. Han, P. Ghosh and V. M. Rotello, *Functionalized gold nanoparticles for drug delivery.* Nanomedicine, 2007. **2**(1): p. 113-123.
48. R. Levy, *Peptide-capped gold nanoparticles: Towards artificial proteins.* Chembiochem, 2006. **7**(8): p. 1141-1145.
49. A. C. Enriquez, I. A. R. Espejel, E. A. Garcia and M. E. Diaz-Garcia, *Enhanced resonance light scattering properties of gold nanoparticles due to cooperative binding.* Analytical and Bioanalytical Chemistry, 2008. **391**(3): p. 807-815.

50. V. Sokolova and M. Epple, *Inorganic nanoparticles as carriers of nucleic acids into cells.* Angewandte Chemie-International Edition, 2008. **47**(8): p. 1382-1395.
51. T. Murakami and K. Tsuchida, *Recent advances in inorganic nanoparticle-based drug delivery systems.* Mini-Reviews in Medicinal Chemistry, 2008. **8**(2): p. 175-183.
52. P. Pandey, M. Datta and B. D. Malhotra, *Prospects of nanomaterials in biosensors.* Analytical Letters, 2008. **41**(2): p. 159-209.
53. I. Palchetti and M. Mascini, *Nucleic acid biosensors for environmental pollution monitoring.* Analyst, 2008. **133**(7): p. 846-854.
54. P. P. Pompa, R. Chiuri, L. Manna, T. Pellegrino, L. L. del Mercato, W. J. Parak, F. Calabi, R. Cingolani and R. Rinaldi, *Fluorescence resonance energy transfer induced by conjugation of metalloproteins to nanoparticles.* Chemical Physics Letters, 2006. **417**(4-6): p. 351-357.
55. I. Willner, B. Shlyahovsky, M. Zayats and B. Willner, *DNAzymes for sensing, nanobiotechnology and logic gate applications.* Chemical Society Reviews, 2008. **37**(6): p. 1153-1165.
56. S. H. Hsu, H. J. Yen and C. L. Tsai, *The response of articular chondrocytes to type II collagen-Au nanocomposites.* Artificial Organs, 2007. **31**: p. 854-868.
57. X. J. Ji, R. P. Shao, A. M. Elliott, R. J. Stafford, E. Esparza-Coss, J. A. Bankson, G. Liang, Z. P. Luo, K. Park, J. T. Markert and C. Li, *Bifunctional gold nanoshells with a superparamagnetic iron oxide-silica core suitable for both MR imaging and photothermal therapy.* Journal of Physical Chemistry C, 2007. **111**(17): p. 6245-6251.
58. H. Z. Jin and K. A. Kang, *Application of novel metal nanoparticles as optical/thermal agents in optical mammography and hyperthermic treatment for breast cancer.* Oxygen Transport to Tissue Xxviii, 2007. **599**: p. 45-52.
59. S. H. Kim, M. J. Kim and Y. H. Choa, *Fabrication and estimation of Au-coated Fe_3O_4 nanocomposite powders for the separation and purification of biomolecules.* Materials Science and Engineering a-Structural Materials Properties Microstructure and Processing, 2007. **449**: p. 386-388.
60. H. Y. Park, M. J. Schadt, L. Wang, I. I. S. Lim, P. N. Njoki, S. H. Kim, M. Y. Jang, J. Luo and C. J. Zhong, *Fabrication of magnetic core @ shell Fe oxide @ Au nanoparticles for interfacial bioactivity and bio-separation.* Langmuir, 2007. **23**(17): p. 9050-9056.
61. C. Alric, J. Taleb, G. Le Duc, C. Mandon, C. Billotey, A. Le Meur-Herland, T. Brochard, F. Vocanson, M. Janier, P. Perriat, S. Roux and O. Tillement, *Gadolinium chelate coated gold nanoparticles as contrast agents for both X-ray computed tomography and magnetic resonance imaging.* Journal of the American Chemical Society, 2008. **130**(18): p. 5908-5915.
62. P. J. Debouttiere, S. Roux, F. Vocanson, C. Billotey, O. Beuf, A. Favre-Reguillon, Y. Lin, S. Pellet-Rostaing, R. Lamartine, P. Perriat and O. Tillement, *Design of gold nanoparticles for magnetic resonance imaging.* Advanced Functional Materials, 2006. **16**(18): p. 2330-2339.
63. K. K. Jain, *Nanomedicine: Application of nanobiotechnology in medical practice.* Medical Principles and Practice, 2008. **17**(2): p. 89-101.
64. T. Powell and J. Y. Yoon, *Fluorescent biorecognition of gold nanoparticle-IgG conjugates self-assembled on e-beam patterns.* Biotechnology Progress, 2006. **22**(1): p. 106-110.

65. C. J. Ackerson, P. D. Jadzinsky and R. D. Kornberg, *Thiolate ligands for synthesis of water-soluble gold clusters.* Journal of the American Chemical Society, 2005. **127**(18): p. 6550-6551.
66. L. A. Porter, D. Ji, S. L. Westcott, M. Graupe, R. S. Czernuszewicz, N. J. Halas and T. R. Lee, *Gold and silver nanoparticles functionalized by the adsorption of dialkyl disulfides.* Langmuir, 1998. **14**(26): p. 7378-7386.
67. Y. S. Shon, C. Mazzitelli and R. W. Murray, *Unsymmetrical disulfides and thiol mixtures produce different mixed monolayer-protected gold clusters.* Langmuir, 2001. **17**(25): p. 7735-7741.
68. Y. L. Liu, K. B. Male, P. Bouvrette and J. H. T. Luong, *Control of the size and distribution of gold nanoparticles by unmodified cyclodextrins.* Chemistry of Materials, 2003. **15**(22): p. 4172-4180.
69. G. H. Woehrle and J. E. Hutchison, *Thiol-functionalized undecagold clusters by ligand exchange: Synthesis, mechanism, and properties.* Inorganic Chemistry, 2005. **44**(18): p. 6149-6158.
70. R. Hong, J. M. Fernandez, H. Nakade, R. Arvizo, T. Emrick and V. M. Rotello, *In situ observation of place exchange reactions of gold nanoparticles. Correlation of monolayer structure and stability.* Chemical Communications, 2006(22): p. 2347-2349.
71. T. J. Dougherty, C. J. Gomer, B. W. Henderson, G. Jori, D. Kessel, M. Korbelik, J. Moan and Q. Peng, *Photodynamic therapy.* Journal of the National Cancer Institute, 1998. **90**(12): p. 889-905.
72. D. Mitton and R. Ackroyd, *History of photodynamic therapy in Great Britain.* Photodiagnosis and Photodynamic Therapy, 2005. **2**(4): p. 239-246.
73. R. Ackroyd, C. Kelty, N. Brown and M. Reed, *The history of photodetection and photodynamic therapy.* Photochemistry and Photobiology, 2001. **74**(5): p. 656-669.
74. G. Jori, C. Fabris, M. Soncin, S. Ferro, O. Coppellotti, D. Dei, L. Fantetti, G. Chiti and G. Roneucci, *Photodynamic therapy in the treatment of microbial infections: Basic principles and perspective applications.* Lasers in Surgery and Medicine, 2006. **38**(5): p. 468-481.
75. U. O. Nseyo, J. DeHaven, T. J. Dougherty, W. R. Potter, D. L. Merrill, S. L. Lundahl and D. L. Lamm, *Photodynamic therapy (PDT) in the treatment of patients with resistant superficial bladder cancer: A long term experience.* Journal of Clinical Laser Medicine & Surgery, 1998. **16**(1): p. 61-68.
76. J. Usuda, H. Kato, T. Okunaka, K. Furukawa, H. Tsutsui, K. Yamada, Y. Suga, H. Honda, Y. Nagatsuka, T. Ohira, M. Tsuboi and T. Hirano, *Photodynamic therapy (PDT) for lung cancers.* Journal of Thoracic Oncology, 2006. **1**(5): p. 489-493.
77. S. M. Fien and A. R. Oseroff, *Photodynamic therapy for non-melanoma skin cancer.* J Natl Compr Canc Netw, 2007. **5**(5): p. 531-40.
78. J. Trachtenberg, A. Bogaards, R. A. Weersink, M. A. Haider, A. Evans, S. A. McCluskey, A. Scherz, M. R. Gertner, C. Yue, S. Appu, A. Aprikian, J. Savard, B. C. Wilson and M. Elhilali, *Vascular targeted photodynamic therapy with palladium-bacteriopheophorbide photosensitizer for recurrent prostate cancer following definitive radiation therapy: Assessment of safety and treatment response.* Journal of Urology, 2007. **178**: p. 1974-1979.
79. N. M. Bressler, S. B. Bressler, L. A. Haynes, Y. Hao, P. K. Kaiser, J. W. Miller, J. Naor, M. J. Potter, C. J. Pournaras, A. Reaves, P. J. Rosenfeld, U. Schmidt-Erfurth, J. S. Slakter, A. Strong and S. Vannier, *Verteporfin therapy for*

subfoveal choroidal neovascularization in age-related macular degeneration: four-year results of an open-label extension of 2 randomized clinical trials: TAP Report No. 7. Arch Ophthalmol, 2005. **123**(9): p. 1283-5.

80. J. D. Macmillan, W. A. Maxwell and C. O. Chichester, *Lethal photosensitization of microorganisms with light from a continuous-wave gas laser.* Photochem Photobiol, 1966. **5**(7): p. 555-65.
81. J. S. Bellin, L. Lutwick and B. Jonas, *Effects of Photodynamic Action on E Coli.* Archives of Biochemistry and Biophysics, 1969. **132**(1): p. 157-&.
82. J. E. Schneider, J. R. Phillips, Q. Pye, M. L. Maidt, S. Price and R. A. Floyd, *Methylene-Blue and Rose-Bengal Photoinactivation of Rna Bacteriophages - Comparative-Studies of 8-Oxoguanine Formation in Isolated Rna.* Archives of Biochemistry and Biophysics, 1993. **301**(1): p. 91-97.
83. R. Bonnett, *Photosensitizers of the Porphyrin and Phthalocyanine Series for Photodynamic Therapy.* Chemical Society Reviews, 1995. **24**(1): p. 19-33.
84. M. Wainwright, *Photodynamic antimicrobial chemotherapy (PACT).* Journal of Antimicrobial Chemotherapy, 1998. **42**(1): p. 13-28.
85. M. Wainwright, *Methylene blue derivatives -- suitable photoantimicrobials for blood product disinfection?* International Journal of Antimicrobial Agents, 2000. **16**(4): p. 381-394.
86. T. C. Oldham and D. Phillips, *Flash photolysis of sensitizers in microbes.* Journal of Physical Chemistry B, 1999. **103**(43): p. 9333-9349.
87. F. Bohm, G. Marston, T. G. Truscott and R. P. Wayne, *Fourier-Transform Detection of Singlet Oxygen and Fluorescence from Cell-Membrane Bound Porphyrins.* Journal of the Chemical Society-Faraday Transactions, 1994. **90**(17): p. 2453-2454.
88. L. W. Ma, J. Moan and K. Berg, *Evaluation of a New Photosensitizer, Meso-Tetra-Hydroxyphenyl-Chlorin, for Use in Photodynamic Therapy - a Comparison of Its Photobiological Properties with Those of 2 Other Photosensitizers.* International Journal of Cancer, 1994. **57**(6): p. 883-888.
89. F. Fischer, G. Graschew, H. J. Sinn, W. Maier-Borst, W. J. Lorenz and P. M. Schlag, *A chemical dosimeter for the determination of the photodynamic activity of photosensitizers.* Clinica Chimica Acta, 1998. **274**(1): p. 89-104.
90. G. P. Tegos, T. N. Demidova, D. Arcila-Lopez, H. Lee, T. Wharton, H. Gali and M. R. Hamblin, *Cationic fullerenes are effective and selective antimicrobial photosensitizers.* Chemistry & Biology, 2005. **12**(10): p. 1127-1135.
91. M. L. Embleton, S. P. Nair, B. D. Cookson and M. Wilson, *Selective lethal photosensitization of methicillin-resistant Staphylococcus aureus using an IgG-tin(IV) chlorin e6 conjugate.* Journal of Antimicrobial Chemotherapy, 2002. **50**(6): p. 857-864.
92. N. Komerik, H. Nakanishi, A. J. MacRobert, B. Henderson, P. Speight and M. Wilson, *In vivo killing of Porphyromonas gingivalis by toluidine blue-mediated photosensitization in an animal model.* Antimicrobial Agents and Chemotherapy, 2003. **47**(3): p. 932-940.
93. M. Wilson, *Photolysis of Oral Bacteria and Its Potential Use in the Treatment of Caries and Periodontal-Disease.* Journal of Applied Bacteriology, 1993. **75**(4): p. 299-306.
94. Y. Itoh, Y. Ninomiya, S. Tajima and A. Ishibashi, *Photodynamic therapy of acne vulgaris with topical delta-aminolaevulinic acid and incoherent light in Japanese patients.* British Journal of Dermatology, 2001. **144**(3): p. 575-579.

95. M. R. Hamblin, D. A. O'Donnell, N. Murthy, C. H. Contag and T. Hasan, *Rapid control of wound infections by targeted photodynamic therapy monitored by in vivo bioluminescence imaging.* Photochemistry and Photobiology, 2002. **75**(1): p. 51-57.
96. M. C. Teichert, J. W. Jones, M. N. Usacheva and M. A. Biel, *Treatment of oral candidiasis with methylene blue-mediated photodynamic therapy in an immunodeficient murine model.* Oral Surgery Oral Medicine Oral Pathology Oral Radiology and Endodontics, 2002. **93**(2): p. 155-160.
97. S. L. Rakestraw, W. E. Ford, R. G. Tompkins, M. A. J. Rodgers, W. P. Thorpe and M. L. Yarmush, *Antibody-Targeted Photolysis - Invitro Immunological, Photophysical, and Cytotoxic Properties of Monoclonal-Antibody Dextran Sn(Iv) Chlorin-E6 Immunoconjugates.* Biotechnology Progress, 1992. **8**(1): p. 30-39.
98. H. M. Tang, M. R. Hamblin and C. M. N. Yow, *A comparative in vitro photoinactivation study of clinical isolates of multidrug-resistant pathogens.* Journal of Infection and Chemotherapy, 2007. **13**(2): p. 87-91.
99. M. E. Wieder, D. C. Hone, M. J. Cook, M. M. Handsley, J. Gavrilovic and D. A. Russell, *Intracellular photodynamic therapy with photosensitizer-nanoparticle conjugates: cancer therapy using a 'Trojan horse'.* Photochemical & Photobiological Sciences, 2006. **5**(8): p. 727-734.
100. A. C. Templeton, D. E. Cliffel and R. W. Murray, *Redox and fluorophore functionalization of water-soluble, tiopronin-protected gold clusters.* Journal of the American Chemical Society, 1999. **121**(30): p. 7081-7089.
101. Z. Malik, J. Hanania and Y. Nitzan, *Bactericidal Effects of Photoactivated Porphyrins - an Alternative Approach to Antimicrobial Drugs.* Journal of Photochemistry and Photobiology B-Biology, 1990. **5**(3-4): p. 281-293.
102. M. Wilson, *Bactericidal effect of laser light and its potential use in the treatment of plaque-related diseases.* Int Dent J, 1994. **44**(2): p. 181-9.
103. R. G. Palgrave and I. P. Parkin, *Surfactant directed chemical vapour deposition of gold nanoparticles with narrow size distributions.* Gold Bulletin, 2008. **41**(1): p. 66-69.
104. N. L. Rosi, D. A. Giljohann, C. S. Thaxton, A. K. R. Lytton-Jean, M. S. Han and C. A. Mirkin, *Oligonucleotide-modified gold nanoparticles for intracellular gene regulation.* Science, 2006. **312**: p. 1027-1030.
105. P. Christou, *Rice transformation: bombardment.* Plant Molecular Biology, 1997. **35**(1-2): p. 197-203.
106. J. M. de la Fuente, C. C. Berry, M. O. Riehle and A. S. G. Curtis, *Nanoparticle targeting at cells.* Langmuir, 2006. **22**(7): p. 3286-3293.
107. R. P. Brinas, M. H. Hu, L. P. Qian, E. S. Lymar and J. F. Hainfeld, *Gold nanoparticle size controlled by polymeric Au(I) thiolate precursor size.* Journal of the American Chemical Society, 2008. **130**(3): p. 975-982.
108. D. G. Duff, A. Baiker and P. P. Edwards, *A New Hydrosol of Gold Clusters .1. Formation and Particle-Size Variation.* Langmuir, 1993. **9**(9): p. 2301-2309.
109. A. C. Templeton, S. W. Chen, S. M. Gross and R. W. Murray, *Water-soluble, isolable gold clusters protected by tiopronin and coenzyme A monolayers.* Langmuir, 1999. **15**(1): p. 66-76.
110. A. Mattoo and D. S. Goldfarb, *Cystinuria.* Seminars in Nephrology, 2008. **28**(2): p. 181-191.
111. J. L. Domingo, *Prevention by Chelating-Agents of Metal-Induced Developmental Toxicity.* Reproductive Toxicology, 1995. **9**(2): p. 105-113.

112. A. M. Prieur and P. Quartier, *Comparative tolerability of treatments for juvenile idiopathic arthritis.* Biodrugs, 2000. **14**(3): p. 159-183.
113. K. G. Thomas and P. V. Kamat, *Chromophore-functionalized gold nanoparticles.* Accounts of Chemical Research, 2003. **36**(12): p. 888-898.
114. L. D'Ilario and A. Martinelli, *Toluidine blue: aggregation properties and structural aspects.* Modelling and Simulation in Materials Science and Engineering, 2006. **14**(4): p. 581-595.
115. V. Decraene, J. Pratten and M. Wilson, *Cellulose acetate containing toluidine blue and rose bengal is an effective antimicrobial coating when exposed to white light.* Applied and Environmental Microbiology, 2006. **72**(6): p. 4436-4439.
116. G. H. Woehrle, J. E. Hutchison, S. Ozkar and R. G. Finke, *Analysis of nanoparticle Transmission Electron Microscopy data using a public-domain image-processing program, Image.* Turkish Journal of Chemistry, 2006. **30**(1): p. 1-13.
117. M. Zheng and X. Y. Huang, *Nanoparticles comprising a mixed monolayer for specific bindings with biomolecules.* Journal of the American Chemical Society, 2004. **126**(38): p. 12047-12054.
118. H. Tang, J. H. Chen, L. H. Nie, Y. F. Kuang and S. Z. Yao, *A label-free electrochemical immunoassay for carcinoembryonic antigen (CEA) based on gold nanoparticles (AuNPs) and nonconductive polymer film.* Biosensors & Bioelectronics, 2007. **22**(6): p. 1061-1067.
119. S. Basu, S. Panigrahi, S. Praharaj, S. K. Ghosh, S. Pande, S. Jana and T. Pal, *Dipole-dipole plasmon interactions in self-assembly of gold organosol induced by glutathione.* New Journal of Chemistry, 2006. **30**(9): p. 1333-1339.
120. J. Malicka, I. Gryczynski, C. D. Geddes and J. R. Lakowicz, *Metal-enhanced emission from indocyanine green: a new approach to in vivo imaging.* Journal of Biomedical Optics, 2003. **8**(3): p. 472-478.
121. S. Banfi, E. Caruso, L. Buccafurni, V. Battini, S. Zazzaron, P. Barbieri and V. Orlandi, *Antibacterial activity of tetraaryl-porphyrin photosensitizers: An in vitro study on Gram negative and Gram positive bacteria.* Journal of Photochemistry and Photobiology B-Biology, 2006. **85**(1): p. 28-38.
122. E. Dulkeith, A. C. Morteani, T. Niedereichholz, T. A. Klar, J. Feldmann, S. A. Levi, F. van Veggel, D. N. Reinhoudt, M. Moller and D. I. Gittins, *Fluorescence quenching of dye molecules near gold nanoparticles: Radiative and nonradiative effects.* Physical Review Letters, 2002. **89**(20).
123. S. K. Ghosh, A. Pal, S. Kundu, S. Nath and T. Pal, *Fluorescence quenching of 1-methylaminopyrene near gold nanoparticles: size regime dependence of the small metallic particles.* Chemical Physics Letters, 2004. **395**(4-6): p. 366-372.
124. X. S. Kou, S. Z. Zhang, Z. Yang, C. K. Tsung, G. D. Stucky, L. D. Sun, J. F. Wang and C. H. Yan, *Glutathione- and cysteine-induced transverse overgrowth on gold nanorods.* Journal of the American Chemical Society, 2007. **129**(20): p. 6402-+.
125. A. Pastore, G. Federici, E. Bertini and F. Piemonte, *Analysis of glutathione: implication in redox and detoxification.* Clinica Chimica Acta, 2003. **333**(1): p. 19-39.
126. R. Hong, G. Han, J. M. Fernandez, B. J. Kim, N. S. Forbes and V. M. Rotello, *Glutathione-mediated delivery and release using monolayer protected nanoparticle carriers.* Journal of the American Chemical Society, 2006. **128**(4): p. 1078-1079.

127. T. G. Schaaff, G. Knight, M. N. Shafigullin, R. F. Borkman and R. L. Whetten, *Isolation and selected properties of a 10.4 kDa Gold : Glutathione cluster compound.* Journal of Physical Chemistry B, 1998. **102**(52): p. 10643-10646.
128. T. G. Schaaff and R. L. Whetten, *Giant gold-glutathione cluster compounds: Intense optical activity in metal-based transitions.* Journal of Physical Chemistry B, 2000. **104**(12): p. 2630-2641.
129. Y. Negishi, K. Nobusada and T. Tsukuda, *Glutathione-protected gold clusters revisited: Bridging the gap between gold(I)-thiolate complexes and thiolate-protected gold nanocrystals.* Journal of the American Chemical Society, 2005. **127**(14): p. 5261-5270.
130. Y. Negishi, Y. Takasugi, S. Sato, H. Yao, K. Kimura and T. Tsukuda, *Magic-numbered Au-n clusters protected by glutathione monolayers (n=18, 21, 25, 28, 32, 39): Isolation and spectroscopic characterization.* Journal of the American Chemical Society, 2004. **126**(21): p. 6518-6519.
131. N. Damrongchai, K. Yun, E. Kobatake and M. Aizawa, *Self-assembling of glutathione S-transferase/calmodulin fusion protein on chemically modified gold surface.* Journal of Biotechnology, 1997. **55**(2): p. 125-133.
132. C. F. Shaw, *Gold-based therapeutic agents.* Chemical Reviews, 1999. **99**(9): p. 2589-2600.
133. D. J. LeBlanc, R. W. Smith, Z. X. Wang, H. E. HowardLock and C. J. L. Lock, *Thiomalate complexes of gold(I): preparation, characterization and crystal structures of 1:2 gold to thiomalate complexes.* Journal of the Chemical Society-Dalton Transactions, 1997(18): p. 3263-3267.
134. B. D. Berezin, *Coordination Compounds of Porphyrins ans Phthalocyanines.* 1981, Chichester U.K.: John Wiley & Sons.
135. M. L. Yarmush, W. P. Thorpe, L. Strong, S. L. Rakestraw, M. Toner and R. G. Tompkins, *Antibody-Targeted Photolysis.* Critical Reviews in Therapeutic Drug Carrier Systems, 1993. **10**(3): p. 197-252.
136. S. B. Brown, E. A. Brown and I. Walker, *The present and future role of photodynamic therapy in cancer treatment.* Lancet Oncology, 2004. **5**(8): p. 497-508.
137. M. J. Hostetler, J. E. Wingate, C. J. Zhong, J. E. Harris, R. W. Vachet, M. R. Clark, J. D. Londono, S. J. Green, J. J. Stokes, G. D. Wignall, G. L. Glish, M. D. Porter, N. D. Evans and R. W. Murray, *Alkanethiolate gold cluster molecules with core diameters from 1.5 to 5.2 nm: Core and monolayer properties as a function of core size.* Langmuir, 1998. **14**(1): p. 17-30.
138. A. M. Awawdeh and H. J. Harmon, *Spectrophotometric detection of pentachlorophenol (PCP) in water using immobilized and water-soluble porphyrins.* Biosensors & Bioelectronics, 2005. **20**(8): p. 1595-1601.
139. D. V. Leff, P. C. Ohara, J. R. Heath and W. M. Gelbart, *Thermodynamic Control of Gold Nanocrystal Size - Experiment and Theory.* Journal of Physical Chemistry, 1995. **99**(18): p. 7036-7041.
140. E. S. Shibu, M. A. H. Muhammed, T. Tsukuda and T. Pradeep, *Ligand exchange of Au(25)SG(18) leading to functionalized gold clusters: Spectroscopy, kinetics, and luminescence.* Journal of Physical Chemistry C, 2008. **112**(32): p. 12168-12176.
141. C. Burns, W. U. Spendel, S. Puckett and G. E. Pacey, *Solution ionic strength effect on gold nanoparticle solution color transition.* Talanta, 2006. **69**(4): p. 873-876.

142. J. Turkevich, P. C. Stevenson and J. Hillier, *The Formation of Colloidal Gold.* Journal of Physical Chemistry, 1953. **57**(7): p. 670-673.
143. L. M. Liz-Marzan, *Tailoring surface plasmons through the morphology and assembly of metal nanoparticles.* Langmuir, 2006. **22**(1): p. 32-41.
144. B. Khlebtsov, V. Zharov, A. Melnikov, V. Tuchin and N. Khlebtsov, *Optical amplification of photothermal therapy with gold nanoparticles and nanoclusters.* Nanotechnology, 2006. **17**(20): p. 5167-5179.
145. N. G. Khlebtsov, V. A. Bogatyrev, L. A. Dykman and A. G. Melnikov, *Spectral extinction of colloidal gold and its biospecific conjugates.* Journal of Colloid and Interface Science, 1996. **180**(2): p. 436-445.
146. G. Bertoloni, F. M. Lauro, G. Cortella and M. Merchat, *Photosensitizing activity of hematoporphyrin on Staphylococcus aureus cells.* Biochimica Et Biophysica Acta-General Subjects, 2000. **1475**(2): p. 169-174.
147. C. Deroe, P. J. Courtoy and P. Baudhuin, *A Model of Protein Colloidal Gold Interactions.* Journal of Histochemistry & Cytochemistry, 1987. **35**(11): p. 1191-1198.
148. J. Gil-Tomas, S. Tubby, I. P. Parkin, N. Narband, L. Dekker, S. P. Nair, M. Wilson and C. Street, *Lethal photosensitisation of Staphylococcus aureus using a toluidine blue O-tiopronin-gold nanoparticle conjugate.* Journal of Materials Chemistry, 2007. **17**(35): p. 3739-3746.
149. B. V. Enustun and J. Turkevich, *Coagulation of Colloidal Gold.* Journal of the American Chemical Society, 1963. **85**(21): p. 3317-&.
150. P. K. Sudeep, B. I. Ipe, K. G. Thomas, M. V. George, S. Barazzouk, S. Hotchandani and P. V. Kamat, *Fullerene-functionalized gold nanoparticles. A self-assembled photoactive antenna-metal nanocore assembly.* Nano Letters, 2002. **2**(1): p. 29-35.
151. A. Ianoul and A. Bergeron, *Spatially inhomogeneous enhancement of fluorescence by a monolayer of silver nanoparticles.* Langmuir, 2006. **22**(24): p. 10217-10222.
152. N. Chandrasekharan, P. V. Kamat, J. Hu and G. Jones, *Dye-Capped Gold Nanoclusters: Photoinduced Morphological Changes in Gold/Rhodamine 6G Nanoassemblies.* J. Phys. Chem. B, 2000. **104**(47): p. 11103-11109.
153. D. C. Hone, P. I. Walker, R. Evans-Gowing, S. FitzGerald, A. Beeby, I. Chambrier, M. J. Cook and D. A. Russell, *Generation of cytotoxic singlet oxygen via phthalocyanine-stabilized gold nanoparticles: A potential delivery vehicle for photodynamic therapy.* Langmuir, 2002. **18**(8): p. 2985-2987.
154. S. Link and M. A. El-Sayed, *Spectral properties and relaxation dynamics of surface plasmon electronic oscillations in gold and silver nanodots and nanorods.* Journal of Physical Chemistry B, 1999. **103**(40): p. 8410-8426.
155. B. Dubertret, M. Calame and A. J. Libchaber, *Single-mismatch detection using gold-quenched fluorescent oligonucleotides.* Nature Biotechnology, 2001. **19**(4): p. 365-370.
156. S. J. Chen and H. T. Chang, *Nile red-adsorbed gold nanoparticles for selective determination of thiols based on energy transfer and aggregation.* Analytical Chemistry, 2004. **76**(13): p. 3727-3734.
157. A. K. Dutta, K. Kamada and K. Ohta, *Spectroscopic studies of nile red in organic solvents and polymers.* Journal of Photochemistry and Photobiology a-Chemistry, 1996. **93**(1): p. 57-64.

158. S. M. Saraiva and J. F. de Oliveira, *Control of particle size in the preparation of colloidal gold.* Journal of Dispersion Science and Technology, 2002. **23**(6): p. 837-844.
159. A. M. Iga, J. H. P. Robertson, M. C. Winslet and A. M. Seifalian, *Clinical potential of quantum dots.* Journal of Biomedicine and Biotechnology, 2007.
160. F. F. Yang, J. S. Yu and Y. Xie, *Synthesis and characterization of water-soluble CdSe/CdS/ZnS core-shell quantum dots.* Chinese Journal of Inorganic Chemistry, 2008. **24**(7): p. 1142-1147.
161. V. Biju, T. Itoh, A. Anas, A. Sujith and M. Ishikawa, *Semiconductor quantum dots and metal nanoparticles: syntheses, optical properties, and biological applications.* Analytical and Bioanalytical Chemistry, 2008. **391**(7): p. 2469-2495.
162. J. M. Klostranec and W. C. W. Chan, *Quantum dots in biological and biomedical research: Recent progress and present challenges.* Advanced Materials, 2006. **18**(15): p. 1953-1964.
163. R. E. Bailey, A. M. Smith and S. M. Nie, *Quantum dots in biology and medicine.* Physica E-Low-Dimensional Systems & Nanostructures, 2004. **25**(1): p. 1-12.
164. W. R. Algar and U. J. Krull, *Quantum dots as donors in fluorescence resonance energy transfer for the bioanalysis of nucleic acids, proteins, and other biological molecules.* Analytical and Bioanalytical Chemistry, 2008. **391**(5): p. 1609-1618.
165. T. Jamieson, R. Bakhshi, D. Petrova, R. Pocock, M. Imani and A. M. Seifalian, *Biological applications of quantum dots.* Biomaterials, 2007. **28**(31): p. 4717-4732.
166. J. F. Weng and J. C. Ren, *Luminescent quantum dots: A very attractive and promising tool in biomedicine.* Current Medicinal Chemistry, 2006. **13**(8): p. 897-909.
167. A. R. Clapp, I. L. Medintz, J. M. Mauro, B. R. Fisher, M. G. Bawendi and H. Mattoussi, *Fluorescence resonance energy transfer between quantum dot donors and dye-labeled protein acceptors.* Journal of the American Chemical Society, 2004. **126**(1): p. 301-310.
168. D. M. Willard and A. Van Orden, *Quantum dots - Resonant energy-transfer sensor.* Nature Materials, 2003. **2**(9): p. 575-576.
169. M. R. Hamblin and T. Hasan, *Photodynamic therapy: a new antimicrobial approach to infectious disease?* Photochemical & Photobiological Sciences, 2004. **3**(5): p. 436-450.
170. G. Jori, *Photodynamic therapy of microbial infections: State of the art and perspectives.* Journal of Environmental Pathology Toxicology and Oncology, 2006. **25**(1-2): p. 505-519.
171. M. L. Embleton, S. P. Nair, W. Heywood, D. C. Menon, B. D. Cookson and M. Wilson, *Development of a novel targeting system for lethal photo sensitization of antibiotic-resistant strains of Staphylococcus aureus.* Antimicrobial Agents and Chemotherapy, 2005. **49**(9): p. 3690-3696.
172. T. N. Demidova and M. R. Hamblin, *Photodynamic therapy targeted to pathogens.* International Journal of Immunopathology and Pharmacology, 2004. **17**(3): p. 245-254.
173. F. Harris, L. K. Chatfield and D. A. Phoenix, *Phenothiazinium based photosensitisers - Photodynamic agents with a multiplicity of cellular targets and clinical applications.* Current Drug Targets, 2005. **6**(5): p. 615-627.

174. M. Wainwright, D. A. Phoenix, J. Marland, D. R. A. Wareing and F. J. Bolton, *A study of photobactericidal activity in the phenothiazinium series.* Fems Immunology and Medical Microbiology, 1997. **19**(1): p. 75-80.
175. M. Wilson, *Lethal photosensitisation of oral bacteria and its potential application in the photodynamic therapy of oral infections.* Photochemical & Photobiological Sciences, 2004. **3**(5): p. 412-418.
176. A. C. S. Samia, X. B. Chen and C. Burda, *Semiconductor quantum dots for photodynamic therapy.* Journal of the American Chemical Society, 2003. **125**(51): p. 15736-15737.
177. W. W. Yu, E. Chang, R. Drezek and V. L. Colvin, *Water-soluble quantum dots for biomedical applications.* Biochemical and Biophysical Research Communications, 2006. **348**(3): p. 781-786.
178. B. R. Fisher, H. J. Eisler, N. E. Stott and M. G. Bawendi, *Emission intensity dependence and single-exponential behavior in single colloidal quantum dot fluorescence lifetimes.* Journal of Physical Chemistry B, 2004. **108**(1): p. 143-148.
179. I. L. Medintz, S. A. Trammell, H. Mattoussi and J. M. Mauro, *Reversible modulation of quantum dot photoluminescence using a protein-bound photochromic fluorescence resonance energy transfer acceptor.* Journal of the American Chemical Society, 2004. **126**(1): p. 30-31.
180. R. Bakalova, H. Ohba, Z. Zhelev, M. Ishikawa and Y. Baba, *Quantum dots as photosensitizers?* Nature Biotechnology, 2004. **22**(11): p. 1360-1361.
181. M. M. Mathews, *Comparative Study of Lethal Photosensitization of Sarcina Lutea by 8-Methoxypsoralen and by Toluidine Blue.* Journal of Bacteriology, 1963. **85**(2): p. 322.
182. A. J. Gomes, L. O. Lunardi, J. M. Marchetti, C. N. Lunardi and A. C. Tedesco, *Indocyanine green nanoparticles useful for photomedicine.* Photomedicine and Laser Surgery, 2006. **24**(4): p. 514-521.
183. L. X. Shi, B. Hernandez and M. Selke, *Singlet oxygen generation from water-soluble quantum dot-organic dye nanocomposites.* Journal of the American Chemical Society, 2006. **128**(19): p. 6278-6279.
184. M. Ozkan, *Quantum dots and other nanoparticles: what can they offer to drug discovery?* Drug Discovery Today, 2004. **9**(24): p. 1065-1071.